Beamforming and Optimisation of RIS-Assisted UAV Communication Systems

Mohammad Omar Tawfiq Abualhayja'a

Submitted in fulfilment of the requirements for the
Degree of Doctor of Philosophy

School of Engineering
College of Science and Engineering
University of Glasgow

June 2024

Abstract

With the rapid development of wireless technologies, unmanned aerial vehicles (UAVs) are expected to play an increasingly significant role in future mobile networks. Thanks to their low cost, small size, high mobility, and deployment flexibility. UAVs are becoming an attractive solution for various wireless communication applications. UAVs can be utilised as aerial communication platforms for enhancing the coverage, capacity, and energy efficiency of wireless networks. However, to effectively utilise the UAV technology in wireless networks, various technical challenges related to communication links reliability, UAV placement, and trajectory planning need to be addressed. Reconfigurable intelligent surfaces (RISs) may be integrated into UAV networks to overcome some of the UAV communications key challenges, and at the same time, enhance the overall performance of the network in terms of spectrum and energy efficiency. This is due to the ability of the RISs to turn the wireless environment into a controlled entity by shaping and fully manipulating its EM responses. To this end, the main goal of this thesis is to provide an analytical framework for analysing, designing, and optimising RIS-assisted UAV communication systems. In this context, this thesis first begins by investigating the fundamental characteristics of UAV technology, major paradigms for UAV integration into wireless networks and their potential applications, and addresses open problems and challenges in UAV communications. It then examines RIS technology within the emerging concept of smart radio environments (SRE), its structure and applications, and sheds light on the potential RIS-assisted UAV system scenarios. The main theme of the first two contributions centres around the performance evaluation of RIS-assisted UAV communication systems. In the first contribution, RIS-assisted UAV communication systems are studied and analysed through the development of a comprehensive mathematical framework for communication systems performance evaluation. Three different system scenarios are considered to assess the impact of RIS on UAV communications. This framework includes the derivation of accurate closed-form approximations for signal-to-noise ratio (SNR) distributions for the proposed systems, as well as analytical expressions for outage probabilities and average bit-error-rate (BER). The findings demonstrate that RIS can significantly enhance the performance of UAV communication systems by ensuring reliable connections, particularly in complex

and dynamic environments where maintaining line-of-sight (LoS) connections may not always be feasible or optimal. Since power efficiency is a critical aspect of green communication, aimed at reducing the carbon footprint of telecommunication networks, the second contribution explores the integration of RIS into wireless networks as a novel passive technology to enhance energy efficiency. A comprehensive optimisation framework is developed to minimise the total power consumption of RIS-assisted communication systems by optimising the number of RIS elements and their phase shifts while adhering to essential communication constraints. Simulation results provide valuable insights into the intricate dynamics of RIS-assisted communications system design by illustrating the impact of control circuit components, control boards, and dynamic power dissipation factors. Results also highlight the significant advantages of RIS deployment in terms of power efficiency, especially at higher data rates. Additionally, the study emphasises the importance of considering alternative relay techniques when customising wireless communication systems to meet specific rate requirements and operating conditions. Finally, the third contribution proposes an application scenario for integrated RIS-assisted UAV communications, specifically focusing on an RIS-assisted UAV Internet of Things (IoT) data collection framework. This framework is optimised to maximise performance in terms of the number of served IoT devices and their data rates. The proposed algorithm presents a promising approach to address the growing demand for efficient data collection in IoT networks. Simulation results reveal the potential of RIS-assisted UAV solutions in meeting the increasing demands of wireless IoT networks. By coordinating the RIS phase shift matrix and UAV trajectory planning, the framework achieves significant enhancements in the number of served IoT devices and the achievable data rates.

Acknowledgements

I would like to begin by expressing my deepest gratitude to the Almighty God for sustaining my health and guiding me through the challenges of my PhD journey.

I would like to extend my immense gratitude to my supervisors. Dr. *Anthony Centeno*, my primary supervisor, for his encouragement and understanding. His consistent support and constructive criticism have been crucial in shaping the direction of my study. Additionally, I express my deepest gratitude to my co-supervisor, Dr. *Lina Mohjazi*, for her commitment and unwavering guidance. Her continuous support, passion for academic research excellence, and meticulous attention to detail have provided me with the confidence and motivation to overcome various challenges encountered during this research. I would also like to thank Prof. *Mohammad Imran* for his support, guidance, and encouragement throughout the course of my research.

I am deeply thankful to the Nokia team, particularly Dr. *Majid Butt*, Dr. *Philippe Sehier*, and Dr. *Dinh-Hieu Tran*, who supported and guided me throughout my research. Their expertise and assistance were invaluable in achieving this significant milestone.

I am grateful to the University of Glasgow for awarding me the UESTC scholarship, which made it possible for me to undertake this Ph.D. research.

I would like to extend my deepest gratitude to my dear parents, *Omar* and *Maysoon*, as well as my siblings, *Ansam* and *Hamza*. Their support and encouragement have been a source of inspiration and motivation, without which I would not have made this success possible. My heartfelt appreciation also goes to my wife, *Elif*, her patience, understanding, and support throughout this journey have been empowering me to pursue my dreams with unwavering determination.

I also wish to extend my heartfelt thanks to my friends and colleagues who provided invaluable intellectual stimulation and emotional support throughout this challenging process. Their insights, encouragement, and camaraderie were essential in navigating the complexities of my research.

A special thank you to everyone who contributed, no matter how small their role. Your collective efforts and support have been instrumental in achieving this significant milestone.

To my beloved parents, my dear siblings, and my extraordinary wife

Statement of Originality

Name: Mohammad O.T. Abualhayja'a
Registration Number:

I certify that the thesis presented here for examination for a PhD degree of the University of Glasgow is solely my own work other than where I have clearly indicated that it is the work of others (in which case the extent of any work carried out jointly by me and any other person is clearly identified in it) and that the thesis has not been edited by a third party beyond what is permitted by the University's PGR Code of Practice.

The copyright of this thesis rests with the author. No quotation from it is permitted without full acknowledgment. I declare that the thesis does not include work forming part of a thesis presented successfully for another degree.

I declare that this thesis has been produced in accordance with the University of Glasgow's Code of Good Practice in Research.

I acknowledge that if any issues are raised regarding good research practice based on the review of the thesis, the examination may be postponed pending the outcome of any investigation of the issues.

Signature: Mohammad Abualhayja'a
Date: 09-09-2024

Contents

List of Tables

List of Figures

List of Abbreviations

AF	Amplify-and-Forward
AO	Alternating Optimisation
AoI	Age of Information
ABS	Aerial Base Station
AP	Access Point
AR	Augmented Reality
AUE	Aerial User Equipment
AWGN	Additive White Gaussian Noise
A2G	Air-to-Ground
BBU	Baseband Unit
BER	Bit Error Rate
BnB	Branch-and-Bound
BS	Base Station
BW	Bandwidth
B5G	Beyond Fifth Generation
CDF	Cumulative Distribution Function
CDG	Compressive Data Gathering
CH	Cluster Head
CPU	Central Processing Unit
CSI	Channel State Information
DAC	Digital-to-Analogue Converter
D2D	Device-to-Device
Dec-POMDP	Decentralised Partially Observable MDP
DF	Decode-and-Forward
DFT	Discrete Fourier Transform
DoF	Degree-of-Freedom
DRL	Deep Reinforcement Learning
eMBB	Enhanced Mobile Broadband
EM	Electromagnetic
FD	Full-Duplex

FDMA	Frequency Division Multiple Access
FL	Federated Learning
FPGA	Field-Programmable Gate Array
GA	Genetic Algorithm
G2A	Ground-to-Air
HD	Half-Duplex
HO	Handover
i.i.d.	Independent and Identically Distributed
IoT	Internet of Things
LoS	Line-of-Sight
MARL	Multi-Agent Reinforcement Learning
MDP	Markov Decision Process
MEC	Mobile Edge Computing
MIMO	Multiple-Input Multiple-Output
MINLP	Mixed-Integer Nonlinear Programming
MISO	Multiple-Input Single-Output
ML	Machine Learning
MMSE	Minimum Mean Square Error
M-MIMO	Massive Multiple-Input Multiple-Output
mMTC	Massive Machine-Type Communications
NLoS	Non-Line-of-Sight
NOMA	Non-Orthogonal Multiple Access
OMA	Orthogonal Multiple Access
op-amp	Operational Amplifiers
PA	Power Amplifier
PDF	Probability Distribution Function
PSO	Particle Swarm Optimisation
PWM	Pulse-Wave-Modulation
QoS	Quality of Service
RF	Radio Frequency
RLF	Radio Link Failure
RIS	Reconfigurable Intelligent Surface
RV	Random Variable
SC	Selection Combining
SER	Symbol Error Rate
SIC	Successive Interference Cancellation
SINR	Signal-to-Interference-plus-Noise Ratio
SNR	Signal-to-Noise Ratio

SRE	Smart Radio Environment
SWIPT	Simultaneous Wireless Information and Power Transfer
TSPTW	Travelling Salesman Problem with Time Windows
UAV	Unmanned Aerial Vehicle
UC	Unit-Cell
UE	User Equipment
ULA	Uniform Linear Array
UPA	Uniform Planar Array
URLLC	Ultra-Reliable Low-Latency Communications
VR	Virtual Reality
WPT	Wireless Power Transfer
ZF	Zero-Forcing
2D	Two-Dimensional
2D-DTF	Two-Dimensional Discrete Fourier Transform
3D	Three-Dimensional
5G	Fifth Generation
6G	Sixth Generation

List of Symbols

$\mathbf{a}_h(\theta, \phi)$	Horizontal array response vector
$\mathbf{a}_v(\theta)$	Vertical array response vector
A_β, B_β	Parameters for Rice factor fitting
A_η, B_η	Parameters for path loss exponent fitting
α	Path loss exponent
$\alpha(\theta_U)$	Path loss exponent as a function of UAV elevation angle
α_{DQL}	Learning rate in DQL
$\hat{\alpha}$	RIS reflection coefficient
$\beta(\theta_U)$	Rician factor as a function of UAV elevation angle
β_{node}	Transceiver node BBU power consumption per unit throughput
B	UC bit resolution in a single polarisation mode
c_1, c_2	Fitting parameters for of Rician distributions sum approximation
$\hat{c_1}$, $\hat{c_2}$	Acceleration coefficients in PSO
C	Number of radio resources
C_k	Cluster centroid
d	Separation between RIS unit cells
d_{RG}	Distance between RIS and ground user
$d_{R,k\to U}[n]$	Euclidean distance between k^{th} RIS and UAV at time slot n
$d_{R,k\to i}$	Euclidean distance between k^{th} RIS and i^{th} IoT device
d_{RU}	Distance between RIS and UAV
d_{SG}	Distance between source and ground user
d_{SR}	Distance between source and RIS
$d_{SR,i}$	Channel gain between source and i^{th} RIS element
d_{UG}	Distance between UAV and ground user
d_{UR}	Distance between UAV and RIS
$d_{U\to i}[n]$	Distance between UAV and i^{th} IoT device
ϵ_{DQL}	Exploration probability in DQL
ϵ_{node}	Transceiver node power amplifier efficiency factor
$f_{Y_i}(\gamma)$	Probability density function (PDF) of the random variable Y_i
$F(M)$	Discrete Fourier Transform (DFT) matrix

$F(M_v) \otimes F(M_h)$	2D-DTF-based codebook for RIS reflection configurations
F_i	Activation end time for i^{th} IoT device
G	Amplification factor of the AF relay
γ	Signal-to-noise-ratio (SNR)
γ_{DQL}	Discount factor in DQL
γ_{th}	Threshold SNR
$\Gamma(.)$	Gamma function
$\Gamma_i[n]$	SNR for the signal received from i^{th} IoT device at time slot n
$h_{RG,i}$	Channel gain between i^{th} RIS element and ground user
$h_{R,k\rightarrow U}[n]$	Channel gain between k^{th} RIS and UAV at time slot n
$h_{R,k\rightarrow i}$	Channel gain between k^{th} RIS and i^{th} IoT device
h_{RU}	Channel gain between RIS and user
$h_{RU,i}$	Channel gain between i^{th} RIS element and UAV
h_{SR}	Channel gain between source and RIS
$h_{SR,i}$	Channel gain between source and i^{th} RIS element
h_{SU}	Channel gain between source and user
h_{UG}	Channel gain between UAV and ground user
$h_{U\rightarrow i}[n]$	Channel gain between UAV and i^{th} IoT device
I	Total number of IoT devices
I_h	Indicators for UC horizontal polarisation
I_v	Indicator for UC vertical polarisation
$IoTD_{min}$	Minimum number of IoT devices to be served
$j_i[n]$	Size of data collected at time slot n from i^{th} IoT device
K	Total number of RISs
κ_{buffer}	Maximum capacity of replay buffer
Λ_i	Binary variable indicating successful reception (1) or failure (0)
λ	Wavelength
M	Number of RIS elements
M_c	Number of adjustable electronic components within the RIS
M_g	Number of the RIS UCs within the same control group
M_{global}	Global best number of RIS elements
M_h	Number of horizontal elements in RIS
M_s	Number of control signals originated by each drive circuit
M_{sub}	Size of the sub-RIS or grouped elements
M_v	Number of vertical elements in RIS
m	Nakagami-m shape parameter
n	Additive white Gaussian noise
N	Total number of time slots

N_0	Variance of the additive white Gaussian noise
N_{iter}	Maximum number of iterations in PSO
N_{pop}	Population size in PSO
Ω	Nakagami-m fading power
O	Large number used in scheduling constraints
p, q	Modulation scheme parameters
P	Transmitted power
$P_b(E)$	Average bit error rate (BER)
$P_b(E \mid \gamma)$	Conditional BER
$P_{DF}^{\text{Tx}}(\bar{R})$	Transmit power to achieve $\bar{R}$ for DF relay-assisted transmission
P_{AF}^{static}	Static power consumption of AF relay
$P_{\text{AF}}^{\text{Tx}}(\bar{R})$	Transmit power to achieve $\bar{R}$ for AF relay-assisted transmission
P_D^c	Circuit power consumption of the destination node
P_S^c	Circuit power consumption of the source node
$P_{\text{control board}}$	Power dissipation of the RIS control board
P_{DF}^{static}	Static power consumption of DF relay
$P_{\text{DF}}^{\text{Tx}}(\bar{R})$	Transmit power to achieve $\bar{R}$ for DF relay-assisted transmission
$P_{\text{drive circuits}}^{\text{total}}$	Total power dissipation of the RIS drive circuits
$P_{\text{LoS}}(\theta)$	Probability of line-of-sight (LoS)
$P_{i,h}(B_{i,h}, b_{i,h})$	Power dissipation of the i^{th} RIS UC in horizontal polarisation
$P_{i,v}(B_{i,v}, b_{i,v})$	Power dissipation of the i^{th} RIS UC in vertical polarisation
P_{RIS}^{DC}	Total power dissipation in RIS
P_{out}	Outage probability
P_R	Power of the relay transmitted signal
P_S	Power of the source node transmitted signal
$P_{\text{RIS}}^{\text{Total}}$	End-to-end power consumption of RIS-assisted transmission
$P_{\text{RIS}}^{\text{Tx}}(\bar{R})$	Transmit power to achieve $\bar{R}$ for RIS-assisted transmission
P_{static}	RIS static power dissipation
P_{Total}relay	End-to-end power consumption of relay-assisted transmission
PUC	Power dissipation of the RIS metasurface layer
P_{node}^c	Transceiver node circuit power dissipation
$P_{\text{node}}^{\text{static}}$	Static power consumption of the transceiver node circuit
P_{node}^{Tx}	Transceiver node transmit power
$P_{\text{node}}^{\text{Total}}$	Total power consumption of a transceiver node
$q[n]$	UAV trajectory coordinates at time slot n
$Q_\zeta(.,.)$	Generalised Marcum Q-function
σ	Scale parameter for Rayleigh distribution
θ	Phase shift of the i-th RIS element

θ	UAV trajectory parameter in DRL
Θ	RIS phase-shift matrix
$\Theta_k[n]$	Phase shift matrix for k^{th} RIS at time slot n
$\theta_i[n]$	Angle between UAV and the i^{th} IoT device at time slot n
θ_i	Phase shift of the i-th RIS element
T_i	Activation start time for i^{th} IoT device
χ	Composite channel gain for RIS-assisted UAV-aided transmission
Ξ	Composite channel gain for RIS-assisted cellular-connected UAV
ξ	Q-network weights
ξ_1, ξ_2	Environment-dependent variables for LoS probability calculation
ξ_{target}	Target network weights
$w_{\theta,k}[n]$	RIS reflection coefficients vector at time slot n
w_{θ_o}	Optimal phase vector for RIS-assisted transmission
ω	Inertia weight in PSO
x	Transmitted signal
X	Boundary of the UAV's x-coordinate in the service area
x_i, y_i, z_i	Coordinates of the i^{th} IoT device
$x_{R,k}, y_{R,k}, z_{R,k}$	Coordinates of the k^{th} RIS
$x_U[n], y_U[n], z_U[n]$	Coordinates of the UAV at time slot n
X_1	Composite channel gain for multi-hop first transmission stage
X_2	Composite channel gain for multi-hop second transmission stage
y_R	Received signal at the relay in relay-assisted transmission
y_U	Received signal at the user relay-assisted transmission
Y	Boundary of the UAV's y-coordinate in the service area
Z	Number of bits in a data packet
Z_i	Data packet size for i^{th} IoT device
$\bar{h}_{NLoS}$	NLoS link attenuation coefficient
$\bar{h}^{\text{LoS}}_{R,k\to U}[n]$	Deterministic LoS component between k^{th} RIS and UAV
$\bar{h}^{\text{LoS}}_{R,k\to i}$	Deterministic LoS component between k^{th} RIS and i^{th} IoT device
$\bar{R}i$	Average data rate for the i^{th} IoT device over N time slots
$\bar{R}_{\text{AF}}$	Achievable rate at the user for AF relay-assisted transmission
$\bar{R}_{\text{DF}}$	Achievable rate at the user for DF relay-assisted transmission
$\bar{R}_{\text{RIS}}$	Achievable rate at the user for RIS-assisted transmission
$\bar{R}_{\text{th}}$	Minimum rate constraint
$\overline{\gamma}$	Average SNR
$\overline{\gamma}_1$	Average SNR for the first transmission stage
$\boldsymbol{\theta}_{\min}$, $\boldsymbol{\theta}_{\max}$	Range for particle positions
$\boldsymbol{\Theta}_{\text{global}}$	Global best position of phase shifts

Chapter 1

Introduction

1.1 Scope and Motivation

The world of wireless communication continues to evolve, enabling novel applications and services. The fifth generation (5G) wireless networks represent a significant step forward in wireless communication compared to previous generations, offering higher peak data rates, ultra-low latency, enhanced reliability, increased network capacity, and improved availability. At their core, future 5G and beyond (B5G) wireless networks are envisioned to support different service categories, including enhanced mobile broadband (eMBB), ultra-reliable low-latency communications (URLLC), and massive machine-type communications (mMTC) [1]. Yet, the evolving landscape of wireless communication continues to expose the need for even more advanced and robust networks capable of meeting the diverse demands of future applications. These demands require innovative solutions, leading to the growing importance of unmanned aerial vehicles (UAVs) in enhancing communication quality across many applications [2]. With their distinctive mobility and adaptability attributes, UAVs have gained substantial attention presenting potential applications in wireless communications [3]. They can be used as airborne communication platforms, enabling extended coverage, higher capacity, enhanced reliability, and energy efficiency [4, 5]. They can also serve as new aerial user equipment (AUE) terminals, facilitating various tasks ranging from data collection to item delivery [4–6]. Moreover, UAV communications offer significant attributes including line-of-sight (LoS) links and dynamic deployment ability, making them a desirable candidate to complement, or even substitute terrestrial wireless networks [2, 7].

By integrating UAVs into future wireless networks, key scenarios of eMBB, URLLC, and mMTC can be facilitated, especially in public safety and emergency response situations where UAVs play a crucial role in providing network service recovery and improving public safety networks. UAVs can enhance mobile broadband by extending network coverage to remote or congested areas where terrestrial infrastructure is limited.

By acting as aerial base stations (ABSs) or relays, UAVs can augment network capacity and provide high-speed connectivity to users, enabling seamless access to high-definition video streaming and immersive augmented reality (AR)/virtual reality (VR) experiences, even in dynamic or crowded environments [4]. UAVs can also provide URLLC links, crucial for applications requiring real-time data transmission and mission-critical operations. For example, in emergency response situations, UAVs equipped with communication devices can establish reliable links to transmit critical information to emergency responders with minimal delay [4]. Furthermore, UAVs can facilitate massive machine-type communications by serving as platforms for connecting a large number of internet-of-things (IoT) devices over a wide area [8]. With their mobility and flexibility, UAVs can collect IoT data from remote or inaccessible locations, enabling applications such as environmental monitoring, precision agriculture, and smart city infrastructure [5]. Additionally, UAV networks can optimise energy consumption by intelligently managing device connectivity and data transmission, supporting the low-power requirements of mMTC [9].

Despite their potential benefits, UAV networks often encounter critical challenges such as communication reliability, blockages, and dynamic environmental conditions. To reap the benefits of future UAV-based applications, it is essential to achieve reliable and improved communications performance and coverage, particularly in environments featuring fading channels, signal blockages, or long transmission distances. It is worth noting that traditional transmission enhancement techniques, such as multiple-input multiple-output (MIMO), phased arrays, multi-antenna transmitters, and relays, involve active components of complex hardware that exhibit high power consumption. The augmentation of reconfigurable intelligent surfaces (RISs) presents a promising low-cost and energy-efficient solution [1]. This is due to the ability of RISs to turn the wireless environment into a controlled entity by shaping and fully controlling its electromagnetic (EM) response. RISs have been proposed as an enabler technology for the smart wireless environment (SRE) implementation allowing for real-time customisation and control of wireless channels [10, 11]. While 5G networks are meticulously planned with optimised infrastructure placement, the dynamic nature of wireless environments characterised by user mobility, environmental changes, and varying traffic conditions presents ongoing challenges that extend beyond the planning phase.

1.1.1 Smart Radio Environment Empowered by RIS

Current wireless networks have traditionally operated under the assumption that the wireless propagation environment is a random uncontrollable process beyond manipulation. While techniques such as adaptive modulation/coding, beamforming, and power control have been employed to mitigate transmission challenges, their effectiveness is limited by the inherent randomness of the wireless environment, posing significant

obstacles to achieving high-capacity and reliable wireless communications [10]. The evolving wireless communication landscape is characterised by growing demands for eMBB, URLLC, and mMTC [12, 13]. In this context, the notion of a controlled wireless environment becomes essential to realise the ambitious objectives of next-generation networks, wherein wireless channels are dynamically manipulated and controlled in real-time [10, 11, 13]. Here comes the emerging concept of SRE, in this new paradigm, wireless channels are subject to real-time control and customisation by incorporating energy-efficient dynamic configuration and intelligent signal control [10].

The recent advancements in wireless networking, particularly in modern relaying solutions, amplify-and-forward (AF) and decode-and-forward (DF) relaying, have introduced solutions that demonstrate the capability to actively assist transmission from source to destination, effectively enhancing the wireless environment [14, 15]. Relays function by leveraging cooperative diversity, essentially converting non-line-of-sight (NLoS) links into LoS connections. However, this approach requires equipping each relay with dedicated power sources and front-end circuitry for receiving, processing, and re-transmitting signals. Consequently, deploying relays leads to higher power demands within the network.

Additionally, the spectral efficiency of relay-assisted systems relies on the duplexing protocol. For instance, half-duplex (HD) relaying protocols restrict simultaneous transmission by transmitters and relays occupying the same physical resource, thereby constraining network throughput. On the other hand, full-duplex (FD) relaying protocols address this limitation but introduce new challenges such as loop-back self-interference at the relay, co-channel interference at the destination, and increased signal processing requirements and power dissipation [14].

The drawbacks associated with relay deployment underscore the need for alternative solutions that offer enhanced efficiency and scalability. RISs emerge as a superior alternative to active relaying solutions. Unlike relays, RISs operate passively without the need for additional RF chain components [10]. By deploying massive arrays of low-cost reflecting or scattering passive elements, RISs enable dynamic control of wireless channels in real-time [11]. Additionally, RIS technology is compatible with existing wireless technologies and supports wideband full-duplex operation without the need for self-interference cancellation techniques. Furthermore, RISs can be deployed on various surfaces, including indoor walls, buildings, and aerial platforms, offering unparalleled flexibility in controlling diverse wireless environments [13].

RIS presents significant advantages for wireless communication but faces challenges in implementation. Adapting to dynamic environments, such as urban or indoor settings, requires RIS to continuously adjust phase shifts to maintain optimal signal paths. While RIS is more energy-efficient than traditional active systems, it still requires power

for the control circuitry and tuning elements, making efficiency a key concern. The complexity of real-time beamforming due to numerous elements also poses computational challenges, necessitating advanced optimisation algorithms. Addressing these issues through innovation and improved algorithms is crucial for realising RIS's full potential in future networks.

1.1.2 RIS-Assisted UAV Communications

While UAVs revolutionise wireless connectivity in diverse environments, the integration of RIS technology further enhances wireless communication networks by improving transmission efficiency. Together, these technologies pave the way for sustainable, efficient, and reliable wireless communication systems in the era of future connectivity.

RIS technology offers a unique approach to improving UAV communication links by manipulating the propagation of wireless signals. By strategically placing RIS elements, UAVs can benefit from enhanced signal propagation, extended coverage, and increased communication range [16]. This is particularly advantageous in scenarios where UAVs need to operate in remote or challenging environments, where traditional communication infrastructure is limited. RIS technology also improves signal quality by mitigating signal attenuation and multipath fading, ensuring that UAVs receive high-quality signals for reliable communication links [17]. Moreover, RIS elements can be dynamically reconfigured to adapt to changing environmental conditions and optimise communication links in real-time which is crucial for dynamic UAV deployment. Furthermore, integrating RIS with UAV networks contributes to energy efficiency by optimising communication links and conserving power, thereby extending flight endurance and operational capabilities [18]. RIS technology also holds promise for enhancing security and privacy in UAV networks by creating secure communication zones and preventing unauthorised access to sensitive data [19].

1.2 Problem Statement and Objectives

For efficient deployment of RIS-assisted UAV communication systems, jointly optimising UAV positioning, trajectory, and RIS phase shifts is essential. However, this joint optimisation is a complex task, requiring advanced algorithms and real-time adaptability to balance multiple factors and constraints effectively. Moreover, optimising RIS beamforming adds another layer of complexity, as it involves precise control of phase shifts to dynamically steer and enhance the signal, necessitating sophisticated computational techniques and real-time processing capabilities. The complexity is further increased by the need to tailor the optimisation objectives to specific applications or targets, whether it be enhancing coverage, improving signal quality, or maximising energy efficiency.

This thesis aims to develop the theoretical foundations for RIS-assisted UAV solutions leveraging the RIS passive beamforming capabilities jointly with UAV flexible deployment and dynamic mobility. Furthermore, since power efficiency is a critical aspect of green communication, targeting reduced carbon footprint of telecommunication networks this thesis also explores the integration of RIS into wireless networks as a novel passive technology to enhance energy efficiency.

Towards achieving a thorough understanding of RIS-assisted UAV communications, this thesis adopts a systematic approach focusing on the examination of one framework at a time. Specifically, the thesis begins by offering insight into the nature of RIS-assisted UAV communication system behaviour and characterising performance measures. These measures not only facilitate straightforward and precise performance assessment but also offer an understanding of how this performance correlates with crucial system parameters. Subsequently, the investigation transitions towards RIS-assisted communications power efficiency to explore its impact on net zero and green communication aspects for both terrestrial and UAV communications. Next, to enhance the scope of potential applications and contribute to the advancement of RIS-assisted UAV communication technologies, the study explores an application scenario for RIS-assisted UAV communications, namely RIS-assisted UAV communications for efficient IoT data harvesting. This thesis assumes that the core network infrastructure, including the placement of BSs and other network nodes, is pre-planned. However, it addresses the need for solutions that enhance performance beyond these initial plans, particularly in complex and unpredictable environments.

1.2.1 Problem Statement

RIS-Assisted UAV Communication System Performance Evaluation

To develop a better understanding of the RIS-assisted UAV networks, a performance analysis across major paradigms for integrating UAVs into cellular networks is examined. Three system scenarios are considered.

Scenario 1) Cellular-connected UAV system: The cellular-connected UAV system leverages UAVs as AUE in various applications across a wide range of sectors. However, cellular networks often face coverage limitations in remote or rural areas and signal blockages in congested urban environments. Moreover, multipath fading and severe path loss at high altitudes introduce additional complexity, leading to reduced data rates and unreliable connectivity. RIS can enhance coverage and capacity by intelligently reflecting and redirecting signals toward UAVs, improving ground-to-air (G2A) link quality. Therefore, analysing the RIS-assisted UAV system in terms of signal-to-noise ratio (SNR) and outage behaviour is crucial to evaluate its effectiveness in enhancing the performance and reliability of cellular-connected UAV systems.

Scenario 2) UAV-aided communications: UAV-aided communications utilise UAVs as airborne communication nodes, serving as ABS or access points (AP), enhancing network capacity, coverage, and resilience. However, UAVs face limitations due to battery life, payload capacity, and signal blockages in urban environments, leading to coverage challenges and significant path loss. RIS can assist air-to-ground (A2G) links by maximising UAV coverage and improving transmit power efficiency. Comprehensive performance analysis, including SNR and outage behaviour, is essential for effective RIS deployment in UAV-aided systems. This analysis should evaluate communication reliability across varying distances, altitudes, and conditions, helping to identify optimal UAV and RIS placement to maximise coverage, minimise outage probability, and enhance system performance.

Scenario 3) Multi-hop RIS-assisted UAV communication system: Exploring RIS-assisted UAV networks requires delving into a multi-hop RIS-assisted UAV communication system where UAVs serve as relay nodes. This setup is particularly suitable for various scenarios, such as rural connectivity, disaster response, urban connectivity enhancement, and temporary events, to improve wireless communication by extending coverage, mitigating obstacles, and enhancing reliability. The inclusion of RIS and the utilisation of UAV relays present notable challenges to the analysis due to their distinctive characteristics and operational scenarios when compared to ABSs or AUEs. These challenges primarily involve the mathematical modelling and analysis techniques employed.

Beamforming and Power Optimisation for RIS-Assisted Communications

Green communication, aimed at reducing the carbon footprint of telecommunication networks, is an increasingly pivotal aspect of modern wireless technology. Within this framework, RIS technology emerges as a promising solution, holding the potential to significantly contribute to reduced emissions from wireless communication systems. However, most of the works only consider the impact of using RIS on enhancing the network performance in terms of reducing the signalling power and ignore the RIS power dissipation. Therefore, there is a need to investigate RIS power dissipation to ensure efficient operation and deployment. Furthermore, considering power dissipation at the RIS when optimising its phase shift represents a crucial aspect in developing beamforming optimisation techniques. Addressing this aspect not only enhances the accuracy of beamforming strategies but also promotes energy efficiency in RIS-assisted communication systems. Thus, a comprehensive exploration of RIS power dissipation and its integration into beamforming optimisation frameworks is essential for advancing the field and realising the full potential of RIS technology in green communication initiatives.

Application Scenario: Efficient Data Harvesting in Urban IoT Networks

Future IoT networks are expected to rely heavily on UAVs to collect data since they can meet the demands for massive connectivity, ultra-high throughput, and energy efficiency. If UAVs can get closer to ground-based IoT devices, this would increase throughput rates and reduce the energy consumption of the energy-limited IoT devices. However, in environments featuring fading channels, signal blockages, or long distances, maintaining reliable communication links between UAVs and IoT devices becomes essential. Therefore, there is a pressing need to develop solutions that ensure reliable communication links between UAVs and IoT devices in challenging environments. To address these limitations and further enhance the performance of UAV-assisted IoT networks, RISs integration presents a promising solution. By dynamically adjusting the phase shifts of RIS elements and the UAV trajectory in real-time, the system can adapt to changing environmental conditions, mitigate signal blockages, and maximise throughput rates. As such, there is a need to establish a theoretical foundation for RIS-assisted UAV IoT data collection framework to enhance IoT network performance. Consequently, it is crucial to develop algorithms that jointly optimise the beamforming of RIS elements and the UAV trajectory.

1.2.2 Objectives

Given the technical challenges outlined, this thesis aims to achieve the following objectives:

O1: Present a comprehensive study on applications and design aspects of RIS-assisted UAV communications in future wireless networks. To achieve this objective, the study will explore RIS-assisted UAV communications elements. Firstly, review the fundamental characteristics of the UAVs, major paradigms for integrating the UAVs into wireless networks, and their possible applications, as well as addressing open problems and challenges in UAV communications. Next, conduct a comprehensive review of the concept of RIS technology and its architecture. This involves delving into the fundamental principles behind RIS technology, its components, and how it operates within wireless communication systems with particular emphasis on aspects such as improved signal quality, enhanced power efficiency, and its role in promoting sustainability. Finally, this study will shed light on the possible RIS-assisted UAV systems scenarios and applications.

O2: Develop accurate analytic tools and frameworks that facilitate a thorough performance evaluation of RIS-assisted UAV communication systems across different scenarios. These tools will enable system designers to gain a comprehensive understanding of the fundamental limits of system performance, offering detailed insights into performance dynamics in terms of coverage and communication

reliability, and assessing the effectiveness of RIS deployment across various scenarios including cellular-connected UAV systems, UAV-aided communications, and multi-hop RIS-assisted UAV communication systems.

O3: Investigate power dissipation at the RIS, with a specific focus on beamforming and power optimisation strategies for RIS-assisted communications by developing a framework to minimise total power consumption in RIS-assisted communication systems, optimising the number of RIS elements and configuration to reduce power dissipation while maintaining necessary channel gain for service requirements. This objective aims to bridge a critical gap in current research by considering the impact of RIS power dissipation on overall system efficiency and performance. Ultimately, this comprehensive exploration will advance the field of RIS technology by providing concrete performance metrics, beamforming techniques, and power control optimisation strategies. These insights will facilitate the integration of RIS-assisted communication systems into green communication initiatives.

O4: Develop a framework for RIS-assisted UAV IoT data collection, focusing on enhancing key performance metrics. This will involve designing and implementing a comprehensive optimisation strategy that uses machine learning (ML) algorithms to optimise UAV trajectory and IoT devices scheduling decisions. Additionally, the optimisation strategy will incorporate the design of a beamforming algorithm to optimise the RIS configuration. This study aims to contribute to the advancement of RIS-assisted UAV implementation in IoT networks by providing a robust framework for enhancing overall IoT network performance.

1.3 Contributions and Research Outcome

Based on the objectives outlined earlier, this research develops an analytical framework for analysing, designing, and optimising RIS-assisted UAV communication systems. This section outlines the main contributions and research outcomes described in the thesis.

1.3.1 Contributions

The major contributions of this thesis are summarised and listed as follows:

- A comprehensive foundation is established to study the integration of UAVs into wireless networks and the potential enhancements offered by RIS technology. It encompasses a thorough review of UAV characteristics, integration paradigms, applications, and challenges. Furthermore, an in-depth exploration of the fundamentals of RIS technology, its components, and operational principles is

undertaken, with special attention given to how RIS technology can improve signal quality, enhance power efficiency, and promote sustainability within wireless communication systems. The findings of this contribution are represented in [J1], [J3], [Ch1], and [Ch2].

- A theoretical framework to analyse the performance of RIS-assisted UAV communications is proposed. Specifically, the outage probability of RIS-assisted UAV communications is investigated in two deployment scenarios: UAV-aided communications and cellular connected-UAV systems, considering Rician fading channels. Accurate closed-form approximations for the SNR distributions and the outage probability were derived for both scenarios. This contribution offers insights into outage probability characterisation, derives analytical approximations validated by simulations, provides asymptotic analysis for high SNR regimes, and studies the impact of optimal UAV altitude and RIS elements on performance. The findings of this contribution are represented in [C2].

- Provide a comprehensive analysis of power dissipation in RIS-assisted communication systems to offer valuable insights into their energy footprint. Furthermore, a precise optimisation problem considering RIS power dissipation is formulated. The formulated problem aims to minimise total power dissipation while meeting essential communication constraints. Factors such as rate requirements and phase shift constraints are also considered, ensuring practical relevance in real-world network scenarios. Moreover, this contribution also includes comparing RIS with traditional active solutions like relaying, specifically AF and DF relaying protocols, showcasing RIS's potential to significantly reduce power consumption and enhance overall network sustainability. The findings of this contribution are partially published in [C1], with the remaining part currently under review for publication, as referenced in [J5].

- Investigate a multi-hop RIS-assisted UAV communication system, with the UAV acting as a relay node. This integration paradigm addresses various application scenarios like rural connectivity, disaster response, and urban enhancement, aiming to enhance wireless communication by extending coverage. The study employs a generic Nakagami-m distribution to model the fading channels, providing flexibility in representing both pure LoS and NLoS fading characteristics. A realistic scenario with a direct NLoS link between the source and destination is also considered. Accurate approximations for system outage probability and bit error rate (BER) for binary modulation schemes are obtained based on the approximated SNR distribution. Furthermore, an asymptotic analysis of outage probability in the high SNR regime is conducted. This study represents a novel examination of RIS-assisted

multi-hop systems operating in composite fading environments with a direct link between source and destination, contributing significantly to the understanding of such systems' performance. The findings of this contribution are represented in [J2].

- An innovative framework for RIS-assisted UAV IoT data collection in urban environments is proposed with objectives to maximise the number of served devices and average throughput. In a framework that considers energy conservation each IoT device operates in sleep mode, activating only during data transmission, with varied time windows for data collection. This necessitates solving the NP-hard travelling salesman problem with time windows (TSPTW) for UAV trajectory design. To tackle the problem's complexity and randomness of the environment, the problem is divided into sub-problems. A deep reinforcement learning (DRL) algorithm is employed for UAV trajectory optimisation and scheduling decisions, alongside a beamforming codebook for RIS phase optimisation. Additionally, a clustering algorithm based on activation time windows and physical location is proposed to enhance data collection efficiency and reduce complexity. The findings of this contribution are partially published in [C3], with the remaining part currently under review for publication, as referenced in [J4].

1.3.2 Research Outcomes

The findings of this thesis, in addition to collaborations with fellow research students, have led to the following publications:

Journals

[J1] Hassouna, S., Jamshed, M.A., Rains, J., Kazim, J.U., Rehman M.U., **Abualhayja'a, M.**, Mohjazi, L., Cui, T.J., Imran, M.A., Abbasi, Q.H., "A Survey on Reconfigurable Intelligent Surfaces: Wireless Communication Perspective", *IET Communications*, vol. 17, no. 5, pp. 497-537, 2023 Mar.

[J2] **Abualhayja'a, M**., Centeno, A., Mohjazi, L., Butt, M.M., Sehier, P., and Imran, M. A., "Exploiting Multi-Hop RIS-Assisted UAV Communications: Performance Analysis," in *IEEE Communications Letters*, vol. 28, no. 1, pp. 133-137, Dec. 2023, DOI: 10.1109/LCOMM.2023.3339969.

[J3] Katwe, M., Kaushik, A., Mohjazi, L., **Abualhayja'a, M**., Dardari, D., Singh, K., Imran, M. A., Butt, M.M., and Dobre, O. A., "An Overview of Intelligent Metasurfaces for 6G and Beyond: Opportunities, Trends, and Challenges," submitted to *IEEE Communications Standards Magazine* (Under review).

[J4] **Abualhayja'a, M**., Centeno, A., Mohjazi, L., Butt, M.M., Sehier, P., and Imran, M. A., "Optimizing RIS-Assisted UAV Solutions for Efficient IoT Data Collection: A Reinforcement Learning Approach," submitted to *IEEE Transactions on Vehicular Technology* (Under review).

[J5] **Abualhayja'a, M**., Wagih, M., Centeno, A., Mohjazi, L., and M. A. Imran, "Beamforming and Power Optimization for RIS-Assisted Communications," submitted to *IEEE Open Journal of the Communications Society* (Under review).

Conferences Proceedings

[C1] **Abualhayja'a, M**., Centeno, A., Mohjazi, L., Abbasi, Q.H. and Imran, M.A., "Performance of Reconfigurable Intelligent Surfaces vs. Relaying for UAV-Assisted Communications", in *2021 IEEE USNC-URSI Radio Science Meeting (Joint with AP-S Symposium)*, Singapore, Singapore, Dec. 2021, pp. 58-59, doi: 10.23919/USNC-URSI51813.2021.9703626.

[C2] **Abualhayja'a, M**., Centeno, A., Mohjazi, L., Abbasi, Q.H. and Imran, M.A., "On the Outage performance of Reconfigurable Intelligent Surface-Assisted UAV Communications", in *2023 IEEE Wireless Communications and Networking Conference (WCNC)*, Glasgow, United Kingdom, March 2023, pp. 1-6, doi: 10.1109/WCNC55385.2023.10118821.

[C3] **Abualhayja'a, M**., Centeno, A., Mohjazi, L., Butt, M.M., Sehier, P., and Imran, M. A., " RIS-Assisted UAV for IoT Data Harvesting," accepted for publication at *ICC 2024 Workshops*, June 2024, Denver, CO, USA.

Book Chapters

[Ch1] **Abualhayja'a, M**., Ansari, S., Popoola, O.R., Mohjazi, L., Bariah, L., Muhaidat, S., Abbasi, Q.H. and Imran, M.A., (2022). RIS-Assisted UAV Communications. *Intelligent Reconfigurable Surfaces (IRS) for Prospective 6G Wireless Networks*, pp.213-232.

[Ch2] **Abualhayja'a, M**., Hassouna, S., Centeno, A., Abbasi, Q. H., Rehman, M. U., Imran, M. A., and Mohjazi, L. (2023). "Intelligent Reflective Surfaces (IRSs) for Green Networks". In *The Role of 6G and Beyond on the Road to Net-Zero Carbon* (Chapter 9, pp. Chapter page range). Institution of Engineering and Technology.

1.4 Thesis Outline

The remainder of this thesis is structured as follows: Chapter 2 provides a comprehensive overview of both UAV communications and RIS technology aimed at establishing a framework for RIS-assisted UAV communications. Chapter 3 focuses on conducting a comprehensive analysis of energy dissipation in RIS systems to showcase RIS's potential in reducing power consumption and enhancing network sustainability. Chapter 4 introduces a theoretical framework to analyse the performance of RIS-assisted UAV communications given different deployment scenarios. In Chapter 5, an innovative framework for RIS-assisted UAV IoT data collection in urban environments is presented. This framework aims to maximise the number of served devices and average throughput while considering energy conservation. Finally, Chapter 7 concludes the dissertation and discusses potential avenues for future extensions of this work.

Chapter 2

Background and Literature Review

In this chapter, the role of UAVs in future mobile networks is explored, highlighting their unique characteristics and discussing their potential impact. Additionally, open problems and challenges in UAV communications are presented while shedding light on the potential for RIS to address these problems. Then, the focus shifts towards a comprehensive study of applications and design aspects of the RIS in future wireless networks focusing on promoting the use of RIS in green communication and achieving sustainable development goals. It also delves into the techniques adopted in the literature for RIS beamforming optimisation and thoroughly examines the strengths and limitations of each approach and technique. Finally, a brief exploration of the fundamental aspects of RIS-assisted UAV communications is provided, including an examination of their deployment scenarios and strategies, followed by an extensive exposition of the applications of RIS-assisted UAV systems within wireless communication systems. This comprehensive review is aligned with the objectives outlined in *O1*, providing a thorough exploration of RIS-assisted UAV communications within wireless networks.

2.1 The Role of UAVs in Future Wireless Networks

The use of UAVs has recently experienced tremendous development in applications such as public safety, traffic monitoring, photography, delivery services, and communication networks [4–6]. To create a clear image of how UAVs may be utilised in wireless networks, this section will list their unique characteristics compared to traditional terrestrial networks. These characteristics will be investigated to highlight opportunities and challenges. It's worth noting that this part emphasises potential uses and opportunities of the UAV networks, with integrated RIS-assisted UAV systems discussed in greater depth in the following sections.

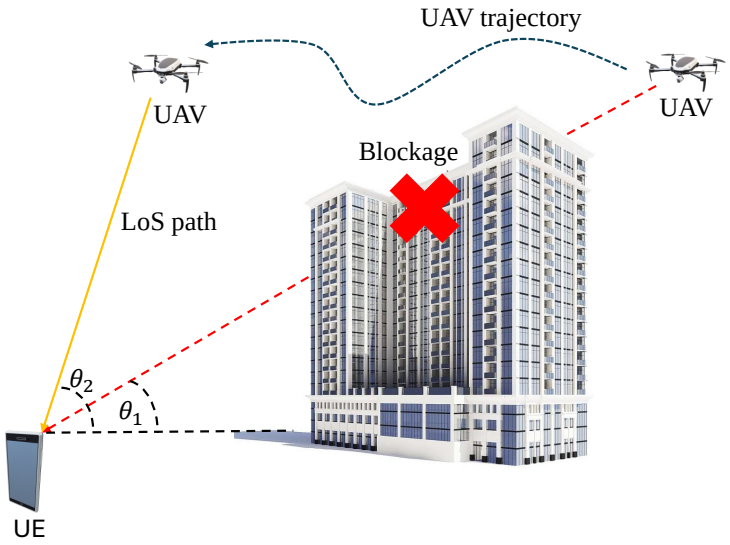

Figure 2.1: UAV dynamic deployment properties.

2.1.1 UAV Characteristics

From a research perspective, providing a full horizon of UAV applications and benefits necessitates highlighting the fundamental differences between UAV communications and conventional terrestrial communications. The novelty of UAV communications lies in several key characteristics. Compared to traditional terrestrial communications, UAV communications offer several compelling benefits, as detailed below.

Dynamic deployment

Due to their flexible placement and 3D mobility, UAVs are ideal for on-demand deployment at specific locations, creating a cost-effective and fast solution appropriate for unexpected and emergency cases or temporary coverage [4, 20]. At the same time, their trajectory can be planned to enhance communication links in real-time by providing shorter link distance and less signal obstruction as shown in Figure 2.1 [21]. Moreover, dynamic deployment of UAVs as ABSs can be utilised to maximise the lifetime of mobile terminals, minimise the average latency, and maximise the number of covered users under energy and spectrum constraints [21–23].

High LoS probability

The A2G channels present distinct features compared to other terrestrial communication channels. As illustrated in Figure 2.2, the UAV A2G link offers a notable advantage in LoS probability over traditional terrestrial communications [2, 24]. This direct loS link facilitates minimal signal attenuation, resulting in heightened signal strength and quality.

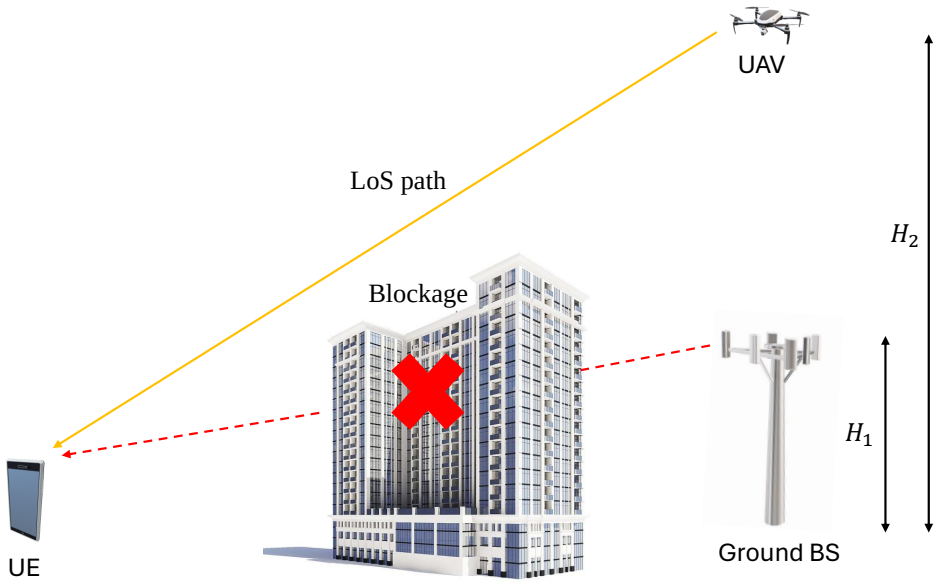

Figure 2.2: UAV high LoS probability.

Unlike terrestrial links subject to obstruction by buildings, trees, and other obstacles, A2G links often enjoy clearer paths, reducing signal blockage. Furthermore, high LoS probability enhances the overall reliability of A2G links by minimising signal fading caused by multipath propagation effects. Consequently, UAVs offer enhanced communication reliability, particularly in urban or densely populated areas [2].

The probability of LoS primarily depends on three factors: UAV altitude, elevation angle, and the propagation environment. This aspect underscores the importance of these variables in determining communication reliability and performance [2]. The deployment of stronger and more reliable communication links with relatively larger diversity gains is facilitated by the high LoS probability of UAV communications [6, 24].

Easy deployment and affordably low infrastructure cost

In contrast to terrestrial networks, UAV networks are easy to deploy and do not require costly infrastructure. This enables network access to remote regions. Google's Loon project and Facebook Aquila are examples of a contemporary initiative to build massive UAV networks to deliver low-cost broadband access to rural areas [25].

2.1.2 Applications and Use Cases in Wireless Networks

Based on their functionality, there are two major paradigms for integrating UAVs into cellular networks. On the one hand, UAV-aided communications, in which UAVs serve as airborne communication platforms. On the other hand, under the cellular-connected category UAVs operate as AUE in a cellular network to serve different applications [4, 5].

Cellular-connected UAV

This paradigm integrates UAVs into the wireless network as a new AUE. Compared to conventional cellular communication with ground users, this communication paradigm involving cellular-connected UAVs exhibits distinct characteristics, opening the door for new applications and opportunities.

Typical applications:

- Remote sensing: Coming in almost all possible shapes, types, and sizes, UAVs may function as airborne platforms loaded with various kinds of sensors such as high-definition and thermal cameras, as well as radio scanners. UAVs with their sensor payloads and data communication capabilities, facilitate remote sensing across various domains. This technology finds application in agriculture, weather forecasting, disaster monitoring, archaeology, surveillance, geological scanning, and environmental monitoring [26–28].

- Edge computing: Mobile edge computing (MEC) is a distributed computing paradigm that integrates network features, processing, storage, and other intelligence services closer to the data source. Mobile computing platforms are equipped with high processing power edge servers, reducing the demand for data processing at a distant data centre. This architecture meets the demands of latency-sensitive applications that use a massive amount of geographically distributed terminals and sensors [29]. UAVs with MEC capabilities can be used by mobile users to offload computationally demanding operations. This will not only alleviate network congestion but also enable faster deployment of new applications. Leveraging their wide coverage and high LoS probability, cellular-connected UAVs offer seamless and continuous MEC services for users with high mobility requirements, without necessitating frequent handovers [29, 30].

- Public safety: UAVs can play a pivotal role in establishing a robust disaster response system. For instance, swift evacuation is critical in preventing significant loss of life during natural disasters. UAVs can be equipped with speakers enabling them to broadcast emergency announcements and guide individuals to evacuate to safety zones more efficiently. Moreover, they can monitor evacuation routes using cameras and offer ground personnel guidance. Additionally, UAVs can scan disaster areas to locate individuals in need of evacuation [31].

- Delivery services: Cellular-connected UAVs will play a significant role in delivery applications. Different corporations have previously created drone delivery systems, such as Amazon Prime Air and Google's Project Wing.

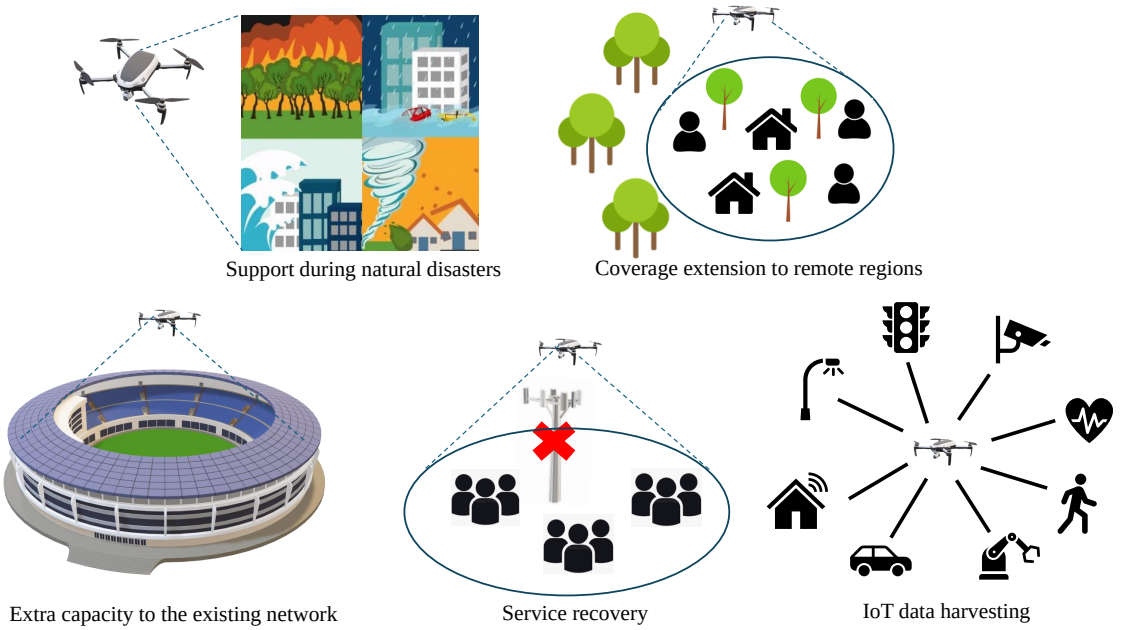

Figure 2.3: Typical applications of UAV-assisted communications.

UAV-assisted communications

In the UAV-assisted communication paradigm, UAVs serve as aerial communication platforms, ABS or relays, for terrestrial users [32]. Unlike stationary terrestrial infrastructure, UAVs can be dynamically deployed to meet real-time demand, enabling flexible network reconfiguration based on traffic demands and user locations [33]. Hence, integrating UAV-assisted communication systems into wireless networks offers significant advantages and opportunities. As shown in Figure 2.3, typical uses include coverage expansion, service recovery during emergencies, data traffic offloading, aerial relaying between distant clusters, and efficient data collection for IoT and machine-type communications.

Typical applications:

- Capacity enhancement and coverage extension: Future wireless networks are driven by ever increasing demand for high mobile data rates, reduced end-to-end latencies, and connectivity across a diversity of new applications such as the IoT, mMTC, etc. Dense cell deployment and millimetre-wave communications are mandatory for serving these demands. However, dense cell networks face several challenges related to backhaul transmission and interference. In addition, the millimetre-wave bands are affected by high propagation loss and sensitivity to blockage. UAVs can provide a low-cost and flexible solution for offloading the macrocells and providing energy-efficient connectivity [4, 5]. Furthermore, UAVs can be developed as a cost-effective aerial communication platform to extend network coverage to remote regions that

are difficult to access or add extra capacity to the existing networks. They may also be used as wireless relays to improve ground wireless device connectivity and coverage [32].

- Mission critical communications and service recovery: In the events of large-scale natural disasters and emergencies, the existing terrestrial networks may suffer from huge damages. UAV-assisted communication is a promising technology that can provide fast, flexible, and reliable solutions to overcome network failure in similar scenarios [34, 35]. By providing the essential coverage UAVs can play a significant role in public safety scenarios during natural disasters to support search and rescue operations and disaster response.

- IoT data harvesting: The number of IoT devices is experiencing an exponential surge, with projections indicating billions of devices will soon be integrated into wireless networks [36]. These devices cover various domains, from household settings to vehicles and wearable devices. However, their operational capabilities are constrained by limited energy resources and environmental obstructions. Simultaneously, the massive volume of data transmitted by these devices necessitates real-time processing in most scenarios [37]. Failure to achieve this real-time processing renders the transmitted data essentially useless. Therefore, the development of reliable connectivity solutions capable of addressing both time and energy constraints is crucial. UAV-assisted communications emerge as an ideal solution to confront these challenges, thanks to their inherent flexibility, cost-effectiveness, and dynamic deployment capabilities [9, 38–41].

2.1.3 Challenges of UAV Neworks

Due to their unique characteristics and physical attributes UAVs will play a fundamental role in realising the development of future mobile networks. However, in order to integrate reliable UAV communications systems, several challenges and limitations must be addressed. This section provides an overview of the key technical challenges that arise in UAV communications for different deployment paradigms.

Accurate propagation channel modelling

An accurate channel model is essential for the proper planning of a communication system. When employing UAVs in applications like UAV-assisted communications and IoT networks, accurate propagation channel modelling is critical to predicting the performance of UAV networks in terms of coverage, reliability, and capacity [5, 24]. The characteristics of UAV communication channels differ substantially from those of traditional terrestrial

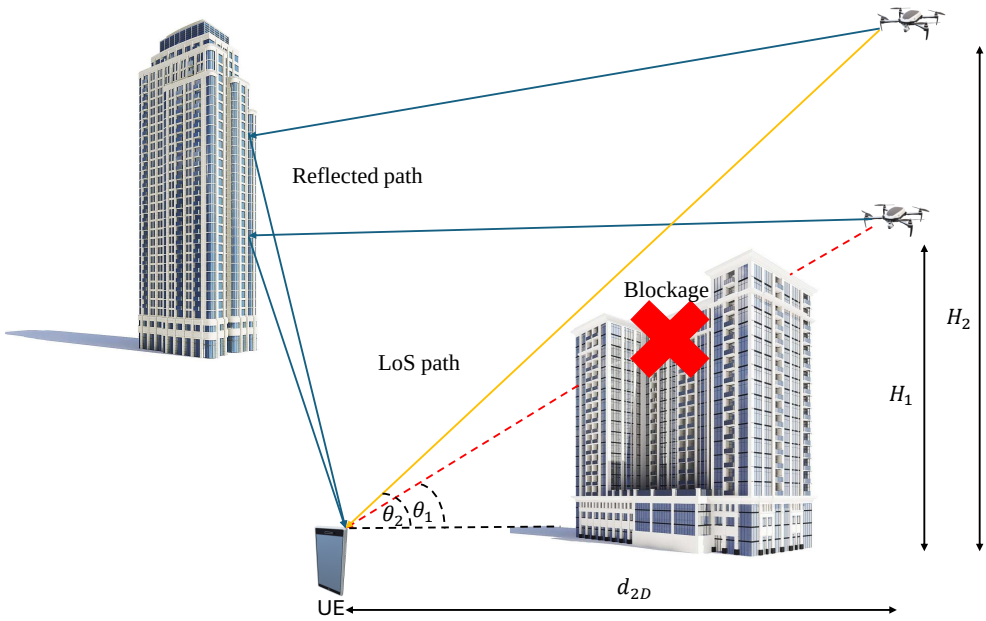

Figure 2.4: UAV communication A2G propagation scenario.

communication channels. Specifically, due to their unique attributes, UAVs experience higher LoS probability. As shown in Figure 2.4, the propagation channel for UAVs depends on multiple factors such as UAV height, elevation angle, and the wireless environment [24]. Furthermore, due to UAV's dynamic mobility patterns, A2G propagation channels can experience greater spatial and temporal variations in non–stationary channels than traditional terrestrial communication channels. Consequently, factors such as Doppler shifts and spread become crucial for certain communication applications [42].

The three-dimensional deployment of UAVs

Optimal 3D placement is one of the critical aspects of UAV-assisted communications. Energy-efficient maximal coverage can be achieved by utilising flexible UAV deployment as aerial communications platforms [21, 43]. However, due to their high mobility, it is a challenging task to achieve optimal UAV 3D deployment, especially in multi-UAV deployment scenarios. Multiple factors must be considered such as inter-cell interference, energy and spectrum constraints, geographical distribution ground nodes, traffic demands, and the varying A2G channel characteristics [23, 44]. These factors introduce additional variables and uncertainties that must be accounted for during deployment planning and optimisation.

Optimal trajectory planning

Optimising the UAV trajectory maintains the quality of communication links by providing shorter and more reliable connections resulting in higher data rates and enhanced latency

[32, 45]. However, planning the optimal UAV path brings new challenges since it requires considering several factors such as propagation environment, traffic demands, and other physical constraints such as UAV dynamics, flying speed, and acceleration [5]. Addressing these challenges effectively requires the development of sophisticated algorithms and techniques that can optimise UAV trajectory while balancing competing objectives such as communication performance, energy efficiency, and operational constraints.

Network planning for cellular-connected UAV applications

The existing cellular networks are planned to serve conventional ground users, which have different characteristics from aerial users such as UAVs. For instance, terrestrial base station (BS) antennas are typically down-tilted to provide coverage for ground users and minimise inter-cell interference [46]. At the same time, UAVs which fly at relatively high altitudes can be served by antennas sidelobes [47]. This may lead to degraded communication quality due to weaker signal strength, increased interference from adjacent cells or non-associated users, and lower antenna gain [46]. Hence, further enhancements and new technologies are needed to reshape the traditional terrestrial networks to provide sufficient coverage and signal quality to support cellular-connected UAV applications. Additionally, due to their rapid movement, cellular-connected UAVs pose new challenges in terms of mobility management and underscore the essential requirement for URLLC for navigation and control links [48].

2.2 Overview of RIS Technology

This section aims to present a comprehensive study on applications and design aspects of the RIS in future wireless networks focusing on promoting the use of RIS in green communication and achieving sustainable development goals. The concept of RIS technology, its architecture, and control mechanisms are presented. Next, the advantages and possible use cases for integrating RISs into the wireless network are highlighted. Finally, the RIS is compared with active solutions in terms of its benefits in terms of signal quantity, power efficiency, and sustainability.

2.2.1 Smart Radio Environment

Future wireless networks such as the sixth generation (6G) wireless networks, are driven by explosive growing demands for ultra-high throughput, ultra-low latency, and ultra-reliable communications, hence, the controlled wireless environment is becoming necessary to realise the development of these networks [49]. As illustrated in Figure 2.5, SRE is an emerging concept that refers to the process of turning the wireless environment into a

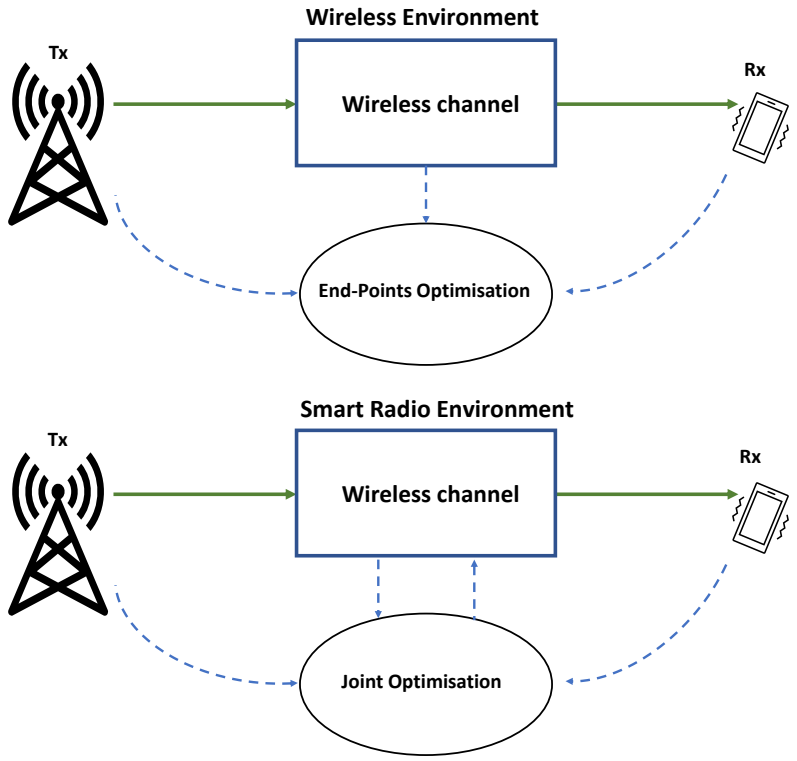

Figure 2.5: The difference between wireless environment and SRE.

controllable and reconfigurable variable [10].

RIS is a novel passive technology that can improve the efficiency of wireless networks and realise the concept of SRE. The integration of RISs into the wireless network reduces the number of active transceivers, enhances coverage, and improves the quality of wireless signals. In contrast to active technologies such as MIMO, active beamforming, and relay networks, which demand extra energy and complicated hardware, RIS is a passive solution, that does not need any RF chains, thus, it can be easily integrated into the network, leading to lower energy consumption and a smaller carbon footprint.

Figure 2.6 illustrates the difference between the conventional cellular networks and the SRE empowered by RIS. In general, as shown in Figure 2.6(a), the user equipment (UE) is served by the closest BS, however, due to the blockage caused by objects in the environment such as buildings which cause signal attenuation, the user will be served by another BS with better signal conditions, but reflections of the signal coming from the closer BS can result in unwanted interference. Moreover, there might be security issues in case of eavesdropper presence. In conventional wireless networks, once the signal is transmitted by the BS, it interacts with the environment causing a degradation in the signal quality with no control over the radio environment and the only thing that can be done to improve the signal quality is to alter the signal at the endpoints. On the other hand, in SRE where it is assumed that RIS is integrated into the environment. RIS can

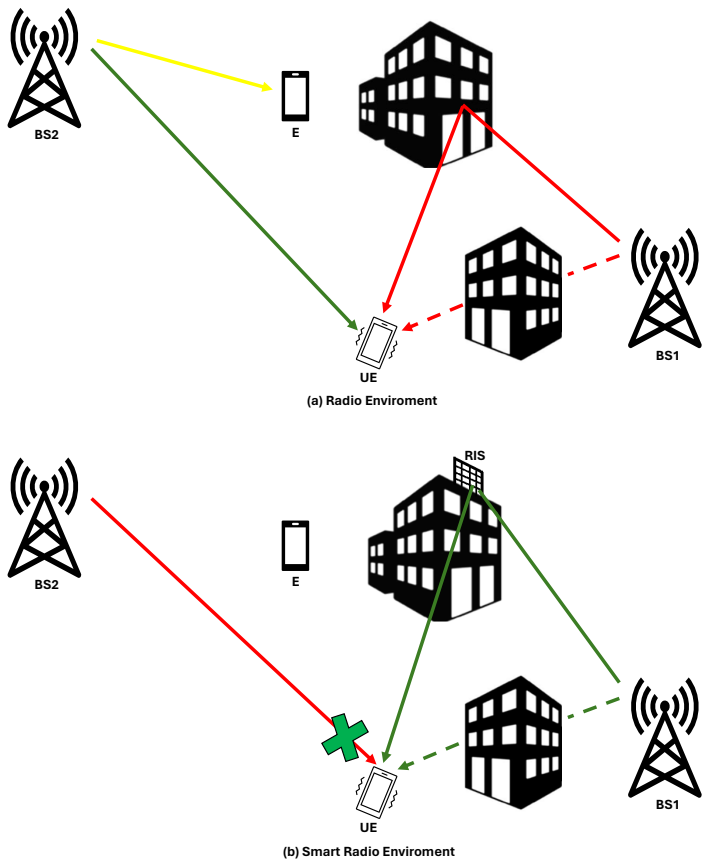

Figure 2.6: RIS-empowered SRE.

be programmed to control the signal reflections to be combined at the UE terminal and get rid of any source of interference or security threats, as shown in Figure 2.6(b).

A RIS is a massive array of low-cost reflecting or scattering passive elements, each can be configured using a simple controller to change the incident wave phase, amplitude, frequency, or polarisation. It coherently adds the signal reflections and focuses them where they are most needed, and at the same time, eliminates any source of noise or interference. RIS can be easily deployed on different surfaces such as indoor walls, buildings, and even aerial platforms providing the opportunity to control various wireless environments. In addition to its easy deployment, RIS is lower cost and more energy-efficient than the active relaying solutions, where it creates virtual LoS links between the transmitter and the receiver via passive beamforming, without the need for any transmit RF chains [50–52]. By leveraging RIS technology, the SRE can enhance the signal strength, coverage, and capacity of wireless networks.

2.2.2 RIS Structure and Control Mechanism

RIS is a two-dimensional (2D) electromagnetic surface made up of several passive scattering units or metamaterial elements whose reflection characteristics can be modified

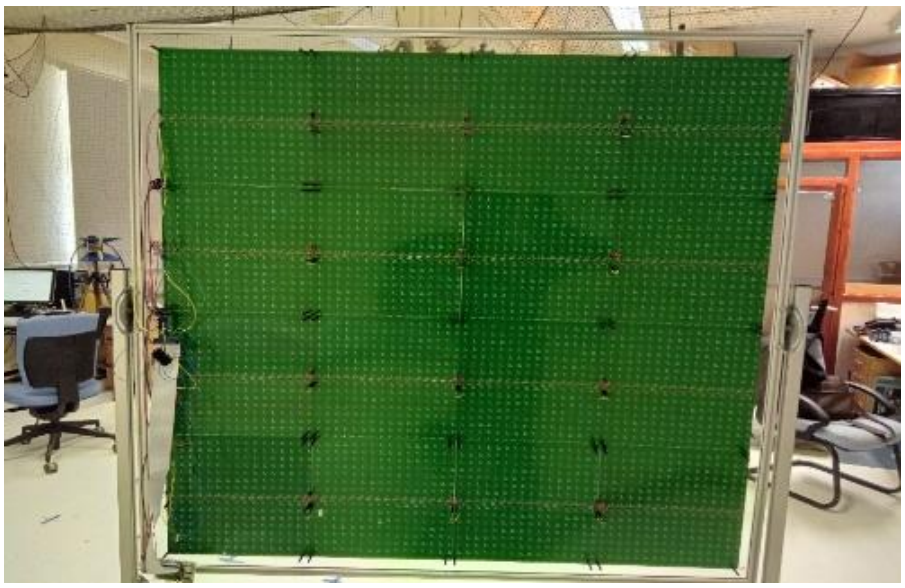

Figure 2.7: RIS prototype.

to produce the desired EM response [11, 14]. A prototype of a RIS developed by the University of Glasgow is shown in Figure 2.7. The model consists of 4096 1-bit elements arranged in a 64X64 rectangular array.

RIS Structure

As shown in Figure 2.8, the RIS structure comprises three layers, each playing a vital role in its operation. Recognising the intricate interplay between these layers is crucial for understanding the operation and power dissipation dynamics of RIS technology and paves the way for developing strategies to enhance its efficiency and effectiveness.

- RIS metasurface layer: Composed of a substrate containing metamaterial unit-cell (UC) elements arranged periodically with spacing smaller than half of the wavelength. UCs commonly consist of metamaterial, dielectric media, and adjustable components, such as varactor diodes and PIN diodes. These UC elements function as individual scatterers, receiving incoming waves and reflecting them with controlled phase [53]. Metamaterials, the building blocks of this layer, are engineered to exhibit unique EM properties by manipulating the interaction of EM radiation. This manipulation allows for precise control over signal propagation and reception, critical for optimising transmission efficiency [54].

- RIS configuration network layer or drive circuit: Responsible for controlling the reflection characteristics of the UC elements. The structure and operation of this layer are determined by tuning mechanisms and desired degrees of EM control freedom. Effective management of these properties is crucial for minimising power dissipation while maximising signalling performance [53].

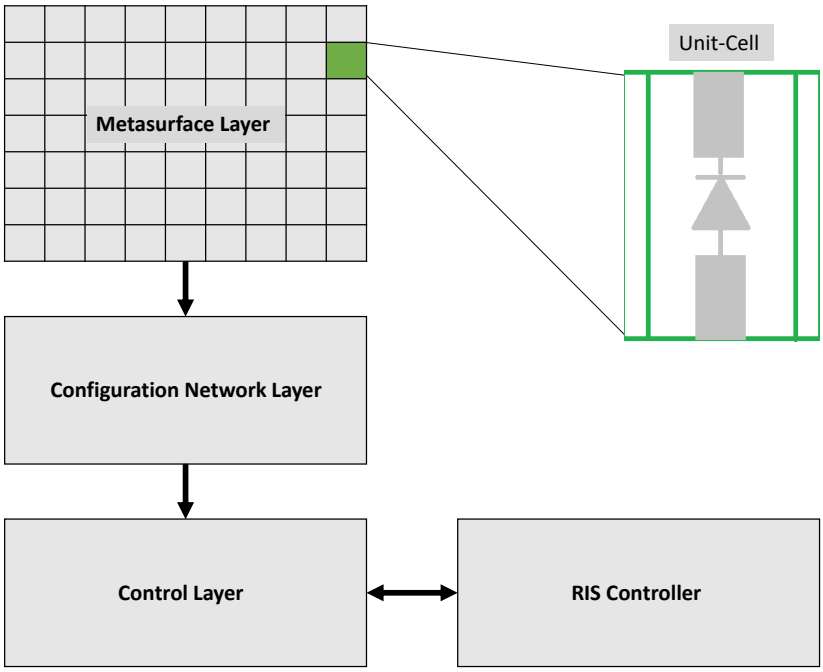

Figure 2.8: Structure of RIS.

- The RIS control layer: Interfaces with the network to execute configuration commands, transmit signals to the configuration network, and process feedback from onboard sensors. This layer facilitates communication through various wireless technologies such as Wi-Fi, Bluetooth, or cellular networks, adapting to specific application and performance requirements [10, 53].

Passive beamforming is a critical element that empowers RISs to dynamically adjust their electromagnetic properties, ensuring adaptation to wireless channel conditions and enhancing system performance. The controller unit acts as the central processing unit, generating configuration commands based on real-time channel conditions, and employing optimisation algorithms or machine learning techniques. This area of research is dynamic and continuously evolving, with focused efforts aimed at developing advanced optimisation techniques to enhance RIS performance and efficiency.

RIS metasurface tuning

The RIS consists of a programmable metasurface that can control the phase changes of individual scattering components by applying an external stimulus to manipulate their physical properties. This allows for modification of the EM properties of the metasurface without the need for refabrication. Metasurface tuning processes refer to techniques used to modify the properties of metasurfaces [53].

The behaviour of reflected and diffracted waves is governed by Snell's law and the Fresnel equations. However, when EM waves encounter a metasurface, a shift in the

resonance frequency can occur due to the periodic arrangement of scattering components. As a result, additional phase shifts are introduced to the reflected and diffracted waves. The EM properties of the metasurface are determined by its physical structure and can be used for specific purposes, such as perfect absorption at a particular frequency [53, 55].

There are different categories of tuning processes that have been identified in the literature, including geometrical or structural tuning, material tuning, and circuit tuning. Structural tuning involves modifying the geometrical properties of the metasurface elements, such as their shape and size, in order to change the response of the surface to incident waves. Material tuning involves adjusting the EM properties of the metasurface elements, such as their permittivity and permeability, to achieve the desired response. Circuit tuning involves incorporating or adjusting the impedance of each unit cell's circuit model using variable capacitors and switches within and between the unit cells to control their properties, such as electric or magnetic fields [53, 56, 57].

2.2.3 Design Parameters of the RIS

The design of a RIS involves several critical parameters that directly influence its performance in wireless communication systems:

- **Number of elements**: RIS is composed of a large array of reflective or refractive elements, typically sub-wavelength-sized units, capable of manipulating the phase, amplitude, and sometimes polarisation of incoming signals. The number of elements significantly impacts the RIS's ability to control the electromagnetic environment, with more elements generally offering finer control and improved performance.

- **Element size and spacing**: The size of each element and the spacing between them (usually less than half the wavelength) is crucial to avoid grating lobes and ensure optimal beamforming capabilities.

- **Phase shift resolution**: RIS elements can adjust the phase of reflected signals, and the resolution of these phase shifts (e.g., 1-bit, 2-bit, continuous) determines how accurately the RIS can control the signal path. Higher phase shift resolution provides more precise signal manipulation.

- **Control method**: The RIS control mechanisms may include electronic, mechanical, or optical methods, influencing the response speed and adaptability of the RIS in dynamic environments. Electronic control is preferred for rapid, real-time adjustments.

- **Material properties**: The RIS's frequency range and tunability are dictated by the materials used, such as metasurfaces or varactor diodes. Advanced materials like liquid crystals or graphene offer additional tunability and control.

- **Polarisation control**: Certain RIS designs can manipulate the polarisation of incoming signals, adding a further layer of control and flexibility.
- **Power consumption**: Despite being generally passive, RIS consumes some power for control circuitry. Using low-power components is crucial for energy efficiency, particularly when compared with active solutions.
- **Beamforming capabilities**: The RIS's ability to form and steer beams is dependent on parameters such as element size, number, and control resolution.

2.2.4 RIS Passive Beamforming

Using its passive beamforming capabilities, RIS can reflect the signal and focus it at the receiver. This is achieved by combining the LoS path between the transmitter and receiver with the reflections from all metasurface elements in the RIS, which work together to form a beam that is directed toward the receiver. This is known as constructive superposition and can improve communication with RIS-assisted technology. In other words, by intelligently adjusting the phase shifts of RIS elements reflected signals in a RIS-assisted communication system can be combined coherently at the intended receiver. The RIS beamforming comprises a controller unit and communication interfaces that use different wireless technologies to send and receive configuration commands and status updates, as well as other components, such as sensors and power sources, depending on the application and performance requirements. The controller unit is the brain of the RIS and it is responsible for generating configuration commands for the RIS based on real-time communication conditions.

A model of a RIS-assisted communication system can be described as shown in Figure 2.9, a downlink transmission system consisting of a BS and a UE. The transmission is supported by a RIS, where the RIS reflects the signal with the optimised phase shifts to enhance the quality of the communication link between the transmitter and the receiver.

Recent studies have proposed several RIS passive beamforming techniques based on different optimisation methods and algorithms. The authors in [58] developed an optimisation approach for multiple-input single-output (MISO) systems that improves the received SNR, and hence, the achievable rate. The suggested approach is based on the alternating optimisation (AO) technique, which optimises the phase shifts of the transmit beamformer and the RIS element. The spectral efficiency optimisation for a single-user MISO system in [59] was accomplished by applying fixed-point iteration to jointly optimise the transmit beamformer and RIS element phase shifts in wideband systems. The authors in [60] offered a viable transmission protocol for estimating the channels in a MIMO-OFDM system using pilot training, and then an AO method for optimising the RIS phase shifts and power allocation matrix. The authors in [61] used the AO approach

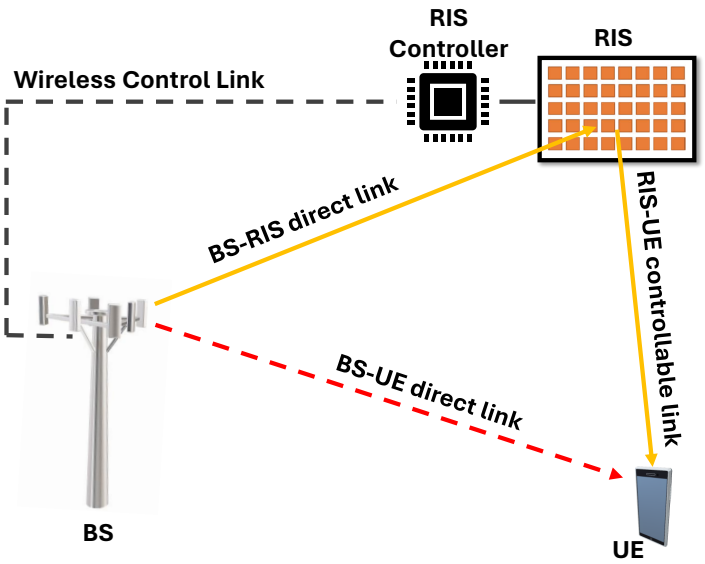

Figure 2.9: RIS-assisted communications system model.

to improve the achievable rate of a multi-stream MIMO communication system with RIS. Authors in [62] proposed zero-forcing (ZF) precoder-based algorithms, leveraging the extra signal routes provided by RIS, which perform comparably to minimum mean square error (MMSE) precoder-based methods. Work in [63] proposed a branch-and-bound (BnB) algorithm to optimise both active and passive beamformers at the AP and the RIS, respectively, aiming to maximise spectral efficiency for a single-user MISO communication. Authors in [64] investigated an uplink RIS-aided massive MIMO system, where RIS phase shifts are optimised using statistical channel state information (CSI). They addressed sum-rate maximisation and minimum user rate maximisation problems through phase shift optimisation using genetic algorithms (GA). Other studies have proposed different machine-learning methods for RIS control. For instance, authors in [65] proposed a novel approach to optimise the performance of RIS using DRL. The authors show that DRL can be used to optimise the reflection coefficients of a RIS without the need for external control signals or feedback. The proposed approach allows the RIS to adapt to changing communication environments and improve the quality of service for users.

Currently, the most commonly used algorithms to solve the non-convex beamforming optimisation problem in RIS-assisted wireless networks rely on the AO method. This approach has an advantage in that the transmit beamforming design can be treated as a standard problem once the passive beamforming vector is determined, which has been extensively studied. However, developing the passive beamforming design given the transmit beamforming vectors is still a challenging task.

2.2.5 RIS Applications

RIS technology has a wide range of applications in wireless communications, including B5G and 6G networks, smart cities, smart IoT networks, wireless power transfer, and UAV-enabled networks [11, 52]. It also has the potential to revolutionise a range of industries and enable new applications that were previously not possible in fields like industrial IoT, healthcare, and entertainment [52].

RIS-assisted B5G and 6G networks

As shown in Figure 2.10, RIS applications in future wireless networks are currently being explored for a variety of use cases, including:

- Improve signal quality and coverage: RISs have the capability to establish virtual LoS links, enabling them to overcome obstacles and enhance signal strength and coverage, particularly in areas with poor reception [10, 11]. Additionally, RISs can be used to mitigate interference and improve the reliability of wireless networks [10]. By optimising the signal strength and reducing interference, RIS can enable more efficient use of the available spectrum and improve the overall network coverage, and hence, reduce the need for a high-power transmission [50, 58, 66, 67]. Furthermore, by deploying RISs inside buildings, the signal quality and coverage can be improved without the need for additional access points or repeaters, reducing the overall cost and complexity of the indoor networks [68].

- Increase network capacity: In cellular networks, inter-cell interference is a significant problem that limits network capacity. RIS can be used to reduce inter-cell interference by selectively reflecting the wireless signal toward the desired user and away from other users, thereby improving the overall network capacity [69, 70]. Moreover, RIS has the potential to enhance indoor mmWave communication by optimising signal propagation and overcoming LoS obstacles [71]. Hence, RISs can be deployed in high-density user areas such as stadiums or transportation hubs to enhance network capacity without the need for additional infrastructure.

- Improve physical layer security: By selectively reflecting the signals to the intended receiver and blocking them from unintended recipients, RIS can ensure that the signals are received with high-quality, and prevent eavesdropping by unauthorised receivers. This makes it much more difficult for attackers to intercept and tamper with the transmitted signals [72–74]. RIS can also mitigate jamming, which is a common security threat that can affect the performance of wireless networks. By reflecting the wireless signals to the intended receiver and using interference

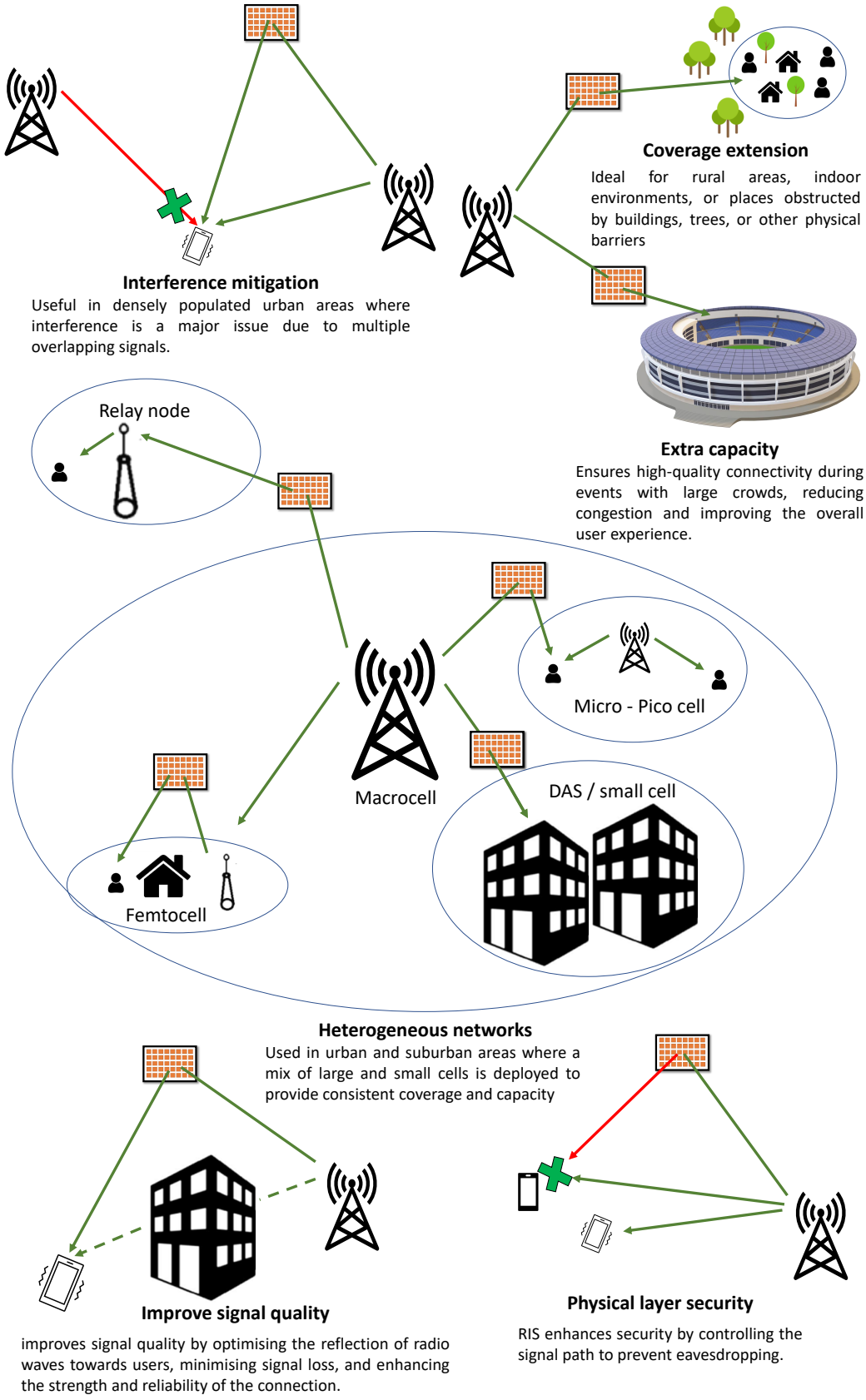

Figure 2.10: RIS applications in B5G and 6G networks.

cancellation techniques to eliminate jamming signals, RIS can enhance the resilience of the network against jamming attacks [75].

- RIS-assisted heterogeneous networks: Heterogeneous networks, which integrate various wireless technologies such as Wi-Fi, cellular, and satellite networks, are increasingly prevalent due to their ability to provide comprehensive coverage and interoperability across different communication systems. However, managing these diverse networks presents several challenges, including the need for high-quality wireless coverage, dynamic network reconfiguration, and scalable, cost-effective solutions [76]. RIS offer a promising approach to address these challenges by providing a flexible and adaptable solution for managing wireless network resources. Rather than combining all network types on a single RIS element, RIS can be strategically adjusted and positioned to cater to different network types and use cases. For instance, RIS can be optimised to enhance communication for Wi-Fi, cellular, or satellite networks independently, depending on the specific requirements of the network in question [14]. In heterogeneous network environments, RIS can be configured to support various scenarios such as air-to-ground communications or air-to-air communication between UAVs. Each RIS installation must be tailored to meet the unique demands of the networks and use cases it supports. This involves adjusting the configuration and positioning of the RIS elements to ensure optimal performance for each network type. For instance, an RIS deployed to support cellular and Wi-Fi networks might need to have different beamforming patterns and configurations to effectively serve both types of networks. Similarly, RIS used for UAV communications would require specific adjustments to support the unique connectivity needs of aerial vehicles. This nuanced approach ensures that RIS can adapt to the varied requirements of heterogeneous networks, providing effective and efficient wireless coverage and communication without necessitating the integration of all networks on a single RIS element.

- RIS-enhanced device-device (D2D) communications: In recent years, there has been growing interest in D2D communications, which enables direct communication between two or more devices without the need for a central BS. This can lead to more efficient use of network resources, reduced latency, and improved user experience [77]. One of the main challenges in D2D communications is to ensure reliable and efficient communication between the devices, especially in environments with high path loss and interference. One solution to this problem is to use RIS, which essentially enhances communication by increasing the signal strength, reducing interference, and improving the overall spectral efficiency [78].

RIS-enabled smart cities and IoT networks

RIS-assisted communication has the potential to significantly improve the reliability and efficiency of wireless communication in a variety of settings, such as smart cities and IoT networks, as shown in Figure 2.11 [52].

Thriving smart city services owe their success to a remarkable array of technological innovations, with communication networks, artificial intelligence, the Internet of Things, and edge computing standing out as key pillars. Smart city services are enabled by the widespread use of smart sensing devices that generate large amounts of valuable data. However, for this data to be useful, it requires a strong and reliable network infrastructure. In urban environments where communication channels may be subject to blockage or severe fading, RIS provides a game-changing solution for ensuring reliable and enhanced connectivity, especially for IoT devices that are resource-constrained [10, 18, 79]. By dynamically adjusting signal paths and reducing interference, RIS enhances the performance and resilience of smart city networks, ensuring low-latency and ultra-reliable data links for effective decision-making.

RISs can be used in smart city applications to improve the efficiency of services and reduce energy consumption. For example, by using RIS to reflect and redirect wireless signals, they can be combined with other smart city technologies, such as sensors and data analytics, to create more efficient and effective urban systems [18, 80]. Another exciting use case for RIS integration is in smart home automation. RIS deployed on walls can be employed to improve quality of service (QoS) in indoor environments with high data rate requirements. IoT devices like smart thermostats, smart lights, and smart security systems can communicate more efficiently and effectively [52]. RIS integration in healthcare monitoring represents another promising use case. Wearable IoT devices used for remote patient monitoring can benefit from RIS technology. By integrating RIS, signal strength and coverage can be improved, resulting in more reliable and accurate data collection. This allows healthcare professionals to monitor patients remotely and make informed decisions based on accurate data [81, 82].

RIS can also be used in industrial automation applications to improve the communication between IoT devices in factories, warehouses, and other industrial settings [83]. RIS integration can improve the signal strength and coverage of IoT devices, and the capacity of the IoT network can be also increased. This results in faster and more efficient production processes, which can save companies time and money. Moreover, RIS can be used to improve wireless communication in harsh environments. By using RIS to reflect and redirect wireless signals, communication can be maintained even in areas with poor reception, such as underground mines and oil rigs. This can improve safety, reduce downtime, and increase productivity [18, 83].

In autonomous vehicle networks, RIS can be used to improve the communication

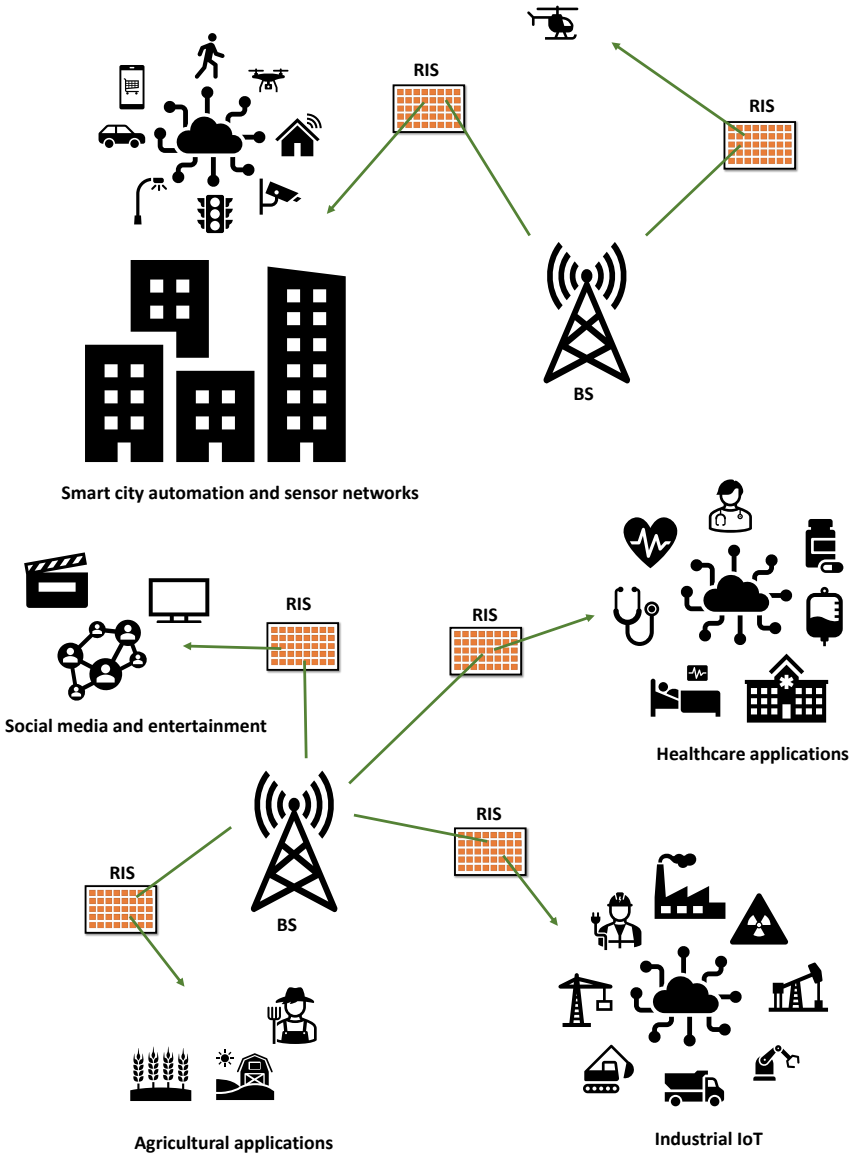

Figure 2.11: RIS applications in smart cities and IoT networks.

between IoT devices used in self-driving cars. By integrating RIS into the wireless network, the signal strength and coverage of IoT devices can be improved, resulting in more accurate and reliable data collection and decision-making. This can improve the safety and efficiency of self-driving cars, which is a critical factor in the adoption of autonomous vehicles [84]. Furthermore, RIS can be used in agriculture applications to improve the communication between IoT devices used in precision agriculture systems. RIS can support efficient and accurate monitoring of crops and soil, which can help farmers make informed decisions about irrigation, fertilisation, and other important factors in crop production [52, 83]. Applications of the RIS can be also extended into entertainment applications to improve the delivery of content to users. By using RIS to reflect and

redirect wireless signals, coverage, and signal strength can be improved, enabling high-quality streaming of video and audio content in areas with poor reception. This can enhance the user experience and increase revenue for content providers.

RIS for wireless power transfer

Wireless power transfer (WPT) offers an innovative solution to the challenges of battery-powered devices by providing a new method for energy acquisition [85]. With the coming future 6G communication networks, the interest in this innovative technology has skyrocketed, with many envisioning a future where wireless devices can receive a steady supply of energy without relying on traditional power sources. However, there are some main challenges in WPT systems such as significant power loss over long distances, limited coverage area, and interference from other wireless devices. Moreover, the effectiveness of WPT systems can be affected by various factors, such as the orientation and distance of the receiving device, the alignment of the transmitting and receiving antennas, and the presence of obstacles in the propagation path [86]. RIS is considered a highly attractive solution for assisting in WPT. This is mainly because RIS possesses a large aperture that can be utilised to power numerous heterogeneous devices by compensating for the significant power loss over extended distances via customised signal reflections. This results in a significant enhancement of the overall efficiency of WPT systems [86].

As shown in Figure 2.12, an interesting scenario arises when sources are capable of supporting simultaneous wireless information and power transfer (SWIPT), enabling a remote, controllable, and readily available energy source [86, 87]. SWIPT offers an efficient means of powering a large number of devices within a wireless-powered IoT network. SWIPT can greatly reduce the energy consumption and carbon footprint of wireless communication systems by enabling wireless devices to harvest energy from the environment, while also transmitting and receiving data. This eliminates the need for wired power sources or batteries, which can have a significant impact on the environment due to their production and disposal processes. SWIPT technology can also enable the development of energy-efficient wireless communication networks, where devices can be powered by energy harvested from other devices or renewable energy sources, such as solar or wind power. This can lead to the creation of self-sustainable communication networks, which can operate without the need for external power sources. However, the substantial loss of power over extended distances decreases the energy received by the energy receiver, ultimately resulting in reduced SWIPT system performance [87]. The use of RIS in SWIPT systems can result in improved information and power transfer, where the RIS can assist in power transfer by reflecting the incident signal towards the receiver, while also providing signal enhancement by optimising the phase shift coefficients of the reflecting elements.

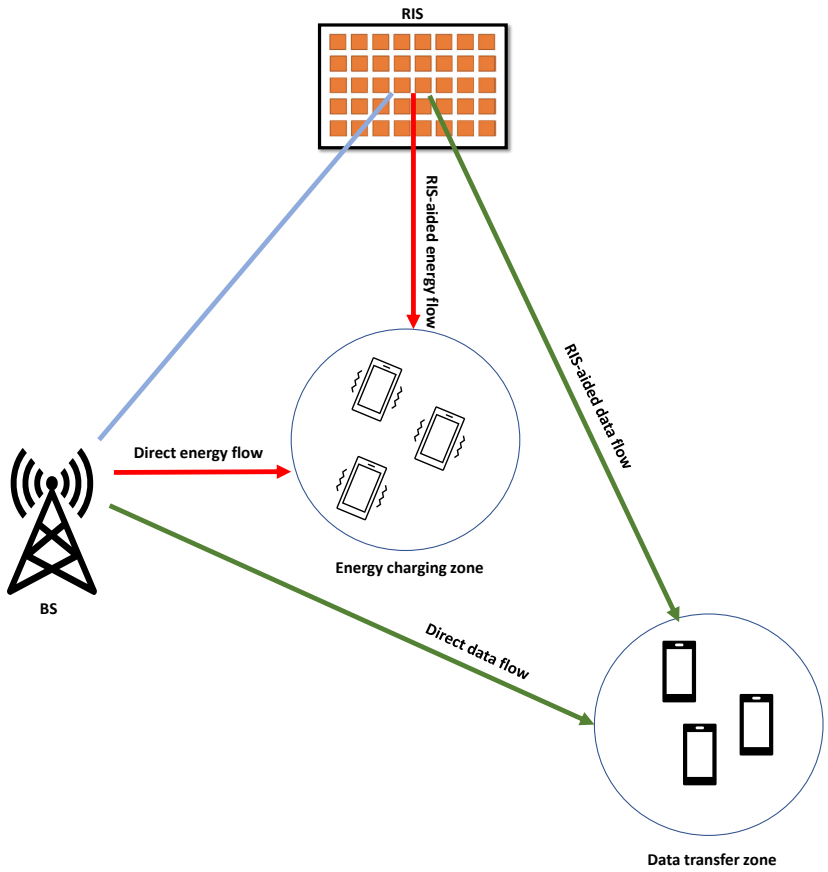

Figure 2.12: RIS-enabled SWIPT.

Implementing RIS in SWIPT systems involves careful consideration of several factors. These include the design and placement of the RIS to maximise its effectiveness, the development of algorithms for optimal phase shift adjustments, and the integration of RIS with existing network management systems. Additionally, the scalability of RIS solutions and their ability to handle varying levels of device density and movement are important aspects to address. The successful deployment of RIS in SWIPT systems requires a thorough understanding of both the technological capabilities of RIS and the specific needs of the wireless communication environment.

2.2.6 RIS Vs. Active Solutions: An Environmental Point of View

This section discusses existing technologies such as active beamforming and relays and explains how RIS is distinguished from these technologies. Both technologies aim to improve wireless communication by enhancing signal strength, reducing interference, and increasing network capacity. However, they differ in their fundamental approach to achieving these goals [15]. RIS technology involves a passive surface made up of a

large number of individually controllable reflecting elements that can be configured to manipulate the propagation of electromagnetic waves. In contrast, active solutions such as MIMO active beamforming and relays use multiple antennas and active processing to achieve similar goals. MIMO active beamforming adjusts the phase and amplitude of transmitted signals to improve signal quality, while relays amplify and forward signals to improve coverage and reduce interference [66, 88].

Power efficiency

The RIS has the potential to be easily deployed into wireless communication networks, enabling smart control over the unpredictable radio environment to enhance coverage, throughput, and energy efficiency. Relays are also viewed as a viable solution for expanding wireless network coverage, with relay-supported connections experiencing superior channel propagation conditions compared to direct transmission links when dealing with weak or NLoS paths. Relay solutions can be classified into two categories depending on the types of relaying protocols; AF and DF, while AF relays may offer a simpler solution, they come with the unwanted side effect of amplifying signal noise. In contrast, DF relays not only provide better performance in terms of SNR and achievable rate but also prove that sometimes, however, they introduce higher complexity [66, 88].

Previous work [14], [88], and [66] suggested examining RIS and relaying-assisted communications. According to their findings, in order to surpass the performance of the relay. Their results show that the RIS should be equipped with a sufficient number of elements to overcome a relay-assisted transmission performance in terms of achievable rate and power efficiency. However, it is also shown that both technologies have their advantages and limitations. RIS performance depends on various factors such as the number of elements, channel conditions, and the type of modulation. RIS has the potential to outperform relaying in certain scenarios, particularly in low-power, high-rate, and high-density networks. However, further research is needed to fully explore the capabilities of the RIS and its practical implementation in real-world wireless communication systems.

Massive MIMO (M-MIMO) antennas and beamforming are crucial technologies for enhancing the performance of communication systems in terms of throughput, capacity, spectral efficiency, and connectivity. However, the adoption of M-MIMO technology poses significant challenges related to design complexity, energy usage, and expenses, making it necessary to focus on developing low-cost and low-complexity solutions [89]. RIS can provide a low-cost, simple, and energy-efficient solution to intelligently adjust the wireless environment to enhance coverage, throughput, and security [11]. Furthermore, RIS can be used in coexistence with M-MIMO systems to improve network performance through the use of passive and active beamforming techniques [58].

Sustainable infrastructure

The integration of the RIS into the network not only enhances power efficiency and capacity but also accomplishes these performance gains without requiring the installation of expensive, intricate infrastructure. By leveraging the capabilities of the RIS, the network can effectively optimise its use of resources and improve overall performance, all while keeping costs in check. Using less communication infrastructure can have a positive impact on the environment in several ways. Here are some potential benefits:

- Energy efficiency: Communication infrastructure requires a significant amount of energy to operate, particularly when it comes to powering equipment and cooling systems. By reducing the amount of infrastructure required, the energy consumption of the network can be lowered. This can help to reduce the carbon footprint of the network and lower greenhouse gas emissions, which is beneficial for the environment [90].

- Reduced waste: Communication infrastructure requires a significant amount of resources to manufacture, deploy, and maintain. By reducing the amount of infrastructure required, the amount of waste generated can also be reduced. This can be particularly important when it comes to electronic waste, which can have a significant impact on the environment [91].

- Lower construction costs: Communication infrastructure can be expensive to build and maintain, particularly in rural or remote areas. By reducing the amount of infrastructure required, the overall construction costs can be lowered. This can help to make communication networks more accessible and affordable, particularly in areas where it may be difficult or expensive to deploy traditional infrastructure [92].

- Reduced environmental impact: Communication infrastructure can have a significant impact on the environment during the construction and deployment phases. This can include disruption to ecosystems and habitats, as well as the release of pollutants and emissions. By reducing the amount of infrastructure required, the overall environmental impact can be reduced.

To ensure that RIS delivers on its potential, ongoing research and development are essential. A key area of focus should be the rigorous validation of theoretical models through real-world testing. This involves conducting experiments to confirm the predicted benefits of RIS and to uncover any practical limitations that may require refinement. Additionally, real-world deployment trials are crucial for assessing the performance and feasibility of RIS in diverse environments. These trials will help identify potential challenges and inform best practices for effective deployment. Continued innovation is

also necessary, with investment directed towards developing new materials, designs, and technologies that enhance RIS performance and functionality. Collaboration between academia and industry will play a vital role in advancing RIS technology and ensuring its successful integration into future wireless networks.

2.3 RIS-Assisted UAV Communications

As outlined earlier, UAVs offer significant advantages to wireless networks, due to their easy deployment, dynamic mobility, extended coverage area, high LoS probability, and efficient data collection capabilities. However, to unlock the potential of UAV network applications, many factors must be taken into account, including energy and spectrum constraints, traffic demands, and the characteristics of A2G channels. RIS integration promises to enhance wireless network power efficiency by reducing active transceivers and the energy demands of active technologies like relay networks [93]. RISs also offer flexibility in deployment, as they can be installed on indoor walls, buildings, and aerial platforms, enabling effective control over diverse wireless environments. Capitalising on those unique features RIS can be used to create a reliable and improved communication environment. This combination of UAVs and RIS technology presents a powerful integrated system that can revolutionise wireless communication systems, enabling efficient and scalable connectivity solutions for diverse applications and industries [94, 95].

The literature lacks a comprehensive exploration of the use cases and performance analysis of RIS-assisted UAV communication systems. Nonetheless, recently, due to their potential to enhance the wireless environment, RIS-assisted UAV networks started to receive significant attention from both academia and industry. In [96], the authors proposed an algorithm for jointly optimising UAV trajectory and RIS passive beamforming to maximise the average achievable rate in RIS-assisted UAV communication systems. In another work, a UAV equipped with a RIS acted as a passive relay between a ground BS and ground UEs to maximise the secure energy efficiency against an eavesdropper by optimising the UAV trajectory, RIS passive beamforming, user association, and transmitted power [97]. Additionally, a performance analysis of a RIS-assisted UAV communication system was proposed in [16], where a UAV acts as a relay and RIS is deployed to support the link from BS to the UAV. Their results show that RIS deployment can improve the system's reliability, average BER, and average capacity. In [88], the authors offered a comparison between the performance of RIS and relay-assisted UAV communications. Results show that the RIS should be equipped with more than one hundred reflecting elements to match up to a single DF relay performance in terms of the achievable rate. It was also observed that a RIS with a sufficiently high number of elements attains a better performance, in terms of power requirements, in the case of high

UAV altitudes.

2.3.1 RIS-Assisted UAV Integration Scenarios

Research on RIS-assisted UAV communication systems is being explored from various angles. Figure 2.13 shedding light on the possibility of integrating RIS alongside UAV under diverse scenarios. These scenarios can be classified into three representative categories based on RIS installation points and UAV roles:

1. RIS-assisted UAV-enabled communications: The high mobility of the UAVs allows them to act as a reliable and responsive communication platform. RISs can be implemented to assist A2G links between the aerial platforms and ground users to maximise UAV coverage area and increase transmit power efficiency. RIS-assisted UAV communications can improve signal quality by mitigating obstacles and signal blockages. Jointly optimising UAV positioning and RIS phase shifts can increase signal strength and reduce interference, leading to higher data rates and improved energy efficiency [17, 96]. Furthermore, RIS-assisted UAV communications can enhance security and privacy by providing secure communication channels and protecting sensitive data from unauthorized access [19].

2. RIS-assisted cellular-connected UAV: Since RISs are intended to provide coverage in a limited local area, they typically have shorter operating ranges compared to active BSs or relays. This characteristic facilitates the practical deployment of RIS without causing interference between them. As a result, RIS can effectively solve the SNR degradation that occurs due to strong interference when a UAV is flying at relatively high altitudes. Additionally, cellular-connected UAVs often face challenges with weak signal strength due to the down-tilt of terrestrial BS antennas. Deploying RISs on building walls to direct reflected signals towards specific UAVs can increase their received signal strengths and maximise the communication channel gain [98].

3. RIS mounted UAV communications: This context involves equipping UAVs with RIS to aid communication between ground nodes and aerial platforms or even extending the coverage area and facilitating communication between distant ground users and terrestrial base stations. By deploying RIS on UAVs, communication range and coverage can be extended, particularly in areas with challenging terrain or obstacles that obstruct direct LoS paths. Moreover, RIS-mounted UAVs offer the advantage of mobility, allowing for dynamic positioning and adaptability to changing communication needs and environmental conditions.

   However, since RIS usually consist of hundreds of elements, this scenario is less feasible compared to other options. Furthermore, the coordination and control

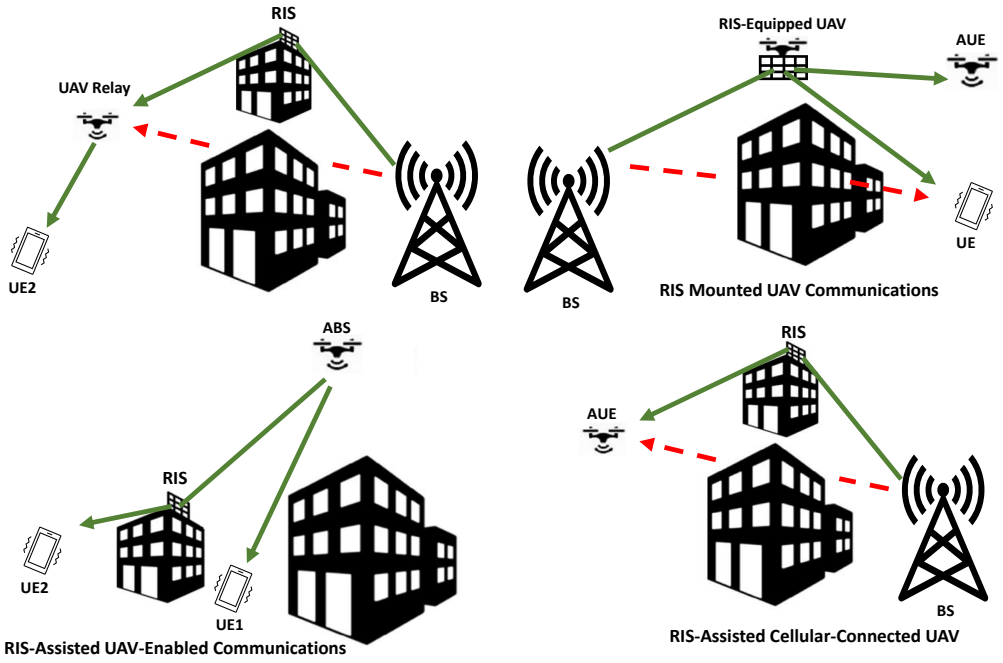

Figure 2.13: RIS-assisted UAV implementation scenarios.

overhead associated with managing RIS elements on a moving platform like a UAV can be significant, requiring efficient algorithms and protocols for real-time operation.

These scenarios illustrate the versatility of RIS-assisted UAV communications and the potential for optimising system configurations for various applications. Ongoing research aims to optimise systems for each scenario and explore combinations of multiple scenarios to serve diverse application requirements.

2.3.2 RIS-Assisted UAV Communications Applications

The integration of RIS with UAV holds promise for revolutionising communication systems across various domains. This discussion delves into the diverse applications of RIS-assisted UAV communications, showcasing their potential to enhance communication efficiency, facilitate IoT data collection, optimise mobile edge computing (MEC), and bolster security measures. Through a series of use cases, this discussion also explores how RIS technology, coupled with UAV capabilities, can address key challenges and unlock new opportunities in wireless communication networks.

Enhanced communication efficiency

RIS-assisted UAV communications offer a solution to minimise energy consumption and maximise communication reliability and throughput, particularly in dense urban environments. By jointly optimising UAV trajectory, RIS phase shifts, and power allocation, researchers have demonstrated significant performance improvements over

traditional methods. The integration of RIS with UAV to enhance communication efficiency in dense urban environments is explored in [99]. The authors proposed a framework to minimise overall energy consumption in 5G networks with QoS constraints by jointly optimising the UAV trajectory and RIS phase shifts. The authors in [17] investigated the potential of RIS-assisted UAV communications for enhancing spectrum and energy efficiency in wireless systems. An efficient framework is proposed to maximise the received power at a ground user by jointly optimising active beamforming at the UAV, passive beamforming at the RIS, and UAV trajectory. In [100], the authors introduced RIS-assisted UAV networks, utilising the mobility of UAVs and the reflection capabilities of RIS for performance enhancement. To maximise energy efficiency, UAV power allocation and RIS phase-shift matrix were jointly optimised using a DRL approach. The study in [101], presented a framework for integrating RIS in UAV-enabled wireless networks to enhance service quality. Non-orthogonal multiple access (NOMA) technique is employed to improve spectrum efficiency, considering continuously roaming mobile users. The objective of minimising energy consumption is achieved by jointly designing UAV trajectory, RIS phase shifts, power allocation from UAV, and dynamic decoding order. The work in [102] explored using RIS in multi-UAV NOMA networks to maximise the network sum rate. By optimising UAVs, RIS phase shifts, and NOMA decoding the system can enhance channel quality, effectively mitigate interference, and boost the overall sum rate. Meanwhile, in [103], the focus was on energy-efficient communication with UAVs equipped with RIS allowing a multi-antenna base station to seamlessly communicate with single-antenna users. The authors developed an algorithm to optimise beamforming and phase shifts, leading to over 45% improvement in energy efficiency compared to conventional relaying methods.

IoT data collection

In the realm of IoT networks, timely and reliable data collection is important for various applications. Leveraging RIS technology, UAVs can efficiently collect data from sensor networks distributed across different areas. Authors in [18], investigated how RIS technology can aid UAVs in achieving timely and reliable data collection in IoT networks. Their work addressed a time-constrained data collection problem from a network of sensing devices by leveraging DRL for UAV trajectory planning and block coordinate descent for RIS configuration to maximise the total number of served devices during their activation periods. The work in [104] proposed RIS-assisted UAV solution for collecting data from IoT networks within urban settings, Their approach aims to minimise the age of information (AoI) for all IoT devices by jointly optimising UAV trajectories, IoT devices scheduling decisions, and RIS phase shifts. In a separate investigation, authors in [105] delve into RIS-assisted UAV communication for IoT applications, incorporating WPT. They introduced a

two-phase operation where IoT devices first harvest energy from the UAV, followed by data collection via information transmission. The study explores both hovering and mobile UAV scenarios to optimise the UAV's trajectory, power allocation, energy harvesting scheduling, and RIS phase-shift matrix, with an objective to maximise the total network sum rate.

Mobile edge computing

The fusion of RIS-assisted UAVs with MEC holds the potential for optimising energy efficiency and enhancing communication links between UAVs and edge clouds. Authors in [106], explored the potential of integrating UAV-mounted RIS to optimise energy efficiency in MEC systems. They develop a joint optimisation framework considering UAV trajectory, RIS beamforming, and MEC resource allocation to maximise system energy efficiency. In a related work by authors in [107], the focus remains on MEC optimisation with RIS-assisted UAVs, where UAVs offload tasks to the edge cloud. Here, RIS assists in improving communication between UAVs and the edge cloud. The authors contributed by proposing a joint optimisation framework for UAV trajectory, task allocation, cache management, and RIS phase shifts to enhance overall system performance to improve energy efficiency and QoS. The authors in [108] proposed a joint trajectory planning and communication scheduling algorithm for UAVs equipped with central processing units (CPUs), serving IoT devices on uneven terrain. RISs are deployed to enhance communication links. The proposed algorithm maximises the number of successfully completed computing tasks while minimising UAV energy consumption.

2.4 Summary

This chapter provides a comprehensive overview of two key technologies shaping the future of wireless networks, namely UAV communications and RIS-assisted communications. It begins by discussing the role of UAVs in future wireless networks, highlighting their characteristics, diverse applications, and the challenges they pose. Then the discussion shifts to RIS technology, explaining its concept as a key enabler for SRE. Then it delves into RIS structure, control mechanisms, passive beamforming capabilities, and various applications. A comparison between RIS and active solutions is also provided from an environmental perspective. Furthermore, the chapter explores the integration of RIS into UAV communications, presenting different scenarios for their joint deployment and the wide range of applications enabled by this integration. It covers both the theoretical aspects and practical implementations of RIS-assisted UAV communications, providing valuable insights into the potential of these technologies to revolutionise wireless communication systems. The insights provided in this chapter are strategically placed to furnish readers with a thorough groundwork, laying the groundwork for an easy

understanding of the innovative contributions outlined in this thesis in the following chapters.

Chapter 3

Analytical performance analysis for RIS-assisted UAV communications

In this chapter, theoretical frameworks to analyse the performance of RIS-assisted UAV communications were proposed, aligning with the aims specified in *O3*. The fundamental limits of the performance of three different systems, namely, RIS-assisted UAV-aided communications, RIS-assisted cellular-connected UAV communications, and multi-hop RIS-assisted UAV communication systems, are analysed and characterised. Accurate closed-form approximations for the statistical distributions of the RIS-assisted channels are derived, which are then exploited to derive an analytical expression for the SNR, outage probability, and BER. In the first scenario, UAV-aided communications, where UAVs act as airborne base stations or access points to extend coverage. Despite challenges like limited battery life and urban blockages, RIS optimises A2G links, increasing coverage and power efficiency. The second scenario involves cellular-connected UAVs facing coverage issues due to high altitude and signal blockages, but RIS improves G2A links by reflecting signals towards UAVs, enhancing SNR and reducing outages. The third scenario examines multi-hop RIS-assisted UAV systems, where UAVs serve as relay nodes to extend coverage and improve reliability in challenging environments like rural areas, disaster zones, and urban centres. This setup enhances communication but requires careful modelling due to the complexities of UAV relays and RIS. Overall, RIS technology enhances SNR, reduces outages, and extends UAV-based network performance across diverse scenarios.

3.1 Introduction

Understanding the impact of RIS on UAV communication systems helps quantify the benefits, such as improved coverage and enhanced data rates. Detailed performance analysis is essential to realise the performance gains, ensuring that the full impact on network performance is understood and providing insights into the optimal design

and configuration of RIS and UAV parameters, to unlock the maximum efficiency and effectiveness of the integrated system. That helps to identify potential challenges and solutions for large-scale deployments in diverse environments and facilitates informed decision-making for deployment into the wireless network.

Performance analyses of RIS-assisted UAV communication systems have not been thoroughly explored in the literature. However, recent research efforts have increasingly focused on examining the performance of RIS-assisted UAV systems, yielding significant insights. Authors in [109], examined crucial performance metrics of RIS-assisted UAV communications such as the outage probability, BER, and average sum rate. The system model considered in this work includes a source node, a UAV equipped with a RIS, and a destination node. They modelled wireless channels assuming Rician fading channels for the RIS-assisted link with a blocked direct link. Similarly, the work in [110] proposed a performance analysis of a RIS-assisted UAV communication system with a blocked direct link. It introduced a unified elevation-angle dependent path loss model, incorporating unique LoS probabilities between the UAV and other communication nodes. Furthermore, the work established tight upper and lower bounds on the average SNR provided a closed-form expression for the probability distribution function (PDF) of the SNR upper bound, and derived closed-form expressions for the achievable symbol error rate (SER), outage probability, and ergodic capacity. Considering a dual-hop RIS-assisted UAV communication system, with the assumption that the UAV serves as a relay to extend the coverage of a ground source node, the work in [16] proposed a performance analysis framework to investigate the outage probability, BER, and average capacity of the system under study. While the findings of this work are useful for understanding the impact of the RIS on the performance of UAV communication networks, they do not offer practical design insights. This stems from the fact that the framework in [16] is based on the assumption that the link between the source and the RIS undergoes Rayleigh fading, and hence, a LoS component does not exist. Nonetheless, it is widely known in the literature on RIS, such as the study in [13], that the RIS attains its highest channel gain when positioned in close proximity to either the source or the destination, and hence, increasing the likelihood of establishing a link with a LoS component between the RIS and the source. Additionally, the derived BER expression in [16] is useful to examine the BER performance for one modulation scheme only, rendering the use of this expression to be limited.

The analysis in this chapter concentrates on specific scenarios within RIS-assisted UAV communication systems, including UAV-aided communications, cellular connected-UAV systems, and multi-hop RIS-assisted UAV networks. These scenarios represent various UAV integration paradigms within wireless networks, with the frameworks and results specifically designed to address their unique characteristics, such as the UAV's function, the nature of fading channels, and the inclusion of RIS. The analysis spans a range of

use cases, such as emergency response operations in disaster-hit areas, UAV deployments in densely populated urban environments, and UAV-aided communications aimed at enhancing coverage in rural regions. Each scenario brings its own set of constraints and requirements. Additionally, the analysis explores variations in UAV positioning, different fading models, and varying numbers of RIS elements.

3.2 Contributions

In this chapter, the outage probability and BER for different RIS-assisted UAV communication systems are studied and analysed considering both UAV integration paradigms, (i) UAV-aided communications: UAV ABS serving a ground user, and a RIS supports A2G communication, (ii) cellular connected-UAV system: where UAV acts as an aerial UE served by a ground BS and a RIS supports G2A communication. Furthermore, a multi-hop RIS-assisted UAV communication system is proposed and analysed. In this system, the UAV acts as a relay node, suitable for various scenarios such as rural connectivity, disaster response, urban connectivity enhancement, and temporary events. This system considers a realistic scenario with a direct NLoS link between the source and the destination, using the generic Nakagami-m distribution to model fading, which can be simplified into the Rayleigh distribution, signifying the presence of pure NLoS fading characteristics. Furthermore, a one-to-one mapping between the m parameter and the Rice K factor enables the Nakagami-m distribution to serve as an approximation for the Rice distribution.

The specific contributions of this work can be summarised as follows:

- Develop an analytical framework to evaluate the coverage probability and reliability of the proposed systems, by deriving the channel distributions of the RIS-assisted link distributions and approximate the SNR distribution. The framework is designed to handle the unique characteristics and operational scenarios of UAV communications.

- Derive approximate closed-form expressions for the proposed system models outage probability and BER for generic binary modulation schemes. This analytical approach allows for a clearer understanding of the trade-offs and optimisations necessary for effective system design.

- Offer deeper insights into the systems' performance through asymptotic analysis at high SNR regimes. This analysis helps to identify the behaviour and performance limits of the proposed systems providing a deeper understanding of the potential and limitations of RIS-assisted UAV communication systems.

- Validate the analytical expressions through Monte Carlo simulations and investigate the UAV optimal positioning and the optimal number of RIS elements for performance enhancement.

3.3 Performance Metrics

In evaluating the efficacy of a digital communication system, it is crucial to utilise appropriate performance metrics that can provide insights into the system's reliability and overall quality. These metrics are significant in assessing how well the system behaves under varying conditions, particularly in environments subject to noise and fading impairments. This section defines basic performance metrics that are used in the proposed analysis, namely, outage probability and average BER.

3.3.1 Outage Probability

A widely recognised and comprehensively understood performance metric for communication systems operating over fading channels is the outage probability. It is defined as the probability that the instantaneous SNR probability, γ, becomes less than a certain specified threshold, γ_{th}. This metric measures the reliability of the communication system and can be expressed as

$$P_{\text{out}} = \int_0^{\gamma_{\text{th}}} P_\gamma(\gamma) d\gamma, \tag{3.1}$$

which is the cumulative distribution function (CDF) of γ, namely, $P_\gamma(\gamma)$, evaluated at $\gamma = \gamma_{th}$.

3.3.2 Average Bit Error Rate

The main objective of digital communications is to transmit a stream of nits, which can encode any type of data, such as text or images. As a result, an important performance metric, and arguably the most challenging to compute, is the average BER. The primary challenge in calculating the average BER comes from the conditional probability, given the fading conditions, which is typically a nonlinear function of the instantaneous SNR. This non-linearity varies based on the system modulation scheme. The average BER can be formulated as follows

$$P_b(E) = \int_0^{\infty} P_b(E \mid \gamma) P_\gamma(\gamma) d\gamma, \tag{3.2}$$

where $P_b(E \mid \gamma)$ is the conditional BER.

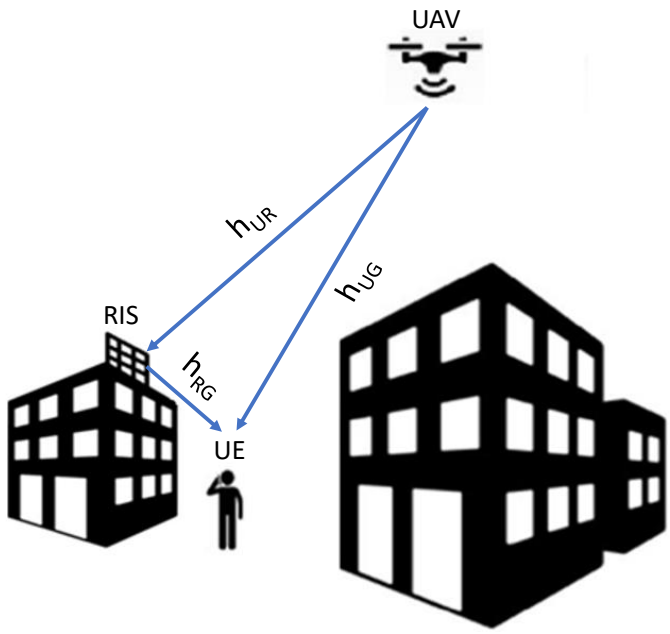

Figure 3.1: RIS-assisted UAV-aided communication system model.

3.4 System model

This section describes the proposed RIS-assisted UAV models. Three models are considered, RIS-assisted UAV-aided communications, RIS-assisted cellular-connected UAV communications, and multi-hop RIS-assisted UAV communications.

3.4.1 RIS-assisted UAV-aided communications

This setup considers a communication network scenario where a UAV acts as an aerial BS (U) serving a ground UE (G), and a RIS (R) of M reflecting elements is deployed on a wall of a building to assist the link between UAV and a ground user, as depicted in Figure 3.1. The UAV trajectory is assumed to be optimised to maintain a LoS connection with the ground user. Moreover, UAVs usually fly at relatively high altitudes and RISs are commonly placed on the facade of a building [96], this will increase the probability of having a LoS link between the RIS and the UAV. In addition to the LoS component, the U-R link is assumed to have scattered multi-path components. Hence, the channel gain for the U-R link can be modelled by a Rician distribution. RIS achieves the maximum channel gain when it is close to the source or the destination [13], thus, the RIS will be placed close to the serving area, which can guarantee a LoS link between the RIS and the ground user. The signal received by the UE can be written as

$$y = \left[h_{UG} + \sum_{i=1}^{M} h_{UR,i} e^{j\theta_i} h_{RG,i} \right] x + n, \tag{3.3}$$

where θ_i is phase-shift applied by the i^{th} element of the RIS, x is the transmitted signal from the BS, $n \sim \mathcal{CN}(0, N_0)$ is the AWGN at the G with zero mean and N_0 variance, $h_{UG} = \sqrt{\rho d_{UG}^{-2}} e^{-j\phi_{UG}}$, $h_{UR,i} = \sqrt{\rho d_{SR}^{-\alpha}} \mu_i e^{-j\phi_{UR,i}}$, and $h_{RG,i} = \sqrt{\rho d_{RU}^{-2}} e^{-j\phi_{RG,i}}$, are the channel gains for U-G, U-R, and R-G links, respectively, ρ is the path loss at the reference distance of 1m, d_{UG}, d_{UR}, and d_{RG} are the distances between the communication nodes U-G, U-R, and R-G, respectively, α is the pathloss exponent, and μ_i denotes the multipath fading coefficients represented by an independent Rician distribution.

As a result, the SNR at the G can be written as

$$\gamma = \frac{P \left| h_{UG} + \sum_{i=1}^{M} h_{UR,i} e^{j\theta_i} h_{RG,i} \right|^2}{N_0}. \tag{3.4}$$

where P is the transmitted power.

From [96], the maximum instantaneous SNR at G can be achieved by the phase alignment of the signals at the user, therefore, (3.4) can be rewritten as

$$\gamma = \frac{P \left(|h_{UG}| + \sum_{i=1}^{M} \left| h_{UR,i} \right| \left| h_{RG,i} \right| \right)^2}{N_0}. \tag{3.5}$$

3.4.2 RIS-assisted cellular-connected UAV communications

As shown in Figure 3.2, for the cellular-connected UAV scenario, a system setup is considered where a UAV (U) acts as an aerial user served by a single antenna terrestrial BS (S), and a RIS (R) with M reflecting elements deployed on a building to assist the link between the S and the U. In addition to the LoS components, the links comprise scattered multi-path components. Hence, the channel gains can be modelled by Rician fading. The received signal at the UAV can be written as

$$y = \left[\sum_{i=1}^{M} h_{SR,i} e^{j\theta_i} h_{RU,i} \right] x + n, \tag{3.6}$$

where $h_{SR,i} = \sqrt{\rho d_{SR}^{-2}} \Psi_i e^{-j\phi_{SR,i}}$ and $h_{RU,i} = \sqrt{\rho d_{RU}^{-\alpha}} \kappa_i e^{-j\phi_{RU,i}}$ are the channel gains for S-R and S-U links, respectively. ρ is the path loss at the reference distance of 1m, d_{SR} and d_{RU} are the distances between the communication nodes S-R and R-U, respectively, α is the path loss exponent, Ψ_i and κ_i denotes the multipath fading coefficients represented by independent Rician distributions, θ_i is phase-shift applied by the i^{th} element of the RIS, x is the transmitted signal from the BS, and $n \sim \mathcal{CN}(0, N_0)$ is the AWGN at U with zero mean and N_0 variance.

As a result, the SNR at U can be written as

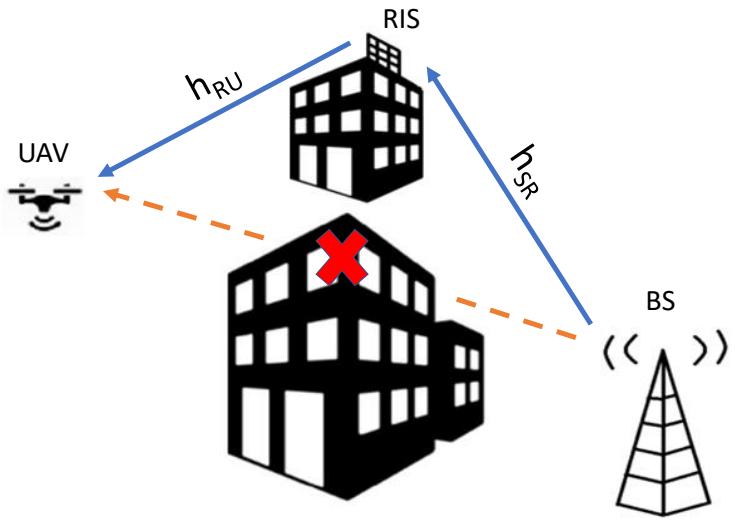

Figure 3.2: RIS-assisted cellular-connected UAV communication system model.

$$\gamma = \frac{P\left|\sum_{i=1}^{M} h_{SR,i} e^{j\theta_i} h_{RU,i}\right|^2}{N_0}. \tag{3.7}$$

Hence, the maximum instantaneous SNR at the U can be expressed as

$$\gamma = \frac{P\left(\sum_{i=1}^{M} \left|h_{UR,i}\right| \left|h_{RG,i}\right|\right)^2}{N_0}. \tag{3.8}$$

3.4.3 Multi-hop RIS-assisted UAV communications

A RIS-assisted multi-hop UAV wireless communication system is shown in Figure 3.3. A system setup is considered where a source node (S) is serving a ground user (G) and there is an aerial relay node (U) available to assist in transmission. A RIS (R) equipped with M reflecting elements is positioned atop a building to assist the link between S and U. U receives the signal from S through a RIS-assisted G2A link, it then transmits the signal to the ground user using the DF relaying protocol. In the proposed framework, it is assumed that each node is equipped with a single antenna, and G uses selection combining (SC) to select between signals received from either the direct or the relay links. A time-division channel allocation scheme comprising two time slots is implemented. This configuration enables multiple terminals to collaborate in transmitting to the destination. During the first time slot, source S transmits its signal to both nodes U and G. If the received SNR at node U is above a certain threshold, it decodes the received message and then forwards the source signal to destination D in the second time slot [111]. In this paper, the generic Nakagami-m distribution is adopted as a multipath fading model of S-R and R-U channels.

It is also assumed that the envelope of the direct channel between S and G is modelled as a Rayleigh distribution.

G2A RIS-assisted Link

In the first transmission stage, the S transmits the signal to U through the RIS-assisted G2A link. The signal received by the UAV can be written as

$$y_1 = \left[\sum_{i=1}^{M} h_{SR,i} e^{j\theta_i} h_{RU,i}\right] x_1 + n_1, \tag{3.9}$$

where $h_{SR,i} = \sqrt{\rho d_{SR}^{-\alpha}}\Upsilon_i e^{-j\phi_{SR,i}}$ and $h_{RU,i} = \sqrt{\rho d_{RU}^{-\alpha}}\Pi_i e^{-j\phi_{RU,i}}$ represent S-R and R-U links channel gains, respectively, ρ is the path loss at reference distance of 1m, d_{SR} and d_{RU} are the distances between S-R and R-U, respectively, α is the pathloss exponent, Υ and Π denote the multipath fading coefficients modelled by independent Nakagami-m distributions, θ_i is phase-shift applied by the i^{th} element of the RIS, x_1 is the transmitted signal from S, and $n_1 \sim \mathcal{CN}(0, N_0)$ is the AWGN at U with zero mean and N_0 variance.

From [96], the instantaneous SNR can be maximised by aligning the phases of the signals at U, i.e., $\theta = \phi_{SR,i} + \phi_{RU,i}$, therefore, from (3.9), the maximum instantaneous SNR at U can be written as

$$\gamma_{SU} = \frac{P_1(\sum_{i=1}^{M} h_{SR,i} h_{RU,i})^2}{N_0} = \overline{\gamma}_1 X_1^2, \tag{3.10}$$

where P_1 is the transmit power, $\overline{\gamma}_1 = \frac{P_1}{N_0}$ is the average transmit SNR, and $X_1 = \sum_{i=1}^{M} h_{SR,i} h_{RU,i}$. It can be noticed that X_1 is the sum of M double Nakagami-m independent random variables (RVs). The PDF of double Nakagami-m is expressed as [112]

$$\begin{aligned} f_{Y_i}(\gamma) = &\frac{4\gamma^{m_1+m_2-1}}{\prod_{\ell=1}^{2}\Gamma(m_\ell)\left(\Omega_\ell/m_\ell\right)^{(m_1+m_2)/2}} \\ &\times K_{m_1-m_2}\left(2\gamma\prod_{i=1}^{2}\sqrt{\frac{m_i}{\Omega_\ell}}\right), \end{aligned} \tag{3.11}$$

where $\Gamma(\cdot)$ is the gamma function, Ω_l is the average fading power, m_l is the shape parameter, and $K_\nu(\cdot)$ is the ν^{th}-order modified Bessel function of the second kind.

The n^{th}-order moment of the RV Y_i, can be given by [112]

$$\mathbb{E}\left\langle Y_i^n \right\rangle = \prod_{\ell=1}^{2} \frac{\Gamma\left(m_\ell + n/2\right)}{\Gamma\left(m_\ell\right)} \left(\frac{\Omega_\ell}{m_\ell}\right)^{n/2}. \tag{3.12}$$

Since $\mathbb{E}\left\langle Y_i^n \right\rangle$ is a linear operator, implying that $E(X_1) = M(E(Y_i))$ holds true. Additionally, assuming that Y_i is independent for all values of i, then $Var(X_1) = M(Var(Y_i))$.

Using the first term of a Laguerre series, PDF of X_1 can be tightly approximated as

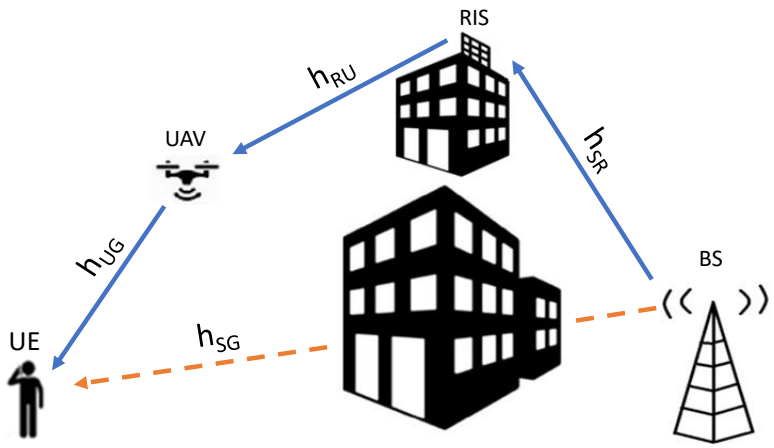

Figure 3.3: Multi-hop RIS-assisted UAV communication system model.

follows [113]

$$f_{\gamma_{SU}}(\gamma) = \frac{1}{b\Gamma(a+1)} \left(\frac{\gamma}{b}\right)^a \exp\left[-\frac{\gamma}{b}\right], \tag{3.13}$$

where $a = \frac{(E(X_1))^2}{\mathrm{Var}(X_1)} - 1$ and $b = \frac{\mathrm{Var}(X_1)}{E(X_1)}$ are parameters defined through the mean and the variance of X_1.

A2G link

In the second relay transmission phase, U sends the decoded signal to G. The received signal at G can be represented as

$$y_2 = h_{UG}x_2 + n_2, \tag{3.14}$$

where $h_{UG} = \sqrt{\rho d_{UG}^{-\alpha}}\tau e^{-j\phi_{UG}}$ is the channel gain for the U-G link, d_{UG} is the distances between the nodes U-G, τ denote the multipath fading coefficient modelled as an independent Nakagami-m distribution, x_2 is the transmitted signal from the UAV, and $n_2 \sim \mathcal{CN}(0, N_0)$ is the AWGN at G with zero mean and N_0 variance.

From (3.14), the SNR of the U-G link can be given by

$$\gamma_{UG} = \frac{P_2 |h_{UG}|^2}{N_0} = \overline{\gamma}_2 X_2^2, \tag{3.15}$$

where P_2 is the transmit power of U, $\overline{\gamma}_2 = \frac{P_2}{N_0}$ is the average transmit SNR, and X_2 is modelled by an independent Nakagami-m RV. From [114], the PDF of X_2 can be expressed as

$$f_{\gamma_{UG}}(\gamma) = \frac{2m_3^{m_3}}{\Gamma(m_3)\Omega_3^{m_3}}\gamma^{2m_3-1}\exp\left(-\frac{m_3}{\Omega_3}\gamma^2\right), \tag{3.16}$$

where $\Gamma(\cdot)$ is the gamma function, Ω_3 is the average fading power, and m_3 is the shape parameter.

Direct Link

In addition to the dual-hop cascaded link, a NLoS link between S and G is also assumed. The direct signal received by the user can be represented as

$$y_D = h_{SG}x_1 + n_3, \tag{3.17}$$

where $h_{SG} = \sqrt{\rho d_{SG}^{-\alpha}}ve^{-j\phi_{SG}}$ is the channel gain for S-G link, d_{SG} is the distances between the nodes U-G, v denotes the multipath fading coefficient modelled as an independent Rayleigh distribution, and $n_3 \sim \mathcal{CN}(0, N_0)$ is the AWGN at G with zero mean and N_0 variance. Hence, the SNR of the direct link can be expressed as

$$\gamma_{SG} = \frac{P_1\left|h_{SG}\right|^2}{N_0} = \overline{\gamma}_1 X_D^2, \tag{3.18}$$

where X_D is modelled by an independent Rayleigh RV. From [114], the PDF of X_D can be given by

$$f_{\gamma_{SG}}(\gamma) = \frac{\gamma}{\sigma^2}e^{-\gamma^2/\left(2\sigma^2\right)}, \tag{3.19}$$

where σ is the scale parameter of the distribution.

3.5 Peformance Analysis

In this section, the performance of the proposed systems is characterised in terms of the outage probability and BER.

3.5.1 RIS-assisted UAV-aided communications

The outage probability represents the CDF of the SNR evaluated at the desired threshold SNR, γ_{th}. Using (3.5), the SNR for the first scenario can be re-written as

$$\gamma = \frac{P\left(\left|h_{UG}\right| + \sum_{i=1}^{M}\left|h_{UR,i}\right|\left|h_{RG,i}\right|\right)^2}{N_0} = \overline{\gamma}\chi^2, \tag{3.20}$$

where $\overline{\gamma} = \frac{P}{N_0}$ is the average SNR, and $\chi = \left|h_{UG}\right| + \sum_{i=1}^{M}\left|h_{UR,i}\right|\left|h_{RG,i}\right|$.

The outage probability can be expressed as

$$P_{\text{out}} = P_r\left(\gamma \leq \gamma_{th}\right) = P_r\left(\sum_{i=1}^{M}\left|h_{UR,i}\right| \leq \frac{\sqrt{\frac{\gamma_{th}}{\bar{\gamma}_1}} - |h_{UG}|}{|h_{RG}|}\right). \tag{3.21}$$

The term $\sum_{i=1}^{M}\left|h_{UR,i}\right|$ involves the summation of M independent and identically distributed (i.i.d.) Rician random variables. However, to the best of the author's knowledge, a closed-form expression for this summation does not exist in the literature and its derivation is mathematically intractable. Hence, a simple and accurate closed-form approximation for this sum is derived.

The authors of [115], proposed a closed-form approximation to the sum of Rician distributions based on modifying the sum distribution of the squared Rician random variables. The CDF of the sum of Rician random variables can be presented as

$$F_M(t) = 1 - Q_M\left(\frac{t_1}{c_1}, \frac{t_2}{c_2}\right), \tag{3.22}$$

where $Q_\zeta(.,.)$ is the generalised Marcum Q-function with parameter ζ [116], c_1 and c_2 are constants, $t_1 = \sqrt{\frac{M\beta\Omega}{\beta+1}}$, β is the Rice factor, and $t_2 = \frac{r}{\sqrt{M}}$ is the normalised argument.

Thus, the outage probability can be written as

$$P_{out} = 1 - Q_M\left(\frac{t_1}{c_1}, \frac{1}{c_2}\left(\frac{\sqrt{\frac{\gamma_{th}}{\bar{\gamma}_1}} - \sqrt{\rho d_{UG}^{-2}}}{\sqrt{\rho d_{RG}^{-2}}\sqrt{\rho d_{UR}^{-\alpha}}}\right)\right). \tag{3.23}$$

For a better understanding of the system performance in terms of the achievable diversity order and the coding gain, the asymptotic or high SNR analysis is derived next. From [117], the generalised Marcum-Q function has the following asymptotic form

$$Q_M(x,y) \sim \sum_{n=0}^{\infty}\psi_n, \tag{3.24}$$

where, ψ_n can be written as

$$\psi_n = \frac{\zeta^M}{2\sqrt{2\pi}}(-1)^n\left[A_n(M-1) - \frac{1}{\zeta}A_n(M)\right]\nu_n, \tag{3.25}$$

where, $\zeta = \sqrt{y/x}$, $\nu_n = \left[\frac{(y-x)^2}{2xy}\right]^{n-\frac{1}{2}}\Gamma\left(\frac{1}{2}-n, \frac{(y-x)^2}{2}\right)$, $A_n(M) = \frac{2^{-n}\Gamma\left(\frac{1}{2}+M+n\right)}{n!\Gamma\left(\frac{1}{2}+M-n\right)}$, and $\Gamma(.)$ is the Gamma function.

As $\bar{\gamma} \to \infty$ the first term in the summation in (3.24) becomes dominating over the other terms. Assuming $y > x$, the first term of the asymptotic approximation in (3.24) can be written as [117]

$$Q_M(x,y) \sim \psi_0 = \left(\frac{y}{x}\right)^{M-\frac{1}{2}} Q(y-x). \tag{3.26}$$

where $Q(.)$ is the Gaussian Q function.

Using (3.23) and (3.26), the asymptotic outage probability can be given as

$$P_{out}^{\infty} \simeq 1 - \left(\frac{\frac{1}{c_2}\left(\frac{\sqrt{\frac{\gamma_1}{h_h}} - \sqrt{\rho d_{UG}^2}}{\sqrt{\rho d_{RG}^2}\sqrt{\rho d_{UR}^{\alpha}}}\right)}{\frac{t_1}{c_1}} \right)^{M-\frac{1}{2}} \times Q\left(\frac{1}{c_2}\left(\frac{\sqrt{\frac{\gamma_{hh}}{\bar{\gamma}}} - \sqrt{\rho d_{UG}^{-2}}}{\sqrt{\rho d_{RG}^{-2}}\sqrt{\rho d_{UR}^{-\alpha}}}\right) - \frac{t_1}{c_1}\right). \tag{3.27}$$

3.5.2 RIS-assisted cellular-connected UAV communications

From (3.8) the SNR for the second scenario can be re-written as

$$\gamma = \frac{P\left(\sum_{i=1}^{M} \left|h_{UR,i}\right| \left|h_{RG,i}\right|\right)^2}{N_0} = \overline{\gamma}\Xi^2, \tag{3.28}$$

where $\overline{\gamma} = \frac{P}{N_0}$ is the average SNR, and the term $\Xi = \sum_{i=1}^{M} \left|h_{UR,i}\right| \left|h_{RG,i}\right|$ is the sum of the product of two Rician random variables. The authors in [118] proposed a closed-form approximation for the CDF of this summation.

Using (3.28) and [118, Eq. (7)], the outage probability can be approximated as

$$P_{out} \simeq \frac{\gamma\left(e+1, \frac{\sqrt{\gamma_{th}}}{v\sqrt{\bar{\gamma}_2}}\right)}{\Gamma(e+1)}, \tag{3.29}$$

where, $\gamma(\cdot,\cdot)$ is the lower incomplete gamma function, e and v are parameters related to the mean and variance of X.

Similarly for this setup, from (3.29) and [118, Eq. (14)] the asymptotic outage probability can be written as

$$P_{\text{out}}^{\infty} \simeq \left[\frac{v^2}{\gamma_{\text{th}}[(e+1)!]^{-\frac{2}{(e+1)}}}\bar{\gamma}\right]^{-\frac{(e+1)}{2}}. \tag{3.30}$$

3.5.3 Multi-hop RIS-assisted UAV communications

Outage Probability

With SC, the destination terminal selects the signal with the largest received SNR. The instantaneous end-to-end SNR at G can then be expressed as

$$\gamma_{SC} = \max_{j \in direct, relay} \gamma_j, \tag{3.31}$$

where γ_j is the j^{th} path received signal SNR.

The outage probability corresponds to the probability that the system fails to meet a desired threshold SNR, γ_{th}. Hence, the end-to-end outage probability can be written as

$$P_{\text{out}} = \Pr\left[\gamma_{sc} < \gamma_{th}\right]. \tag{3.32}$$

Since the γ_j's are independent, the outage probability can be expressed as [119]

$$P_{\text{out}} = \prod_{j \in direct, relay} \Pr\left[\gamma_j < \gamma_{th}\right]. \tag{3.33}$$

Assuming a DF protocol at the aerial relay node, an outage occurs when either one of the links is in an outage. According, the outage probability for the relay-assisted transmission can be written as

$$P_{\text{out},relay} = 1 - \left(1 - P_{\text{out},SU}\right)\left(1 - P_{\text{out},UG}\right). \tag{3.34}$$

Similar to [118], from (3.13) the outage probability at the UAV for S-U RIS-assisted link can be given by

$$P_{\text{out},SU} = \Pr\left[\gamma_{SU} < \gamma_{th}\right] = \frac{\gamma\left(a+1, \frac{\sqrt{\gamma_{th}}}{b\sqrt{L_1 \bar{\gamma}_1}}\right)}{\Gamma(a+1)}, \tag{3.35}$$

where $\gamma(\cdot,\cdot)$ is the lower incomplete gamma function and $L_1 = \rho^2 (d_{SR}^{-\alpha})(d_{RU}^{-\alpha})$.
From (3.16), $P_{\text{out},UG}$ can be given by

$$P_{\text{out},UG} = \Pr\left[\gamma_{UG} < \gamma_{th}\right] = \frac{\gamma\left(m_3, \frac{m_3 \gamma_{th}}{\Omega_3 L_2 \bar{\gamma}_2}\right)}{\Gamma(m_3)}, \tag{3.36}$$

where $L_2 = \rho d_{UG}^{-\alpha}$.

It can be seen that P_{out} of the RIS-assisted link is a decreasing function of the square root of the transmission SNR and the path loss between nodes. This suggests that the RIS-assisted link may exhibit better robustness to variations in these parameters compared to the U-G link.
Finally, the outage probability of the direct link can be obtained as

$$P_{\text{out},SG} = \Pr\left[\gamma_{SG} < \gamma_{th}\right] = 1 - e^{-\gamma_{th}/\left(2\sigma^2 \bar{\gamma_1} L_3\right)}, \tag{3.37}$$

where $L_3 = \rho d_{SG}^{-\alpha}$.

Here, a closed-form expression for the outage probability in the high SNR regime is derived to provide further context for the system performance.
At high SNR ($\gamma \to \infty$), the outage performance of the relay-assisted transmission can be asymptotically written as

$$P_{\text{out }, relay} \to P^A_{\text{out},SU} + P^A_{\text{out},UG}. \tag{3.38}$$

By exploiting [120, Eq. (8.354.1)], $P_{\text{out},SU}$ can be evaluated at high SNR values as

$$P^{\infty}_{\text{out},SU} \simeq \frac{\sum_{n=0}^{\infty} \frac{(-1)^n \left(\sqrt{\frac{\gamma_{\text{th}}}{\bar{\gamma_1}}}\right)^{a+n+1}}{(a+n+1)b^{a+n+1}}}{\Gamma(a+1)}. \tag{3.39}$$

The initial term in the summation presented in (3.39) significantly outweighs the remaining terms. Hence, after considering that term only and with some simple mathematical manipulations, (3.39) simplifies to

$$P^{\infty}_{\text{out},SU} \simeq \left[\frac{b^2}{\gamma_{\text{th}}\left[(a+1)!\right] - \frac{2}{(a+1)}} \bar{\gamma_1}\right]^{-\frac{(a+1)}{2}}. \tag{3.40}$$

The asymptotic outage probability over Nakagami-m channels can be evaluated as [121]

$$P_{\text{out},UG} \approx \frac{m_3^{m_3-1}}{\Gamma(m_3)} \left(\frac{\gamma_{\text{th}}}{\bar{\gamma_2}}\right)^{m_3}. \tag{3.41}$$

Similarly, the asymptotic outage probability for the direct channel over the Rayleigh fading can be given by [121]

$$P_{\text{out},SG} \approx \frac{\gamma_{\text{th}}}{\bar{\gamma_1}}. \tag{3.42}$$

Average BER

The unified unconditional average BER expression for SC communication and arbitrary binary modulation schemes is given by [122]

$$P_{BER} = \frac{q^p}{2\Gamma(p)} \int_0^{\infty} e^{-q\gamma} \gamma^{p-1} F_{\gamma_{sc}}(\gamma)\, d\gamma, \tag{3.43}$$

where p and q are modulation scheme related parameters [16].
From (3.33) and (3.34), $F_{\gamma_{sc}}(\gamma)$ can be given by

$$F_{\gamma_{sc}}(\gamma) = (F_{\gamma_{SU}}(\gamma) + F_{\gamma_{UG}}(\gamma) - F_{\gamma_{SU}}(\gamma) F_{\gamma_{UG}}(\gamma)) F_{\gamma_{SG}(\gamma)}, \tag{3.44}$$

where $F_{\gamma_{SU}}$, $F_{\gamma_{UG}}$, and $F_{\gamma_{SG}}$ are the cumulative distribution functions of γ_{SU}, γ_{UG}, and γ_{SG}, respectively. Hence, the integral at (3.43) becomes an integral of three terms as follows

$$P_{BER} = \frac{q^p}{2\Gamma(p)}(I_1 + I_2 - I_3), \tag{3.45}$$

where,

$$I_1 = \int_0^\infty e^{-q\gamma}\gamma^{p-1} F_{\gamma_{SU}}(\gamma) F_{\gamma_{SG}}(\gamma)\, d\gamma, \tag{3.46}$$

$$I_2 = \int_0^\infty e^{-q\gamma}\gamma^{p-1} F_{\gamma_{UG}}(\gamma) F_{\gamma_{SG}}(\gamma)\, d\gamma, \tag{3.47}$$

and

$$I_3 = \int_0^\infty e^{-q\gamma}\gamma^{p-1} F_{\gamma_{SU}}(\gamma) F_{\gamma_{UG}}(\gamma) F_{\gamma_{SG}}(\gamma)\, d\gamma. \tag{3.48}$$

The integral I_1 can be solved through integration by substitution followed by exploiting [123, Eq.(2.10.3.9)] to derive the expression in (3.49)

$$\begin{aligned} I_1 = {} & \frac{1}{\Gamma(a+1)} \times \\ & \left(\frac{\left(\frac{1}{b\sqrt{L_1\gamma_1}}\right)^{a+1}}{2(a+1)} q^{\frac{-(2p+a+1)}{2}} \Gamma\left(\frac{2p+a+1}{2}\right) {}_2F_2\left(\frac{a+1}{2}, \frac{2p+a+1}{2}; \frac{1}{2}, \frac{a+1}{2}+1 : \frac{\left(\frac{1}{b\sqrt{L_1\gamma_1}}\right)^2}{4q}\right) \right. \\ & \left. + \frac{\left(\frac{1}{b\sqrt{L_1\gamma_1}}\right)^{a+2}}{2(a+2)} q^{\frac{-(2p+a+2)}{2}} \Gamma\left(\frac{2p+a+2}{2}\right)_2 F_2\left(\frac{a+2}{2}, \frac{2p+a+2}{2}; \frac{3}{2}, \frac{a+4}{2} : \frac{\left(\frac{1}{b\sqrt{L_1\gamma_1}}\right)^2}{4q}\right) \right). \end{aligned} \tag{3.49}$$

where ${}_aF_b(.)$ is the confluent hypergeometric function [123].
The integral I_2 can be evaluated by applying [123, Eq.(2.10.3.2)] to obtain

$$I_2 = \frac{\Gamma(p+m_3)(\frac{m_3}{\Omega_3 L_2 \bar{\gamma_2}})^{m_3}}{m_3\Gamma(m_3) q^{(p+m_3)}} \times {}_2F_1\left(m_3, p+m_3; m_3+1; -\frac{(\frac{m_3}{\Omega_3 L_2 \bar{\gamma_2}})}{q}\right). \tag{3.50}$$

The third integral term contains two lower incomplete gamma functions with different arguments which makes it difficult to evaluate. To overcome this, a series representation of the lower incomplete gamma function is used to replace the $F_{\gamma_{SU}}(\gamma)$ term, resulting in

$$F_{\gamma_{SU}}(\gamma) = \frac{1}{\Gamma(a+1)} \sum_{k=0}^{\infty} \frac{(-1)^k (\frac{\sqrt{\gamma_{th}}}{b\sqrt{L_1 \bar{\gamma}_1}})^{k+a+1}}{k!(a+k+1)}. \tag{3.51}$$

After some mathematical manipulations the integral I_3 can be rewritten as

$$I_3 = \frac{1}{\Gamma(a+1)} \sum_{k=0}^{\infty} \frac{-1^k (b\sqrt{L_1 \bar{\gamma}_1})^{-(k+a+1)}}{k!(k+a+1)\Gamma(m3)} \times \int_0^{\infty} e^{-q\gamma} \gamma^{\frac{p+k+a-1}{2}} \gamma \left(m_3, \frac{m_3 \gamma_{th}}{\Omega_3 L_2 \bar{\gamma}_2} \right) d\gamma, \tag{3.52}$$

which consists of a sum of integrals of the form given in [123, Eq.(2.10.3.2)]. Consequently, I_3 can be evaluated as in follows

$$\begin{aligned} I_3 = & \sum_{k=0}^{\infty} \frac{-1^k (b\sqrt{L_1 \bar{\gamma}_1})^{-(k+a+1)}}{k!(k+a+1)\Gamma(a+1)} \frac{\Gamma(\frac{2p+k+a+1}{2} + m_3)(\frac{m_3}{\Omega_3 L_2 \bar{\gamma}_2})^{m_3}}{m_3 \Gamma(m_3) q^{(\frac{2p+k+a+1}{2}+m_3)}} \\ & \times {}_2F_1 \left(m_3, \frac{2p+k+a+1}{2} + m_3; m_3+1; -\frac{(\frac{m_3}{\Omega_3 L_2 \bar{\gamma}_2})}{q} \right). \end{aligned} \tag{3.53}$$

3.6 Special Characteristics of the UAV Channels

Due to the special characteristics of the UAV channels, both the Rice factor and the path loss exponent depend on the LoS probability. They can be expressed as a function of θ_U, the angle between the UAV and the communication node as [44, 124]

$$\beta(\theta_U) = A_\beta e^{B_\beta \theta_U}, \tag{3.54}$$

and,

$$\alpha(\theta_U) = A_\eta P_{\text{LoS}}(\theta_U) + B_\eta. \tag{3.55}$$

where $P_{LoS}(\theta_U) = \frac{1}{1+\xi_1 e^{-\xi_2(\theta_U - \zeta_1)}}$ is the LoS probability, A_i, B_i, $i \in (\beta, \eta)$ are parameters that depend on the environment and the transmission frequency, $A_\beta = \beta(0)$, $B_\beta = \frac{2}{\pi} \ln \left(\frac{\beta(\frac{\pi}{2})}{\beta(0)} \right)$, and ξ_1 and ξ_2 are environment variables [117].

3.7 Numerical and Simulation Results

In this section, the numerical and simulation results are represented to verify the analysis and to obtain insights into the effect of the RIS size and the UAV positioning (altitude) on the system's performance. To verify the analysis, MATLAB is employed to generate a Monte Carlo simulation by using 10^8 realisations.

The simulation parameters for both RIS-assisted UAV-aided and RIS-assisted cellular-connected UAV scenarios are set as follows: $\rho = 20$ dB, $\beta(0) = 5$ dB, $\beta(\pi/2) = 15$,

Table 3.1: Multi-hop RIS-assisted UAV communication system nodes coordinates

Node	x (m)	y (m)	z (m)
Source node	0	0	20
RIS	0	70	20
UAV	320	50	UAV_h
Ground user	340	-10	1.5

$A_\eta = 1.5$, and $B_\eta = 3.5$. Also, unless otherwise stated, $P_1 = 0.01$ W, $P_2 = 0.1$ W, and $N_0 = -110$ dBm. It is worth mentioning that the transmit power is selected for the aerial BS to be lower than the terrestrial BS due to the power limitations on the UAV. While the following simulation parameters are chosen for the multi-hop RIS-assisted UAV communication system: $P_1 = P_2 = 49$ dBm, $\rho = -1$ dB, $N_0 = -110$ dBm, $\alpha = 3.5$ and 2.8 for S-G and S-R links, respectively, and 2.2 for both R-U and U-G links. The horizontal distances S-R, R-U, U-G, and S-G are 70, 320, 60 and 320 m, respectively.

Figure 3.4 and Figure 3.5 represent the outage probability as a function of the UAV height for the UAV-aided communication and the cellular-connected UAV communication systems, respectively. Both figures show that the analytical results are consistent with the simulations. It can be observed that the outage probability performance of the two considered scenarios experiences a significant improvement as the number of RIS elements increases. Thus, a RIS with a sufficiently high number of elements can maintain reliable connections between aerial and terrestrial nodes. Moreover, it can also be noticed that the performance improves as the UAV height increases since both the Rician factor and the path loss exponent are affected by the LoS probability, which becomes higher as the elevation angle of the UAV increases, or in other words as the UAV flies at relatively high altitudes. However, the performance degrades again when the UAV elevation angle variations become insignificant and the path loss starts to increase due to the increased UAV altitude. It is also worth noting that although a LoS link exists between the UAV and the ground user, as shown in Figure (3.4), the RIS significantly affects the performance of the system, and even a small increase in the number of the RIS elements can noticeably improve the system performance.

Figures 3.6 and 3.7 examine the outage probability performance of the A2G and G2A setups, respectively, as a function of the transmit SNR for different numbers of RIS elements. The UAV height is selected based on the results presented in Figure 3.4 and Figure 3.5 to achieve the maximum performance, where the UAV heights are set as 130 m for the first systems and 350 m for the cellular-connected UAV system. Again, the analytical results are consistent with the simulations in both scenarios. Figures 3.6 and 3.7 should tell that the effect of RIS elements is significant, and increasing the number of RIS elements greatly improves system performance by reducing the outage probability at any given transmit SNR. In both figures, systems with a larger number of RIS elements show

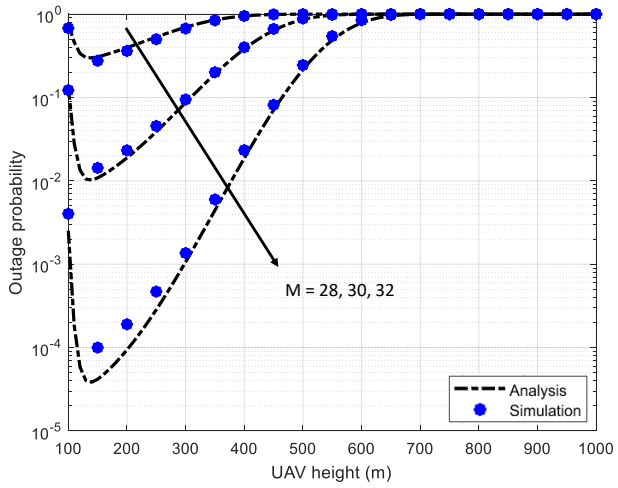

Figure 3.4: P_{out} versus UAV height for different numbers of RIS elements for RIS-assisted UAV communication (A2G).

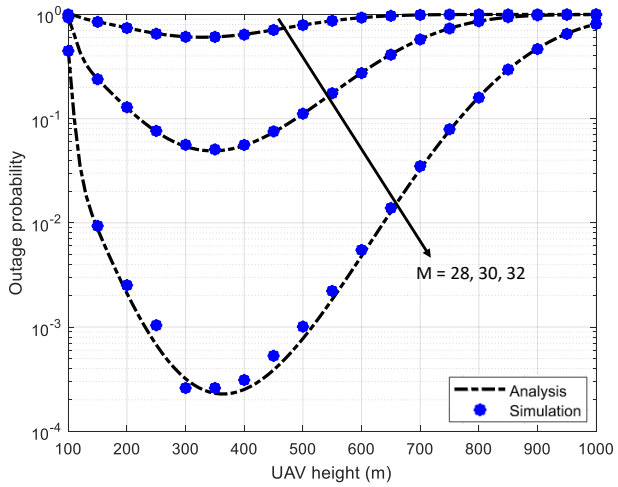

Figure 3.5: P_{out} versus UAV height for different numbers of RIS elements for RIS-assisted UAV communication (G2A).

lower outage probabilities across all SNR values compared to those with fewer elements. This indicates that a larger RIS can capture and direct more signal energy towards the receiver, effectively improving communication reliability. As expected, the RIS with a larger number of elements achieves improved performance. It can be also observed that the performance of the system with a larger RIS is similar to the high SNR performance of the systems with a lower number of RIS elements. Specifically, in Figure 3.7, it can be observed that the RIS with 24 elements achieves a similar outage performance at a transmitting SNR of 76 dB as the 20 elements RIS at SNR of 80 dB. This demonstrates that a modest increase in RIS elements can yield comparable performance to a system with higher SNR, potentially saving transmit power and improving energy efficiency. This will result in maintaining the quality of communication links by providing energy-

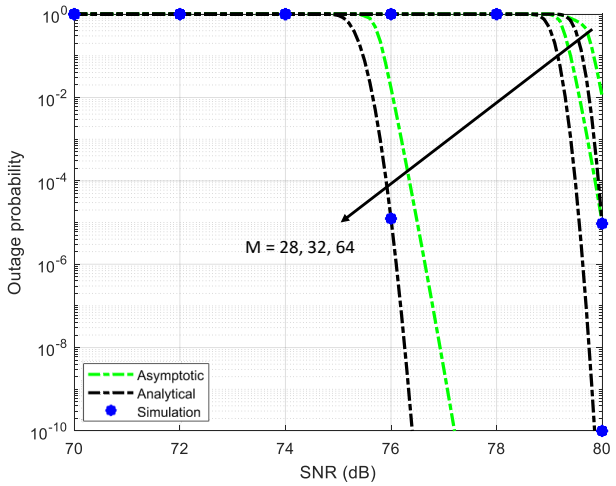

Figure 3.6: P_{out} versus SNR for different numbers of RIS elements for RIS-assisted UAV communication (A2G).

efficient and reliable connections for different propagation environments and users' traffic demands. The practical implications of these findings include improved energy efficiency and reliability, as increasing the number of RIS elements allows systems to maintain the quality of communication links even under lower SNR conditions. This makes RIS a valuable tool in designing energy-efficient and reliable communication systems, especially in variable propagation environments and diverse traffic demands. Furthermore, in the case of cellular-connected UAVs and the expected multiple-cell detection, increasing the number of the RIS elements can overcome the SNR degradation problem which will reduce the radio link failures (RLFs) caused by interference. This improvement will also be reflected in mobility management and reduce any unnecessary handovers (HOs). Moreover, the figures validate that the analytical results are consistent with the simulations in both A2G and G2A scenarios, reinforcing the accuracy of the theoretical models and enhancing the reliability of the study's conclusions.

Figure 3.8 shows end-to-end outage probability as a function of the UAV height with respect to the ground. The analytical results are consistent with the simulations, which demonstrates the accuracy of the proposed approximation. Furthermore, The outage probability of the multi-hop system demonstrates a noteworthy enhancement with the increase in the size of RIS. Thus, a sufficiently high number of RIS elements ensures a reliable connection between S and U, hence, in that case, the outage of the system is mainly determined by A2G link. This result is particularly useful for design considerations, where a certain number of RIS elements are used to reach a desired performance for the UAV operating at a specific height and vice versa. The proposed investigation yields an additional noteworthy insight, indicating that a RIS with a sufficient size can maintain a reliable link between S and U when U moves closer to G.

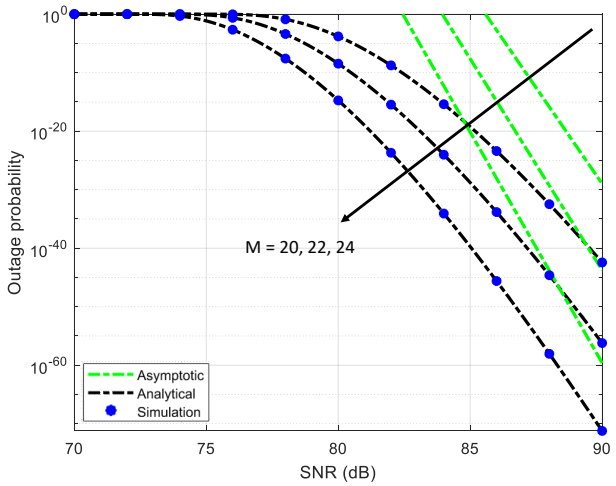

Figure 3.7: P_{out} versus SNR for different numbers of RIS elements for RIS-assisted UAV communication (G2A).

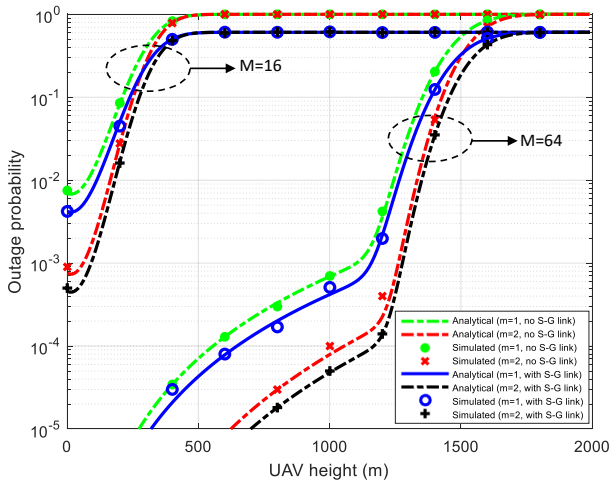

Figure 3.8: P_{out} versus UAV height for different numbers of RIS elements and fading parameter (m).

The system's outage performance, represented in Figure 3.9, is evaluated in relation to the transmit SNR for various numbers of RIS elements. The analytical results closely match the simulation findings, demonstrating the consistency of the proposed analysis. A noteworthy observation is that the performance of the system with a larger RIS closely resembles the high SNR performance of the system with a smaller RIS. For instance, when comparing a RIS with 64-elements to an 16-element RIS, it is observed that the former achieves a similar outage performance at a transmit SNR of 50 dB as the latter does at an SNR of 65 dB indicating that employing a larger RIS can attain energy-efficient and reliable connections to meet the demands of diverse propagation environments. It is also worth noting that the high SNR asymptotic behaviour aligns with the exact results.

Figure3.10 which effectively visualises the influence of the horizontal position of the

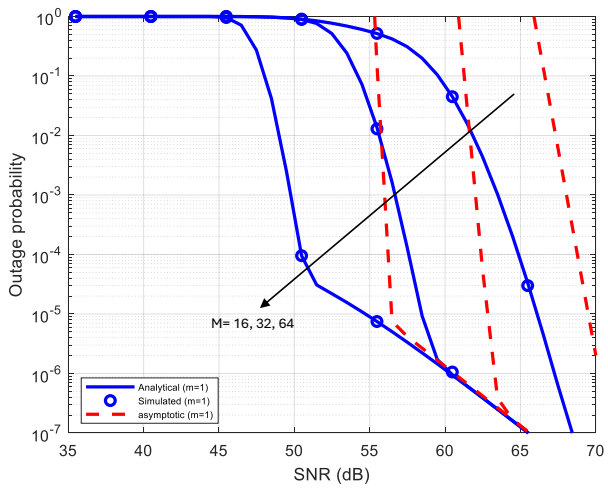

Figure 3.9: P_{out} versus SNR for different numbers of RIS elements for multi-hop RIS-assisted UAV communication system.

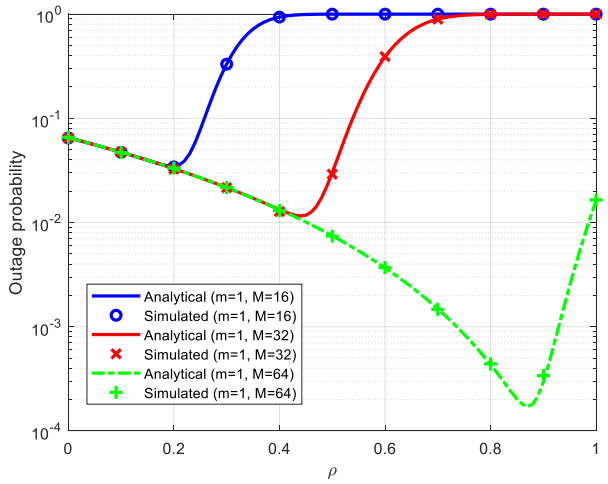

Figure 3.10: P_{out} versus distance ratio for different number of RIS elements.

UAV on the outage probability performance of the multi-hop RIS-assisted UAV system. Specifically, it examines the outage probability of the multi-hop system at a fixed UAV height of $200m$ as a function of $D_r = \frac{r_{SU}}{r_{SU}+r_{UG}}$ which represents the horizontal distance ratio of the distance between, S-U denoted as r_{SU}, to the sum of the distance between S-U and U-G, denoted as r_{UG}, for different numbers of RIS elements. It can be clearly noticed that a RIS with a sufficiently high number of elements can maintain a reliable link between the BS and the UAV. Thus, when the UAV moves closer to the ground user the outage performance improves. However, in the case of the lower number of RIS elements, if the distance between the UAV and the BS is increased further, the first link (BS-UAV) dominates the system performance.

Figure3.11 represents end-to-end BER different modulation schemes as a function of the UAV height. As expected, the simulation matches the analytical results. Moreover, the

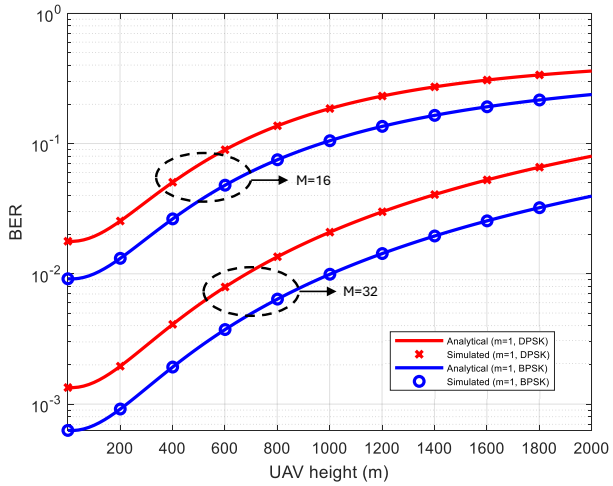

Figure 3.11: The average BER versus UAV height for different numbers of RIS elements and modulation schemes.

series expansion used to replace the lower incomplete gamma function in (3.47) converges for the given parameter values. It can be clearly seen that a RIS with a sufficient size can stabilise the performance and maintain a reliable connection, and the behaviour of the average BER performance is similar to the outage performance behaviour.

3.8 Summary

This study represented a framework to examine the performance of RIS-assisted UAV communication systems, namely, RIS-assisted UAV-aided communications, RIS-assisted cellular-connected UAV communications, and multi-hop RIS-assisted UAV communication systems. Closed-form accurate approximations for the SNR distribution of the RIS-assisted UAV networks over Racian and Nakagami-m fading channels, outage probability, and average BER for the proposed systems were derived. These expressions were exploited to evaluate the outage and error performance of the proposed systems. Furthermore, high SNR outage probability expressions were also derived and analysed. These results highlight the effectiveness of RIS in optimising system performance according to specific requirements or constraints. This study shows that the integration of RIS presents an efficient solution, particularly in complex and dynamic environments where maintaining LoS connections might not always be feasible or optimal. The subsequent chapter delves into RIS optimisation and beamforming techniques to enhance power efficiency, with a particular emphasis on practical considerations such as RIS power dissipation required for operation. Moreover, in order to provide a comprehensive understanding of how the performance gains discussed in this study can be translated into practical, impactful solutions in real-world applications, chapter 5 will transition from theoretical analysis and

performance evaluation to practical application scenarios by exploring the application of RIS-assisted UAV communication systems in IoT data harvesting.

Chapter 4

Beamforming and Power Efficiency Optimisation for RIS-Assisted Communications

After investigating the communication efficiency of RIS-assisted UAV communications and introducing an analysis focused on assessing the reliability and robustness of RIS-assisted UAV communication systems under various operational scenarios, this chapter further extends the analysis by investigating the power efficiency of RIS-assisted communications to determine when they should introduce their best performance gains under practical considerations. This chapter focuses on studying the impact of RIS on enhancing the energy efficiency and sustainability of wireless communication networks. The primary objective, aligned with *O3*, is to present a comprehensive study of the intricacies of power dissipation in RIS, focusing on both static and dynamic components, and providing a detailed breakdown of RIS-assisted communications operational cost. This analysis includes an examination of control circuit components, control boards, and dynamic power dissipation factors. A precise framework that considers RIS power dissipation is also formulated. This framework is designed to minimise the total power consumed by RIS-assisted communication systems while adhering to essential communication constraints. This objective is facilitated by choosing the optimum number of RIS elements and adjusting the phase shifts matrix to achieve power dissipation reduction while maintaining the channel gain required to fulfil service requirements.

4.1 Introduction

Future wireless networks are expected to utilise RIS as a technology enabler, however, understanding the power dissipation of RIS is crucial for efficient operation and deployment. Moreover, to fully observe the power efficiency of RIS, it is important to

compare it with other active solutions such as active relays. These comparisons provide insights into the relative advantages and trade-offs of each technology. Active relays amplify received signals before retransmitting them, which inherently involves higher power consumption due to the active amplification process. In contrast, RIS can achieve similar benefits through passive reflection, potentially consuming less power. Comparing the power dissipation of RIS and active relays can highlight the efficiency gains of RIS, particularly in scenarios where energy consumption is a critical factor.

In the literature, several works examined the power efficiency characteristics of RIS-assisted communications and compared them with other active solutions to evaluate their potential gains. For instance, the authors in [14], [66], and [88] investigated the performance of RIS and relaying-aided communications, examining their basic differences, similarities, and efficiency in various scenarios. The work in [14] aimed to identify potential advantages and limitations of both technologies and outline the contexts in which RIS can outperform relaying. The study also highlighted how factors such as the number of RIS elements, channel conditions, modulation type, and targeted performance metrics can impact the performance of both technologies. The authors in [66] provided a comparative study between RIS and DF relaying. Their main goal was to determine how large an RIS needs to be to overcome a traditional DF relaying system. Their simulation results suggested that a decent number of RIS elements is needed to outperform the performance of relay-assisted transmission in terms of data rate. Moreover, the results emphasised the importance of optimising the size and deployment of RIS to achieve the desired performance gains.

The above studies showed that RIS has the potential to outperform relaying in certain scenarios, particularly in limited power, high throughput, and dense networks. However, several limitations still require further investigation to fully understand RIS capabilities, address practical implementation challenges in a real-world scenario, and unlock the full potential of RIS technology. Firstly, none of the studies conducted a detailed analysis of RIS power dissipation, which is crucial for understanding the overall energy efficiency of RIS-assisted communication systems. Moreover, the consideration of power dissipation at the RIS end in optimising the phase shift of the RIS was not addressed, indicating a gap in understanding the energy dissipation aspect of RIS deployment. Practical considerations regarding phase shifts of the RIS, such as discrete phase shifts and their impact on system performance, were also overlooked in the cited studies. These practical constraints can significantly affect the implementation feasibility and performance of RIS-enabled systems. Lastly, the investigation of beamforming optimisation techniques to minimise power dissipation, particularly at the RIS, was lacking in the referenced research. Incorporating power-efficient beamforming strategies could enhance the energy efficiency of RIS-assisted communication systems, warranting further investigation.

4.2 Contributions

This chapter investigates RIS power dissipation and optimisation, highlighting their potential to enhance energy efficiency and sustainability. Through a detailed analysis of RIS power dissipation and the development of an optimisation algorithm, the study emphasises the practical relevance of RIS deployment for achieving efficient and sustainable wireless networks, while also providing comparisons with traditional active solutions to support decision-making in system design showcasing benefits and drawbacks of each technology that make them suitable for different applications. Contributions are detailed as follows:

- Investigate the impact of RIS on enhancing energy efficiency and sustainability in wireless communication, aligning with the principles of green communication. By providing a detailed breakdown of energy dissipation, including control circuit components and dynamic power factors. Additionally, a comprehensive power consumption cost model for both relay-assisted and RIS-assisted communication systems is introduced, considering the power dissipation at all communication nodes.
- Propose a precise optimisation framework aimed at minimising the total power consumption of RIS-assisted communication systems while adhering to achievable rate constraints. This framework takes into account critical factors such as RIS design and phase shift constraints, ensuring its practical relevance in real-world network scenarios. A novel and practical approach to optimising RIS configuration and phase shifts is proposed leveraging the strengths of metaheuristic algorithms to effectively address the inherent complexities of the problem.
- Provide a comparative analysis between RIS and traditional active relaying solutions, showcasing RIS performance gains compared to AF and DF relaying, examine various factors that influence performance, and discuss the inherent advantages and limitations of each technology.

4.3 RIS Power Dissipation Analysis

Understanding the power dissipation in RIS is crucial for efficient operation and deployment. This section studies the intricacies of power dissipation in RIS, focusing on the static power component coming from the control and configuration network layers and the power dissipation generated by the metasurface layer or the UCs. As shown in Figure 4.1, the operation power cost of RIS can be expressed as the sum of static and metasurface power components [125–127]

$$P_{\mathrm{RIS}}^{DC} = P_{\mathrm{static}} + P_{\mathrm{UC}}. \tag{4.1}$$

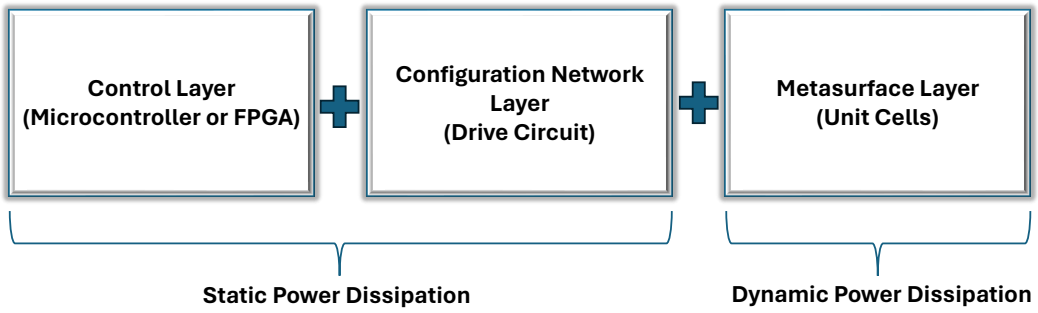

Figure 4.1: RIS power dissipation components.

4.3.1 Static Power Dissipation

As shown in Figure 4.2, the static power dissipation of an RIS primarily originates from the control circuitry, which includes components such as field-programmable gate arrays (FPGAs), registers, as well as digital-to-analogue converters (DACs). Hence, the static power dissipation P_{static} can be represented as the sum of the power dissipation of the control board and the power dissipation of the drive circuit as shown below [127, 128]

$$P_{\text{static}} = P_{\text{control board}} + P_{\text{total drive circuits}}. \tag{4.2}$$

The FPGA control board plays a pivotal role as the "brain" of the RIS. The FPGA control board, responsible for data processing and possessing ample computational capabilities, remains a constant in power dissipation within the RIS system. In practical implementations, a commercial-grade FPGA, such as the XC7K70T, operating at a voltage of 24 V, this FPGA draws a current of 0.2 A, resulting in a power dissipation of 4.8 watts [128, 129]. For RIS prototypes featuring fewer UCs or lower demands in terms of data processing speed, cost-effective and energy-efficient entry-level FPGAs, such as the Xilinx ZYNQ7100, consuming a mere 1.5 watts of power [126, 128]. In [130], a high-end FPGA controller was used in their prototype that only consumes 1.5 W of power. The authors also suggested that the beamforming algorithm could be implemented on a standard microcontroller, reducing the controller's power consumption to approximately 10 mW.

Conversely, the power dissipation of the drive circuits is variable and depends on multiple factors since diverse components necessitate different circuitry of the drive circuits. For instance, PIN-diode-based RIS UCs employ shift registers, while varactor-diode-based UCs utilise DACs, operational amplifiers (op-amps), and pulse-wave-modulation (PWM) signals with level regulators [127, 128].

PIN Diodes with FPGAs and Registers: The integration of PIN diodes with FPGAs and registers forms an essential part of the control circuitry. These components consume power even when the RIS is not actively manipulating signals, contributing to the static

(a) PIN-diode based RIS.

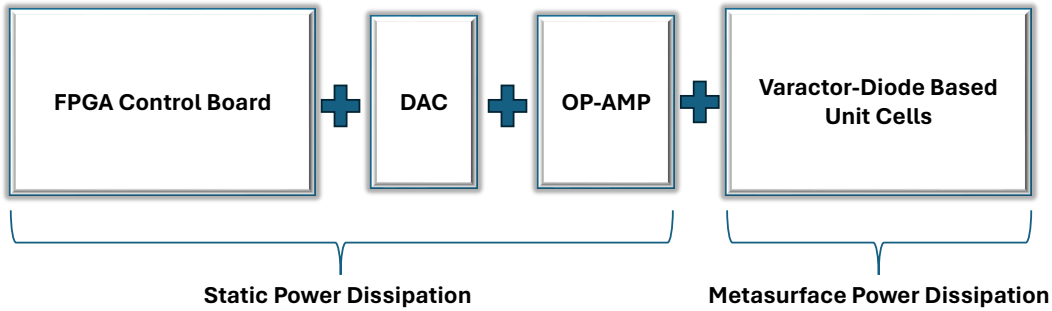

(b) Varactor-diode based RIS.

Figure 4.2: RIS static power dissipation for different RIS structures.

power dissipation.

Varactor Diodes with DACs: Similarly, varactor diodes coupled with DACs play a role in static power dissipation. These components are responsible for tuning the metasurface, and their power dissipation is inherent to the control circuitry.

Drive circuit power dissipation is influenced by the number of control signals, which correlates with the count of adjustable electronic components (M_c), the number of UCs within the same group sharing the same control signal (M_g), and the control degree-of-freedom (DoF) within the RIS system, including UC control, row/column control, and sub-array control. Furthermore, the power of drive circuits comes from several individual circuits, with the power dissipation of each circuit depending on its own inherent self-power dissipation characteristics.

Hence, the power of drive circuits can be written as [127, 128]

$$P_{\text{total drive circuits}} = \left\lceil \frac{M_c}{M_g \cdot M_s} \right\rceil \cdot P_{\text{drive circuit}} \,, \tag{4.3}$$

where M_s represents the number of control signals originated by each drive circuit.

In typical RIS setups, all UCs usually have the same bit resolution. Thus, assuming a linear polarisation, the static power dissipation P_{static} for different RIS types can be defined as [127]

$$P_{\text{static}} = \begin{cases} P_{\text{control board}} + \left\lceil \frac{MB}{M_g \cdot M_s} \right\rceil \cdot P_{\text{drive circuit}}, & \text{PIN-diode/ RF switch-based RIS} \\ P_{\text{control board}} + \left\lceil \frac{M}{M_g \cdot M_s} \right\rceil \cdot P_{\text{drive circuit}}, & \text{varactor-diode-based RIS} \end{cases} \tag{4.4}$$

where M stands for the total number of RIS UCs and B is the UC bit resolution in a single polarisation mode.

4.3.2 Metasurface layer Power Dissipation

In contrast to static power dissipation, the dynamic power dissipation in RIS varies based on its specific configuration and operation [127].

Varactor-Diode-Based RIS: In RIS systems belonging to the family of varactor-diode-based programmable metasurfaces, the dynamic power dissipation is considered negligible. This is due to the fact that the current in the varactor diodes of the UCs remains minimal when the system is operational [125–127].

PIN-Diode-Based RIS: The dynamic power dissipation in PIN-diode-based RIS is influenced by several factors:

Polarisation Mode: When designing a PIN-diode-based RIS for dual polarisation, the power dissipation increases. This is because additional PIN diodes are required to achieve polarisation in both directions simultaneously.

Bit Resolution of RIS UCs: The power dissipation in PIN-diode-based RIS varies depending on the bit resolution of the UCs. A single PIN diode representing a 1-bit binary state consumes less power compared to the scenario where multiple PIN diodes are needed for a multi-bit UC.

UCs Coding Status: Different coding statuses, such as "00," "01," "10," and "11," for a 2-bit RIS UC result in varying numbers of "on-state" PIN diodes. Each coding status leads to different power dissipation levels, further emphasising the significance of coding efficiency in RIS design.

Metasurface layer power dissipation P_{UCs} is given by [127]

$$P_{\text{UCs}} = \begin{cases} \mathrm{I}_v \cdot \sum_{i=1}^{M} \left[P_{i,v}\left(B_{i,v}, b_{i,v}\right) \right] + \mathrm{I}_h \cdot \sum_{i=1}^{M} \left[P_{i,h}\left(B_{i,h}, b_{i,h}\right) \right], & \text{PIN-diode-based RIS} \\ 0, & \text{varactor-diode-based RIS} \end{cases} \tag{4.5}$$

where I_v and I_h represent the indicators for vertical and horizontal polarisations respectively, with a value of "1" indicating that the RIS can manipulate incoming wireless

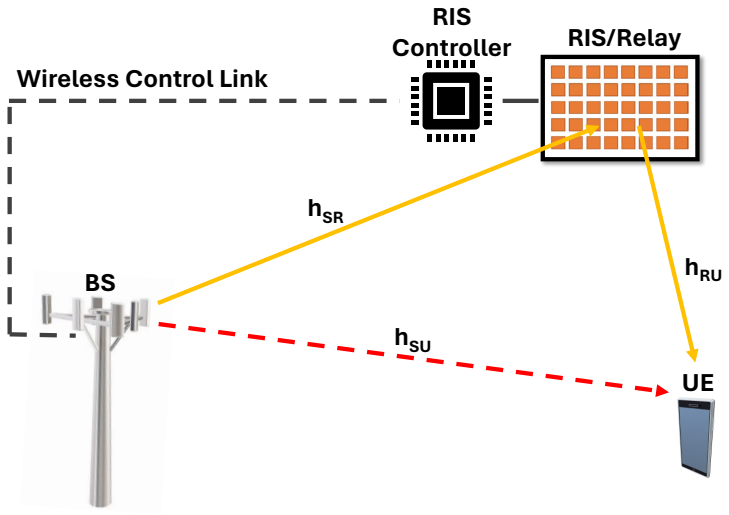

Figure 4.3: RIS/Relay-assisted communication system model.

signals in that specific polarisation direction. M stands for the total number of RIS UCs. $P_{i,x}$ $(B_{i,x}, b_{i,x})$, $x \in [v, h]$, denotes the power dissipation of the i-th RIS UC with B-bit resolution in a single polarisation mode and b bits encoded as "1".

4.4 System Model

As shown in Figure 4.3, the proposed setup considers a communication system in which a single antenna source node (S) serves a user equipment (U). To enhance the performance, the transmission is either assisted by a relay or a RIS (R) equipped with M reflecting elements. Two different modes of data transmission are examined: (i) RIS-supported transmission, (ii) relay-supported transmission.

4.4.1 RIS-supported transmission

In this configuration, the RIS redirects the incident signal from S towards U. Let $\Theta = \left\{e^{j\theta_1}, e^{j\theta_2}, \ldots, e^{j\theta_M}\right\}$ denotes the RIS phase-shift matrix, where $\theta_m \in [0, 2\pi)$, $m \in \{1, \ldots, M\}$ is the phase shift of the m^{th} reflecting element. Then the received signal at the UE is [66]

$$y = \left(h_{SU} + \hat{\alpha} h_{SR}^T \Theta h_{RU}\right) x + n, \tag{4.6}$$

where h_{SU}, $h_{SR} \in \mathbb{C}^{M\times 1}$, and $h_{RU} \in \mathbb{C}^{M\times 1}$ are S-U, S-R and R-U channel gains, respectively, $\hat{\alpha} \in [0, 1)$ represents the RIS reflection coefficient, x is the transmitted signal, and $n \sim \mathcal{CN}(0, N_0)$ is the additive white Gaussian noise (AWGN) with zero mean and N_0 variance.

Based on (4.6), the SNR at the UE can be written as

$$\gamma = \frac{P_S \left| h_{SU} + \hat{\alpha} h_{SR}^T \Theta h_{RU} \right|^2}{N_0}, \tag{4.7}$$

where P_S is the power of the transmitted signal.

Using (4.6) and (4.7), the maximum rate at the UE can be written as

$$\bar{R}_{\text{RIS}} = \log_2 \left(1 + \frac{P_S \left| h_{SU} + \hat{\alpha} h_{SR}^T \Theta h_{RU} \right|^2}{N_0} \right). \tag{4.8}$$

Hence, the transmit power required to achieve a data rate of $\bar{R}$ for RIS-assisted transmission is written as

$$P_{\text{RIS}}^{\text{Tx}}(\bar{R}) = \left(2^{\bar{R}} - 1 \right) \frac{N_0}{\left| h_{SU} + \hat{\alpha} h_{SR}^H \Theta h_{RU} \right|^2}. \tag{4.9}$$

4.4.2 Relay-supported transmission

DF relaying

The DF relaying protocol is divided into two phases; the first phase is when the source node transmits data to the destination node through the relay node, the relay first decodes the received signal from the source [111]. The signal received by the relay node can be written as

$$y_R = h_{SR}\, x_1 \; + \; n_1 \; , \tag{4.10}$$

where $h_{SR} \in \mathbb{C}$ represents the channel gain for S-R link, x_1 is the transmitted signal from the S, and $n_1 \sim \mathcal{CN}(0, N_0)$ is the AWGN at R with zero mean and N_0 variance.

After successfully decoding the signal, the relay re-encodes it and forwards it to the destination in the second transmission phase. The signal received by U from the relay can be written as

$$y_U = h_{RU}\, x_2 \; + \; n2 \; , \tag{4.11}$$

where $h_{RU} \in \mathbb{C}$ is the channel gain for R-U link, x_2 is the transmitted signal from the relay, and $n_2 \sim \mathcal{CN}(0, N_0)$ is the AWGN at U with zero mean and N_0 variance.

The analysis of DF transmission focuses on a specific decoding structure at the relay station. It is essential for the relay to fully decode the signal, when both the relay and destination decode the entire signal, the minimum of the two SNRs is considered. Hence, the SNR of the DF relay-assisted system can be given by [131]

$$\gamma = \min\left(\frac{P_S\left|h_{SR}\right|^2}{N_0}, \frac{P_S\left|h_{SU}\right|^2}{N_0} + \frac{P_R\left|h_{RU}\right|^2}{N_0}\right), \tag{4.12}$$

where P_S and P_R represent the powers of the transmitted signals from S and the relay, respectively. The first term denotes the maximum rate at which the relay can decode the source message. The second term signifies the maximum rate at which U can reliably decode the signal given repeated transmissions from both S and the relay. The minimum function ensures that the SNR calculation accurately reflects the transmission quality, accounting for both direct and relayed paths in the DF relay-supported transmission system. Using (4.12), the achievable rate at the U can be written as

$$\bar{R}_{\mathrm{DF}} = \frac{1}{2}\log_2\left(1+\min\left(\frac{P_S\left|h_{SR}\right|^2}{N_0}, \frac{P_S\left|h_{SU}\right|^2}{N_0} + \frac{P_R\left|h_{RU}\right|^2}{N_0}\right)\right). \tag{4.13}$$

Let $P = P_S = P_R$, similar to the RIS-assisted link scenario the formula for transmit power required to achieve a data rate $\bar{R}$ can be derived from (4.13) as

$$P_{\mathrm{DF}}^{\mathrm{Tx}}(\bar{R}) = \begin{cases} \frac{2^{2\bar{R}}-1}{\left|h_{SR}\right|^2/N_0} & \text{if } \left|h_{SR}\right|^2 \leq \left|h_{SU}\right|^2 + \left|h_{RU}\right|^2 \\ \\ \frac{(2^{2\bar{R}}-1)N_0}{\left(\left|h_{SU}\right|^2+\left|h_{RU}\right|^2\right)} & \text{otherwise} \end{cases}. \tag{4.14}$$

AF relaying

In AF relaying, when a source node transmits data to a destination node through a relay node, the relay first receives the signal from the source node, amplifies it, and then forwards it to the destination. Unlike the DF relaying protocol, the relay in AF relaying does not decode the received signal before retransmitting it [111]. AF relaying offers several advantages, including simplicity in implementation and reduced complexity at the relay node compared to DF relaying. However, it may suffer from noise and interference amplification, especially if the relay amplifies the signal indiscriminately [132]. The received signal at the relay node can be expressed as

$$y_R = h_{SR}\, x \;+\; n_1 \;, \tag{4.15}$$

where $h_{SR} \in \mathbb{C}$ represents the channel gain for S-R link, x is the transmitted signal from the S, and $n_1 \sim \mathcal{CN}\left(0, N_0\right)$ is the AWGN at R with zero mean and N_0 variance.

After receiving the signal, the relay node amplifies it. This amplification process helps to boost the signal strength, compensating for the attenuation that may have occurred during transmission from the source to the relay node. Once amplified, the relay node forwards the signal to the destination node. Therefore, the signal received by the U can

be written as [133]

$$y_U = \sqrt{G}\, h_{RU} h_{SR}\, x_1 \; + \sqrt{G}\, n_1 + \; n_2 \;, \tag{4.16}$$

where $h_{RU} \in \mathbb{C}$ is the channel gain from the relay to U, G represents the amplification factor of the relay, and $n_2 \sim \mathcal{CN}(0, N_0)$ is the AWGN of the second stage.

The UE receiver combines the signals received from S and the relay. Assuming a variable relay gain $G = \frac{P_R}{P_S|h_{SR}|^2+N_0}$ [134], and utilising (4.15) and (4.16), the SNR of the AF relay-supported transmission can be expressed as [131]

$$\gamma = \frac{P_S \left|h_{SU}\right|^2}{N_0} + \frac{P_S P_R \left|h_{SR}\right|^2 \left|h_{RU}\right|^2}{N_0(P_S \left|h_{SR}\right|^2 + P_R \left|h_{RU}\right|^2 + N_0)}. \tag{4.17}$$

Using (4.17), the achievable rate at U is given by

$$\begin{aligned} \bar{R}_{\mathrm{AF}} =& \frac{1}{2} \log_2 \Bigg(1 + \frac{P_S \left|h_{SU}\right|^2}{N_0} \\ &+ \frac{P_S P_R \left|h_{SR}\right|^2 \left|h_{RU}\right|^2}{N_0 \left(P_S \left|h_{SR}\right|^2 + P_R \left|h_{RU}\right|^2 + N_0\right)} \Bigg). \end{aligned} \tag{4.18}$$

Let $P = P_S = P_R$, the following expression can be used to express the power required to achieve a certain rate $\bar{R}$ in the AF relaying system

$$\begin{aligned} P_{\mathrm{AF}}^{\mathrm{Tx}}(\bar{R}) =& \frac{\sigma^2}{2\left(|h_{SU}|^2(|h_{SR}|^2 + |h_{RU}|^2) + |h_{SR}|^2|h_{RU}|^2\right)} \\ &\times \Bigg[\left(\left(|h_{SR}|^2 + |h_{RU}|^2\right) \left(2^{2\bar{R}_{\mathrm{AF}}} - 1\right) - |h_{SU}|^2 \right) \\ &+ \sqrt{\left(|h_{SR}|^2 + |h_{RU}|^2\right)^2 \left(2^{2\bar{R}_{\mathrm{AF}}} - 1\right)^2 + 2|h_{SU}|^2(|h_{SR}|^2 + |h_{RU}|^2) \left(2^{2\bar{R}_{\mathrm{AF}}} - 1\right) + |h_{SU}|^2} \Bigg]. \end{aligned} \tag{4.19}$$

In the AF relaying system, there are two potential sources of noise and channel impairments: the direct link from the source to the destination, the relay link from the source to the relay, and then from the relay to the destination. The minimum function in (4.19) selects the minimum value between these two potential noise sources and impairments, ensuring that the power calculation is based on the most limiting factor for achieving the desired rate.

4.4.3 End-to-End Power Consumption Model

The efficient operation of wireless networks is crucial to reducing their environmental impact. The total power consumption of a transceiver node encompasses both the transmit

power and the circuit power [135]. For a given communication traffic the total power consumption expression can be written as follows [136]

$$P_{\text{node}}^{\text{Total}} = \epsilon_{\text{node}} P_{\text{node}}^{Tx} + P_{\text{node}}^{c} \tag{4.20}$$

where ϵ_{node} is the node power amplifier (PA) efficiency factor, P_{node}^{Tx} is the node transmit power, and P_{node}^{c} is the node circuit power dissipation.

The circuit power consumption of a transceiver node primarily comes from the dynamic power consumption which depends on changes in communication traffic, and the static baseband unit (BBU) power consumption [136]

$$P_{\text{node}}^{c} = P_{\text{node}}^{\text{static}} + \beta_{\text{node}} \bar{R}, \tag{4.21}$$

where P_{node}^{static} represents the circuit static power and β_{node} is the BBU power consumption per unit throughput.

End-to-end power (E2E) power consumed by the RIS-assisted transmission system can be written as the summation of the signalling power and the power dissipated to operate the source node and the RIS as shown below

$$P_{\text{RIS}}^{\text{Total}} = \epsilon_S P_{\text{RIS}}^{\text{Tx}} + P_S^c + P_{\text{RIS}}^{\text{DC}} + P_D^c. \tag{4.22}$$

In relaying-assisted transmission scenarios, the source node is active only half of the time; therefore, E2E power consumption of relay-assisted communication can be given by [66]

$$P_{\text{relay}}^{\text{Total}} = (\epsilon_S + \epsilon_{\text{relay}}) P_{\text{relay}}^{\text{Tx}} + \frac{1}{2}(P_S^c + P_S^{\text{sleep}}) + P_{\text{relay}}^c + P_D^c, \tag{4.23}$$

where relay $\in$ {DF,AF} and P_S^{sleep} is the source node power dissipation when it is sleeping [137].

AF relays are simpler compared to DF relays. They amplify the received signal and forward it without performing complex baseband processing, which would typically require the functions of a BBU. Thus, the primary power consumption in AF relays is related to analogue signal processing and amplification. Therefore, the dynamic power consumption dominates the circuit power consumption of the AF relay node [138].

4.5 RIS-assisted Transmission Power Optimisation

Understanding the power dissipation of RIS is essential for optimising their performance and energy efficiency. This article has highlighted the two main components of power dissipation in RIS: static power dissipation arising from control circuitry and metasurface

power dissipation, which varies based on factors like bit resolution of UCs, and coding status. As RIS technology continues to evolve, managing and reducing power dissipation will be critical in realising its full potential in wireless communication and signal processing applications.

4.5.1 Problem Formulation

In the context of optimising the performance of RIS, an optimisation problem is formulated with the aim of minimising power dissipation while adhering to specific constraints. The objective is to minimise the total power, which includes the transmission power and the operational cost of the RIS. However, the operational cost of the source node is assumed to be fixed and cannot be altered by adjusting the optimisation parameters. Consequently, the objective function considers only the transmission power and the RIS power dissipation.

To ensure efficient communication, a minimum rate constraint ($\bar{R}_{\text{th}}$) is imposed to meet the required QoS. The optimisation variables in the proposed problem are the phase shifts (θ_i) of the RIS elements and the number of grouped elements k, with the relationship $M = kM_{\text{sub}}$, where M_{sub} is the size of a sub-RIS group. The phase shifts (θ_i) are critical as they determine the RIS's ability to manipulate electromagnetic waves, thereby influencing the system performance.

The phase shifts are constrained to fall within the range of 0 to 2π. Furthermore, a discrete structure is imposed on these phase shifts, ensuring they conform to $\theta_i = \frac{2\pi}{2^B}$, where B is the bit resolution, dictating the quantisation level of each phase shift. In this problem, the optimisation focuses on finding the optimal number of sub-RIS groups (k) that effectively minimise the RIS power dissipation while achieving the desired performance since RIS is designed as blocks of elements.

The revised optimisation problem is formally stated as follows:

$$
\begin{aligned}
(\text{P1}): \quad \min_{\Theta,k} \quad & P_{\text{RIS}} = P_{\text{RIS}}^{\text{Tx}} + P_{\text{RIS}}^{\text{DC}} && \text{(4.24a)}\\
\text{S.t.} \quad & \bar{R}_{\text{RIS}} \geq \bar{R}_{\text{th}}, && \text{(4.24b)}\\
& \theta_i = \frac{2\pi}{2^B}, && \text{(4.24c)}\\
& 0 < \theta_i \leq 2\pi, \quad \forall i = 1, \cdots, M, && \text{(4.24d)}\\
& M = kM_{\text{sub}}, \quad k \in \mathbb{Z}^+, && \text{(4.24e)}
\end{aligned}
$$

where constraint (4.24b) represents the rate requirement to ensure a minimum QoS. Constraints (4.24c) and (4.24d) ensure that the phase shifts are restricted to a set of predefined discrete values determined by the RIS's bit resolution B. Finally, the structural

constraint in (4.24e) defines the total number of RIS elements as a multiple of the sub-RIS group size M_{sub}, with k being the integer variable that dictates the number of these groups.

In this formulation, k serves as the key optimisation parameter instead of the number of RIS elements M, allowing us to directly control the number of sub-RIS groups. Optimising k, indirectly adjusts M, enabling the algorithm to determine the most energy-efficient configuration of RIS elements.

4.5.2 Problem Formulation

In the context of optimising the performance of RIS, an optimisation problem is formulated aimed at minimising power dissipation while adhering to specific constraints. The objective is to minimise total power which effectively captures the transmission power in addition to the operational cost of the RIS and the source node. However, it is assumed that the source node operational cost is fixed and cannot be controlled by changing the presented optimisation parameters, and hence, the objective function will only include transmission power and RIS power dissipation. To ensure efficient communication, a minimum rate constraint (R_{th}) is imposed to meet the required QoS. The proposed problem considers the phase shifts (θ_i) of the RIS elements as optimisation variables, with the condition that they fall within the range of 0 to 2π. These phase shifts are intricately linked to the RIS's ability to manipulate electromagnetic waves. Furthermore, a discrete structure on the phase shifts is enforced, ensuring they conform to $\theta_i = \frac{2\pi}{2^B}$, where B is the bit resolution. Additionally, to effectively minimise RIS power dissipation, it is essential to find the optimum number of RIS elements required to achieve the desired performance while simultaneously minimising operational power.

$$
\begin{aligned}
(\text{P1}): \quad \min_{\Theta,k} \quad & P_{\text{RIS}} = P_{\text{RIS}}^{\text{Tx}} + P_{\text{RIS}}^{\text{DC}} && \text{(4.25a)}\\
\text{S.t.} \quad & \bar{R}_{\text{RIS}} \geq \bar{R}_{\text{th}}, && \text{(4.25b)}\\
& \theta_i = \frac{2\pi}{2^B}, && \text{(4.25c)}\\
& 0 < \theta_i \leq 2\pi, \quad \forall i = 1, \cdots, M, && \text{(4.25d)}\\
& M = kM_{sub}, \quad k \in \mathbb{Z}^+, && \text{(4.25e)}
\end{aligned}
$$

where (4.24b) represents the rate constraints, (4.24c) and (4.24d) ensure that the phase shifts are restricted to a predefined set of discrete values for the B control bits of the RIS within their possible range. Constraint in (4.24e) represents structural constraint related to the number of elements in the RIS, to ensure that the total number of RIS elements is a multiple of the size of the sub-RIS or the grouped elements M_{sub}.

Problem (P1) is inherently non-convex due to the discrete nature of its constraints,

particularly with respect to Θ, and its non-concave objective function. The discrete constraints introduce combinatorial complexity, further complicating the optimisation landscape. In addition to the non-concavity of the objective function, constraints involves discrete decision variables, making the problem particularly challenging to solve using conventional optimisation techniques. As such, there is no standard method to guarantee an optimal solution for these types of non-convex optimisation problems. In the subsequent section, an efficient algorithm is proposed to obtain a suboptimal solution to (P1), addressing the discrete constraints and non-convexity effectively.

4.5.3 Proposed Solution

Solving the optimisation problem in (4.16) determines the optimal phase shifts (θ_i) and the number of RIS elements (M) that collectively minimise power dissipation while satisfying the rate and phase shift constraints, thereby enhancing the energy efficiency and effectiveness of the RIS. In other words, to strike the balance between the number of RIS elements and their configuration which maximises the channel gain while minimising the RIS operational cost.

Given the interdependency between M and Θ it's necessary to consider both variables simultaneously during optimisation. Metaheuristic algorithms, such as particle swarm optimisation (PSO), are well-suited for handling complex optimisation problems with multiple variables and non-convex objective functions. Compared to other metaheuristic approaches, PSO offers advantages in terms of simplicity and fast convergence. PSO can effectively explore complex search spaces with multiple variables and non-linear interactions, where it employs a population (swarm) of candidate solutions (particles) and searches the solution space in parallel, thus, increasing the chances of finding the global optimum by exploring multiple areas of the search space simultaneously. PSO's capability to simultaneously optimise both variables aligns well with the nature of (P1). Moreover, PSO does not require gradient information, making it suitable for problems where the objective function is not differentiable, as in the case of discrete phase shifts.

The computational complexity of PSO is given by

$$O(PI_{\text{PSO}} \log(MN)),$$

where I_{PSO} and P represent the number of iterations and particle size, respectively, which is generally more efficient compared to the SDR scheme with complexity

$$O(\sqrt{N}(2N^4 + N^3)).$$

Algorithm 1 Particle Swarm Optimisation (PSO) for Joint Optimisation of M and Θ

Choose population size N_{pop}, maximum number of iterations N_{iter}, inertia weight $\hat{\omega}$, acceleration coefficients $\hat{c_1}$, $\hat{c_2}$.
Initialise range for particle positions $\boldsymbol{\theta}_{\min}$, $\boldsymbol{\theta}_{\max}$, and range for M.
Initialise particle M values randomly within range
for $iter = 1$ **to** N_{iter} **do**
  for each particle **do**
    Initialise particle positions $\boldsymbol{\Theta}$ randomly within range $\boldsymbol{\theta}_{\min}$ to $\boldsymbol{\theta}_{\max}$ based on the current particle's M value
    Evaluate the fitness of the particle using the objective function with respect to both $\boldsymbol{\Theta}$ and M
    Update personal best position, fitness, and M
    Update global best position, fitness, and M
  for each particle **do**
    Update velocity using PSO update equations for $\boldsymbol{\Theta}$
    Update position for $\boldsymbol{\Theta}$ by adding velocity
    Apply position constraints to ensure values remain within range for $\boldsymbol{\Theta}$
Return $\boldsymbol{\Theta}_{\text{global}}$, M_{global}

For the genetic algorithm (GA), the computational complexity is approximately

$$O(GP_{\text{GA}}MN),$$

where G is the number of generations, P_{GA} is the population size, and MN accounts for the fitness evaluations. Although GA is effective in global search, it often converges slower than PSO and involves more complex operations such as selection, crossover, and mutation, leading to higher computational costs.

Algorithm 1 is proposed to solve (P1). First, the number of RIS elements M values are initialised randomly within the specified range and constraints. During each iteration, the phase shift matrix Θ is initialised based on the current particle's M value. Subsequently, the fitness of each particle is evaluated using the objective function with respect to both Θ and M, updating the personal best position, fitness, and M accordingly. Next, the global best position, fitness, and M are updated based on the entire population. While performing velocity update equations, position updates, and constraint applications, the focus remains solely on Θ, as M remains fixed during the iteration. Finally, the global best position Θ_{global} and the global best M_{global}) are returned by the algorithm.

4.6 Numerical and Simulation Results

In this section, simulation results are represented to evaluate each transmission mode. It is assumed that the S-R link is predominantly LoS due to the RIS being typically

deployed with prior knowledge of the BS's location to exploit LoS channels. RIS is assumed to be deployed locally which can guarantee a LoS link between the RIS and the user. Consequently, the channel gains h_{SR} and h_{RU} are modelled by independent Ricain fading and the path loss exponent of 2.8. Owing to user mobility and the complexities of propagation environments, the direct S-U channel is subject to independent Rayleigh fading and a path loss exponent of 3.5. The remaining parameters utilised are detailed in Table 1 unless specified otherwise.

Parameter	**Value**	**Reference**
Noise Figure	10 dB	[66]
Bandwidth (BW)	20 MHz	-
Source Antenna Gain	5 dBi	[66]
Destination Antenna Gain	5 dBi	[66]
Relay Antenna Gain	5 dBi	[139, 140]
RIS Reflection Element Gain	0 dBi	[66]
RIS Bit Resolution B	1	-
$\epsilon_{\mathrm{S}}, \epsilon_{\mathrm{DF}}, \epsilon_{\mathrm{AF}}$	0.5	[66]
P_{S}^{static}	8 W	[137]
P_{DF}^{static}	4 W	[141]
P_{AF}^{static}	1 W	[]
P_{S}^{sleep}	3 W	[137]
$\beta_{\mathrm{S}}, \beta_{\mathrm{DF}}, \beta_{\mathrm{AF}}$	1 W/Mbps	[141]
P_D^c	0.1 W	[66]
$P_{\text{control board}}$	1.5 W	[127, 130]
$P_{i,v}(1,0), P_{i,h}(1,0)$	0	[127]
$P_{i,v}(1,1), P_{i,h}(1,1)$	0.01 W	[127]
$P_{\text{drive circuit}}^{\text{PIN}}$	0.07 mW	[127]
$P_{\text{drive circuit}}^{\text{Varactor}}$	0.43 W	[127]

Table 4.1: System parameters.

The simulation configuration described in Figure 4.4 is examined, wherein the source and RIS/relay are positioned at predetermined locations, while the destination's location is determined by the variable d_1. First, the performance of the PSO algorithm is evaluated. Figure 4.5 shows the total power consumed by the RIS-assisted transmission system progressively decreases as the algorithm experiences additional iterations. For PIN-diode-based RIS, the total power drops significantly, by around 9 dB, within the first few iterations. For the varactor-diode-based RIS, the power decreases rapidly in the first few iterations but not as sharply as the RIS PIN to reach half of the power (3 dB less) after about 10 iterations. The observed differences in the total power between the RIS PIN and RIS Varactor configurations can be attributed to the inherent operational characteristics of the operational cost of each type. For the PIN diode configuration, the power consumption of UCs is generally higher compared to that of varactor diodes. However, the proposed

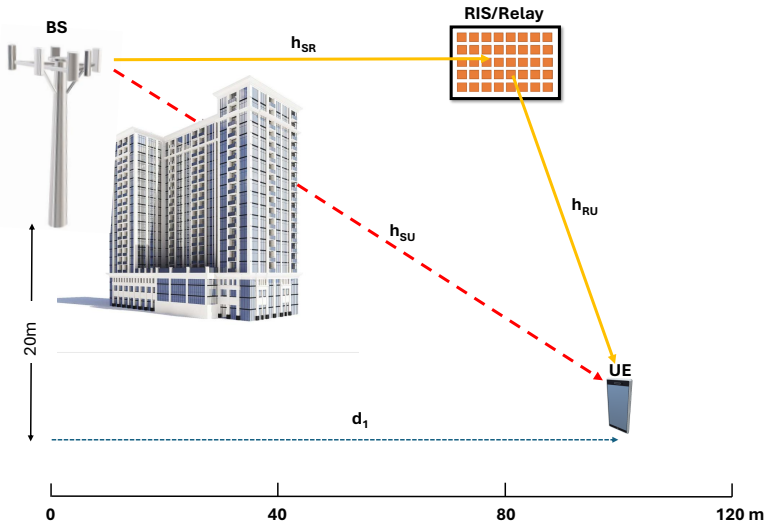

Figure 4.4: Simulation setup.

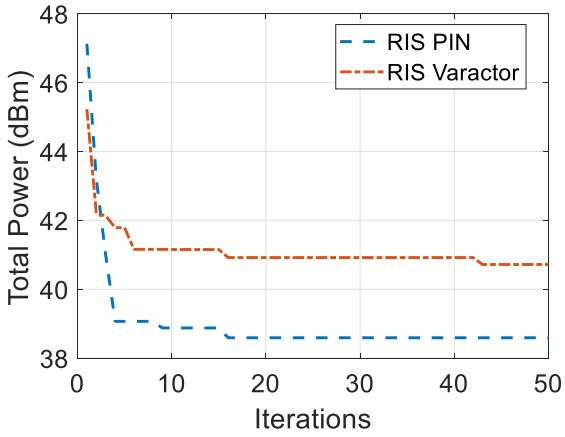

Figure 4.5: The total power consumed by the RIS-assisted transmission system Vs PSO iterations ($\bar{R} = 8$ bit/s/Hz, $d_1 = 80m$).

algorithm can minimise this power by selecting the optimal number of elements and their corresponding configurations, allowing for more efficient use of power through strategic adjustments. In contrast, the power consumption in the varactor diode configuration primarily depends on the drive circuit power in addition to the transmit power. This dependency on drive circuit power leaves less room to optimise overall power consumption.

Figure 4.6 investigates the relationship between the total power consumption and distance d_1 in various wireless communication scenarios. The analysis examines the total power required to achieve the desired data rate $\bar{R}$ as a function of the distance parameter d_1. One striking observation is that RIS-assisted transmission (both PIN-diode-based and varactor-diode-based) is more power-efficient compared to traditional relay methods (DF and AF), especially as the user becomes closer to the RIS/relay position. It can be also noticed that as the target data rate increases from 8 bit/s/Hz to 10 bit/s/Hz, the power

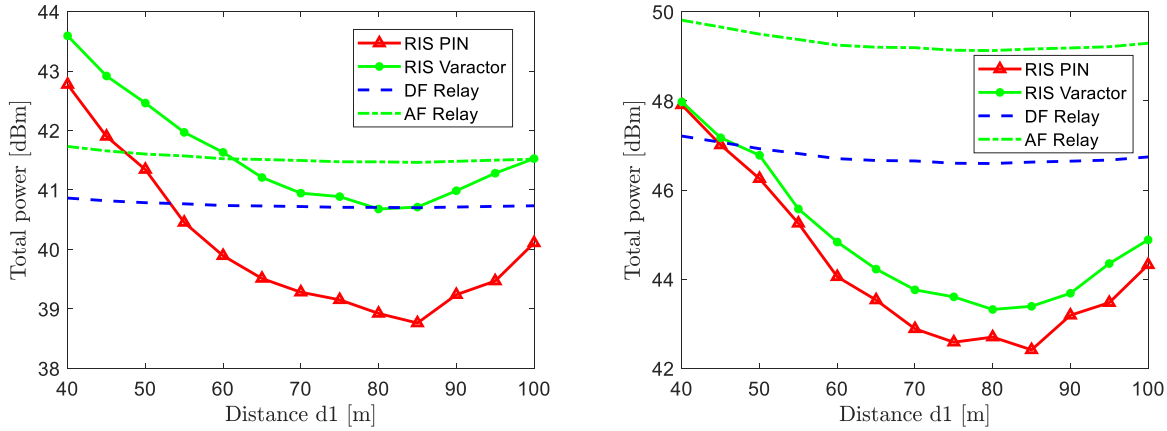

(a) $\bar{R} = 8$ bit/s/Hz (b) $\bar{R} = 10$ bit/s/Hz

Figure 4.6: The total power needed to achieve a spectral efficiency of $\bar{R}$ bit/s/Hz as a function of distance d_1.

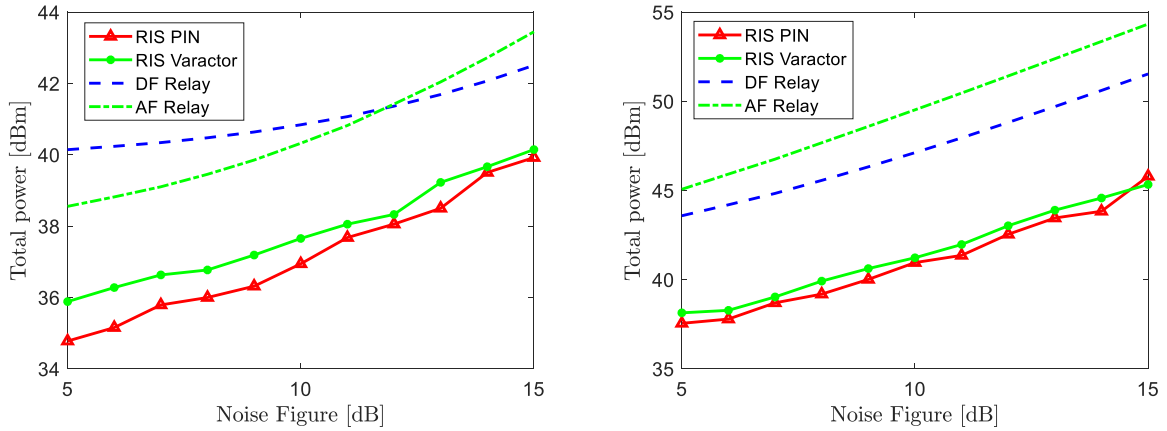

(a) $\bar{R} = 8$ bit/s/Hz (b) $\bar{R} = 10$ bit/s/Hz

Figure 4.7: The total power needed to achieve a spectral efficiency of $\bar{R}$ bit/s/Hz as a function of distance noise figure.

savings from using RIS is even more significant compared to relays. PIN-diode-based RIS-assisted transmission shows the lowest total power consumption, particularly effective in the mid-range value of d_1 (approximately 60 to 90 m), while AF relay-assisted transmission shows the highest power consumption among the compared methods. Another interesting observation is that the gap between total power requirements between DF relay-assisted transmission and AF relay increases with higher data rates, while total power consumption curves of two RIS configurations become closer to each other in case of targeting higher data rates.

For the following simulations, the user location is also chosen at this distance to illustrate the maximum achievable benefits of the RIS placement for the given simulation setup.

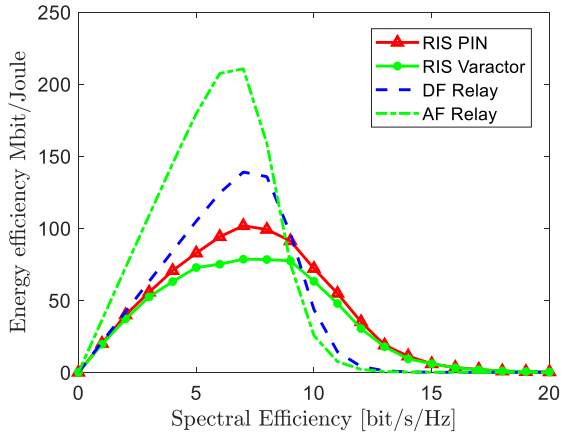

Figure 4.8: End-to-end energy efficiency [Mbit/Jule] as a function of the spectral efficiency [bit/s/Hz].

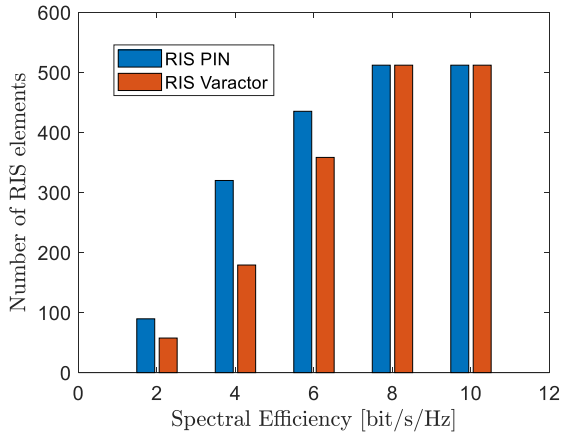

Figure 4.9: Optimal number of RIS elements VS. spectral efficiency.

Figure 4.7 shows the total power consumption for the proposed systems as a function of the noise figure. As expected, the results show that as the noise figure increases, the total power consumption increases for all scenarios. Both RIS types show similar power consumption trends, with the RIS PIN slightly more efficient. Since AF relays do not amplify only the signal but also the noise, AF relay-assisted transmission consistently exhibits the highest power consumption. It can also be observed that the efficiency of RIS-assisted transmission is more pronounced at higher data rates (10 bit/s/Hz), as seen in Figure 4.7a, indicating robustness to noise and their suitability for high-performance communication systems. The performance gap between PIN-diode-based and varactor-diode-based RIS-assisted transmissions is relatively small and tends to decrease slightly as the noise figure increases, this can observed clearly at lower data rates (8 bit/s/Hz) as in Figure 4.7b.

The energy efficiency which is defined as $BW \cdot \bar{R}/P_{\text{total}}$ is represented as a function of spectral efficiency in Figure 4.8. At higher data rates, for example, when $\bar{R}$ is higher

than 10 (bit/s/Hz), the RIS consistently outperforms the relay-assisted transmission. This implies that, in scenarios demanding higher data rates, the RIS-supported transmission can achieve the desired rate with significantly lower transmit power compared to the traditional relaying approaches. This is due to the passive nature of RIS, which does not require additional power for processing and retransmitting signals as relays do. Therefore, the power savings are more substantial at higher rates, where active relaying would otherwise consume significantly more power. The scalability of RIS in terms of energy efficiency with increasing data rates highlights its potential for future high-throughput wireless communication systems. Conversely, when targeting lower data rates, such as setting $\bar{R}$ to 6, the relay-assisted transmission significantly outperforms the RIS-assisted transmission. This suggests that at lower data rates, the advantage of employing an RIS diminishes, and the relay becomes a competitive alternative.

Figure 4.9 shows the optimum number of RIS elements required to achieve different values of targeted spectral efficiency. It demonstrates that while both RIS types require increasing numbers of elements to achieve higher spectral efficiencies, the optimal number of elements for varactor-diode-based RIS generally less than PIN-diode-based RIS for the same performance levels. This can be explained by considering the power consumption characteristics of the drive circuits and the UC elements themselves. On one hand, the power consumption of PIN-diode-based RIS increases linearly with the number of unit cells, is minimally affected by the control DoF due to energy-efficient drive circuits, and can be significantly reduced by minimising the number of PIN diodes in the ON state, making efficient beamforming design crucial to maintain high energy efficiency. On the other hand, despite having nearly zero power dissipation in their UCs, varactor-diode-based RISs are more energy-intensive due to high drive circuit power consumption and their power consumption increases rapidly with the number of unit cells due to the high power requirements of the drive circuits. This characteristic explains why PIN-diode-based RIS offers better energy efficiency at lower data rates, and why the performance gap between the two RIS types decreases as the data rate demand increases.

Simulation is also extended to analyse the performance of UAV communications in urban environments where buildings can obstruct direct signal paths. As shown in Figure 4.10, in this setup the UAV operates at a variable height above the ground and is intended to communicate with the BS. However, due to the presence of tall buildings obstructing direct LoS communication. The channel model and simulation parameters remain the same as in the previous setting, ensuring consistency in the analysis.

Figure 4.11 investigates the relationship between the total power consumption and UAV height. Similar to Figure 4.6, the analysis examines the power required to achieve the desired data rate $\bar{R}$. At lower UAV heights (up to approximately 200 meters), the differences between RIS-assisted transmissions and relay-assisted transmissions are less

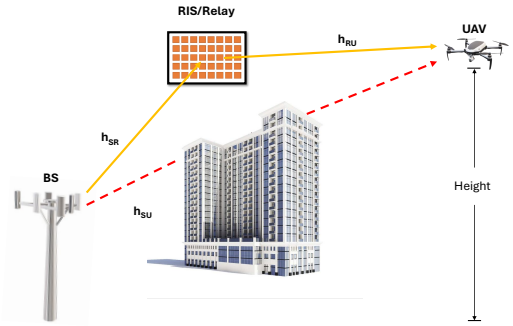

Figure 4.10: RIS-assisted UAV communications simulation setup.

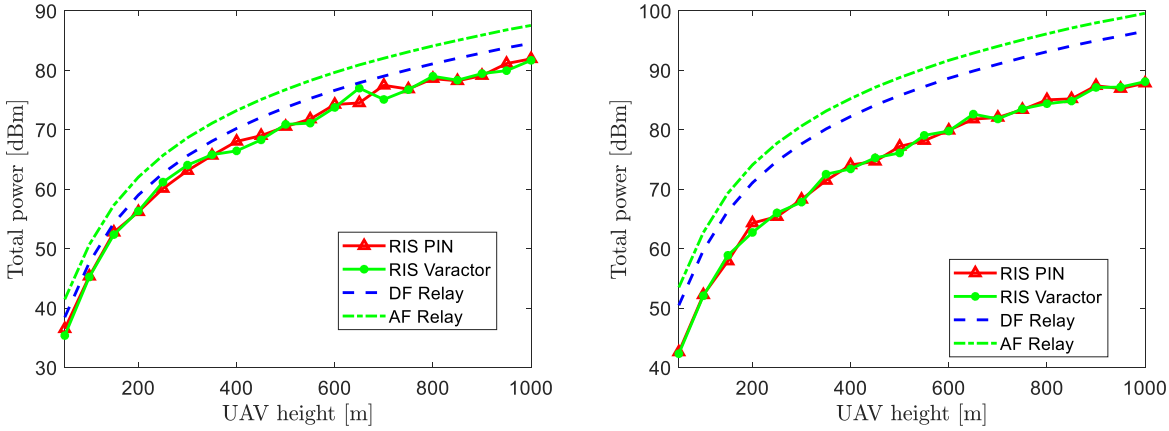

(a) $\bar{R} = 8$ bit/s/Hz (b) $\bar{R} = 10$ bit/s/Hz

Figure 4.11: The total power needed to achieve a spectral efficiency of $\bar{R}$ bit/s/Hz as a function of UAV height.

pronounced, but as the height increases, the advantages of the RIS become more evident. This suggests that in urban environments where buildings obstruct direct signal paths, RIS-assisted UAV communications may provide a more robust solution for maintaining high-quality communication links as UAV height varies. When comparing Figure 4.11a and Figure 4.11b, it can be observed that the gap between RIS-assisted transmissions and Relay-assisted transmissions power requirements increases as the rate increases. This growing gap highlights the relative efficiency of RIS technology in maintaining high data rates with lower power consumption, making it a more suitable choice for scenarios where power efficiency is crucial. Additionally, it is noteworthy that the performance of the PIN diode-based RIS and varactor diode-based is quite similar. Both exhibit a comparable pattern in power consumption across various UAV heights.

4.7 Summary

The imperative of green communication is addressed in this study through an examination of how RIS technology enhances energy efficiency and sustainability in telecommunication networks. RIS is emphasised as an eco-friendly solution to challenges in power efficiency, with its potential to align with the green communication principles highlighted. Both the performance improvement and power dissipation aspects of RIS are considered, with static and dynamic energy dissipation components analysed alongside signalling power. A precise optimisation problem is formulated, incorporating communication constraints, rate requirements, and phase shift limitations. To effectively address this problem, a robust algorithm that iteratively adjusts RIS phase shifts and element numbers is developed. Valuable insights into the intricate dynamics of wireless communication system design are provided by the proposed analysis. The significant advantages of RIS deployment, particularly at higher data rates, are underscored. Moreover, the importance of considering alternative relay techniques and phase optimisation when tailoring wireless communication systems to specific rate requirements and operating conditions is also highlighted.

Chapter 5

Efficient Data Harvesting in Urban IoT Networks: DRL for RIS-Assisted UAV Communications

The previous two chapters have analysed the performance of RIS-assisted UAV communication systems from different aspects. Building on the studies introduced in the previous chapters, this chapter explores a practical application scenario that leverages the performance gains of RIS-assisted UAV communications. Aligning with the objectives outlined in *O4*, this chapter proposes an innovative framework for RIS-assisted UAV IoT data collection, with objectives to maximise the number of served devices and average throughput. This framework addresses the complex problem of UAV trajectory design for data collection, utilising DRL algorithms. Additionally, a beamforming codebook for RIS phase optimisation and a novel IoT devices clustering algorithm are proposed to enhance data collection efficiency and reduce complexity. This chapter establishes a theoretical foundation for RIS-assisted UAV implementation, capitalising on the passive beamforming capabilities of RIS alongside the adaptable deployment and dynamic mobility of UAVs to enhance the performance of IoT networks.

5.1 Introduction

The IoT represents a paradigm shift in how devices interact and communicate with each other, as well as with humans. At its core, IoT relies on a network of interconnected devices equipped with sensors, actuators, and communication modules that collect, exchange, and act on data in real-time. This network infrastructure enables the automation of processes, remote monitoring, and control, leading to increased efficiency, productivity, and innovation across various sectors. However, as the IoT market continues to grow, with projections indicating over 500 billion IoT devices worldwide by 2030 [36], there is a

fundamental need for efficient data collection mechanisms. Traditional methods, such as terrestrial BSs, are limited in their scalability and adaptability to dynamic environments. Moreover, during peak hours, they can quickly become overloaded due to the surge in demand from mobile users. This load is further amplified by the rise of new applications like holographic communications, video streaming, and VR/AR, making terrestrial BSs even more susceptible to overload. To tackle this challenge, there is a growing need for creative solutions that can improve the efficiency of IoT data collection [37]. UAVs with their unique flexibility and high mobility characteristics, present a unique opportunity to address these limitations.

In the forthcoming wireless networks, UAVs emerge as a significant player presenting a multitude of potential applications. Serving as airborne communication platforms, they hold the potential to enhance various aspects of wireless networks, including coverage area, capacity, reliability, and energy efficiency. Their flexible deployment allows for enhancements in communication quality, unlike conventional terrestrial BSs which serve ground users within limited boundaries and lack this capability. Alternatively, they can serve as novel aerial UE terminals within the cellular network, addressing diverse applications [2,4,5,7]. With their extensive coverage and mobility, UAVs present a unique opportunity to tackle the challenges associated with IoT data collection. By optimising their trajectories, UAVs can efficiently collect IoT data, reducing the energy consumption typically associated with IoT data transmission and enabling IoT devices to upload data in real-time [9, 38–41]. Moreover, their high altitude enhances LoS connections with IoT devices, thereby improving communication success rates and coverage [5, 24, 42].

Extensive studies have been conducted to explore UAV-assisted IoT networks [9,38–41]. The work in [9] studied energy efficiency in routing UAVs for IoT data collection. Shedding light on the potential to extend the lifespan of UAVs and enhance their role in IoT data collection this work presented innovative algorithms to minimise energy consumption. The authors in [38] explored a different aspect of IoT data collection using UAVs, emphasising information age as a crucial metric. Their work offered insights into how UAVs can be strategically employed to collect data that is most relevant to real-time IoT processes. In [39], the authors addressed a specific challenge in IoT data collection dealing with time-constrained IoT devices. This study explored innovative trajectory planning strategies for UAVs to efficiently collect data from devices with time constraints. In [40], the authors explored using UAVs as relays for emergency communications in IoT networks. They proposed algorithms for efficient resource allocation, including bandwidth and power allocation, in addition to trajectory optimisation techniques to ensure timely and reliable communication during emergencies, highlighting the significance of these strategies for enhancing communication reliability in critical situations. Aiming to efficiently utilise UAVs for data collection and wireless power transfer to IoT devices, authors in [41],

presented algorithms and frameworks for jointly optimising trajectory planning and resource allocation to maximise the UAV's minimum data collection rate. The work in [142] proposed a multi-agent reinforcement learning (MARL) approach for path planning with multiple autonomous UAVs to collect data from distributed IoT devices. It addresses the challenge of adapting to changes in scenario parameters by formulating a decentralised partially observable Markov decision process (Dec-POMDP) and solving it using DRL.

The focus of the aforementioned works on UAV-assisted IoT networks lies in optimising UAV trajectories, resource allocation, and communication strategies to enhance data collection efficiency. However, these efforts often encounter obstacles in effectively addressing crucial challenges such as communication reliability, blockages, and dynamic environmental conditions. Hence, it is essential to maintain reliable communication links between UAVs and IoT devices particularly in environments featuring fading channels, signal blockages, or long distances. To address these limitations and further improve the performance of UAV-assisted IoT networks, the integration of RIS presents a promising solution. RIS has been proposed as an enabler technology for the smart wireless environment implementation allowing for real-time customisation and control of wireless channels [10, 11]. Capitalising on the unique features RIS can be used to create a reliable and improved communication environment to enable flexible, robust, and scalable IoT networks.

Due to their potential to enhance the wireless environment, RIS-assisted UAV systems for IoT networks received significant attention from both academia and industry [18, 104]. Authors in [18], investigated the potential of utilising RIS technology to aid UAVs in achieving timely and reliable data collection in IoT networks. Their work addressed a time-constrained data collection problem from a network of sensing devices by leveraging DRL for UAV trajectory planning and block coordinate descent for RIS configuration to maximise the total number of served devices during their activation periods. The work in [104] proposed a RIS-assisted UAV solution for collecting data from IoT networks within urban settings, Their approach aims to minimise the AoI for all IoT devices by jointly optimising UAV trajectories, IoT devices scheduling decisions, and RIS phase shifts.

While research in [18] and [104] present promising prospects for integrating RIS with UAVs to enhance IoT data collection, deploying IoT devices in urban environments with varying spatial and temporal attributes poses significant challenges, especially in scenarios involving a large number of IoT devices. Such challenges involve resource constraints, the timeliness of data, and scalability challenges. Effective clustering of IoT devices is therefore crucial to facilitate efficient communication and enhance overall system performance [37, 143, 144]. In clustering, IoT devices are grouped based on their spatial proximity or functional similarity to enhance data collection processes. This clustering process is closely connected with resource allocation and RIS phase shift matrix optimisation. The

authors in [143]introduced a novel approach for IoT efficient data collection using UAVs and compressive data gathering (CDG). The solution involves clustering sensor nodes, constructing forwarding trees based on CDG, and optimising UAV trajectories to minimise total transmission power and flight distance. By leveraging CDG, the proposed solution aggregates data from sensor nodes to designated projection nodes, reducing the number of transmissions and energy consumption. This is achieved by optimising the deployment of cluster heads (CHs) and UAV trajectories using K-means clustering and heuristic algorithms, respectively. In [144], the authors discussed the characteristics of sensor nodes' K-means clustering and proposed a framework for utilising multiple UAVs to minimise deployment and operational costs while adhering to budget and power constraints. The framework involves optimising the number and locations of CHs for efficient sensor data collection and UAV trajectories to minimise data collection flight time.

Despite the benefits of utilising CHs for data collection in IoT networks, there are drawbacks that require careful consideration. Reliance on CHs means that if a CH fails or malfunctions, it can disrupt the entire data collection process for the sensors within its cluster. Moreover, data transmission through CHs introduces additional latency compared to direct communication. Additionally, the scalability of CH-based clustering may become a concern as the network expands or the density of sensors increases. Another drawback is that the effectiveness of CH-based clustering heavily depends on the strategic placement of CHs within the network, hence, suboptimal placement may lead to uneven coverage, increased communication distances, and lower data collection efficiency. Lastly, CHs may become bottlenecks in the network if they cannot handle the volume of data traffic efficiently.

By associating clusters with RIS deployment, data collection efficiency can be optimised, and latency reduced. Introducing clustering based on IoT devices' geographical locations and considering time constraints, such as operational schedules, coupled with deploying multiple RISs, where each RIS can efficiently serve a cluster containing devices with different operating schedules, offers a promising approach to optimising data collection efficiency and reducing latency. Moreover, as the number of devices served by a single RIS increases, the complexity of signal processing and resource allocation also increases, potentially leading to performance degradation and reduced efficiency. Hence, aligning RIS with the operational schedules of the clustered devices enhances network efficiency and maximises the utilisation of RIS resources.

In this context, the incorporation of RIS technology enhances the effectiveness of UAVs by improving signal quality and extending communication ranges, which is crucial for maintaining robust connections with IoT devices. This is particularly significant in environments where traditional communication infrastructure may be inadequate or non-existent. As a result, RIS-assisted UAVs are uniquely positioned to address the challenges

associated with IoT data collection, offering a novel and efficient approach to gathering and transmitting data. This chapter explores how this application scenario not only demonstrates the practical benefits of RIS and UAV integration but also underscores its potential to revolutionise IoT network management and performance.

5.2 Contribution

In this work, a RIS-assisted UAV system for IoT data collection framework is proposed and optimised. Notably, the proposed data collection framework incorporates clustering of IoT devices based on geographical locations and time constraints. The trajectory of the UAV, the radio resource allocation, and the RIS phase shifts are jointly optimised to maximise the number of served IoT devices and their data rates alongside considerations of channel capacity, RIS phase shifts, and time constraints. In the proposed scenario, the UAV is chosen to operate at a fixed altitude to simplify the optimisation process and establish a baseline for comparison. To address the problem's complexity and randomness of the environment, the problem is divided into two sub-problems, leveraging DRL for UAV trajectory and resource allocation optimisation, and a codebook-based beamforming algorithm for RIS phase shifts. The algorithm process can be performed by a distributed network controller for managing IoT devices and data collection activities.

The contributions of this work can therefore be summarised as follows

- First, propose an innovative RIS-assisted UAV IoT data collection model, designed with consideration for obstructive obstacles in urban settings and the restricted energy allocation for each IoT device. Consequently, to conserve energy, each IoT device is required to remain in sleep mode for the majority of the time and only become active during the transmission of information. Particularly, each IoT device has a different time window for the UAV to collect data. Therefore, the UAV trajectory design becomes a TSPTW, which is an NP-hard problem and challenging to find the optimal solution.

- In order to efficiently serve IoT devices, a novel IoT devices clustering algorithm, is proposed, considering their activation time window and physical location. It helps to significantly increase the amount of data collection and reduce complexity.

- To address the complexity of the formulated optimisation problem, a DRL algorithm is employed for UAV trajectory optimisation and scheduling decisions, alongside a beamforming codebook approach for RIS phase optimisation.

- Drawing inspiration from the practical necessities of human safety measurements, it is recognised that the more data is gathered, the more accurate predictions become.

This drives exploration into an optimisation problem aimed at maximising the average data rate while ensuring a predetermined number of served IoT users, as established in the first problem.

5.3 System Model

As shown in Figure5.1, in urban settings, the proposed system assumed a wireless network with I IoT devices. Each IoT device's location within the simulation environment by its coordinates (x_i, y_i, z_i), for $i \in \{1, \ldots, I\}$. The spatial distribution of IoT devices follows a normal distribution, implying that their positions within the simulation environment are statistically clustered around a central tendency. Most devices are concentrated near the mean coordinates $(\bar{x}, \bar{y}, \bar{z})$, with deviations from the mean reflecting the inherent variability captured by the normal distribution. A UAV is available to collect data from these devices over a target time span N. The position of the UAV is denoted by $(x_U[n], y_U[n], z_U[n])$, for $n \in \{1, \ldots, N\}$. Because of their limited energy and blockage caused by the environment, IoT devices are usually unable to communicate over long distances, hence, K RISs each equipped with $M_h \times M_v$ reflecting elements are distributed at $(x_{R,k}, y_{R,k}, z_{R,k})$, for $k \in \{1, \ldots, K\}$, to assist links between the UAV and the IoT devices within their assigned clusters as explained in the following section.

5.3.1 IoT Devices Activation Pattern

To save energy, IoT devices switch between active and sleep modes, transmitting data during short active periods and conserving power during longer sleep periods [145]. This assumption reflects real-world scenarios where IoT devices operate based on sensor data or predefined schedules i.e. a scheduler table containing network grouping information is broadcasted by the network. This activation sequence of the IoT devices follows a uniform distribution [18]. While the activation times follow random distribution, they are not entirely unpredictable; rather, they exhibit periodic or predictable patterns to facilitate the formation of clusters within the network. The randomness in activation times is influenced by factors such as environmental conditions, energy availability, and node density. This assumption enables the adaptability of the proposed framework to be assessed and its effectiveness in handling dynamic IoT environments to be evaluated. Additionally, UAV-enabled data collection in this setting enables the collection of diverse data types from multiple locations, encompassing spatial and contextual information.

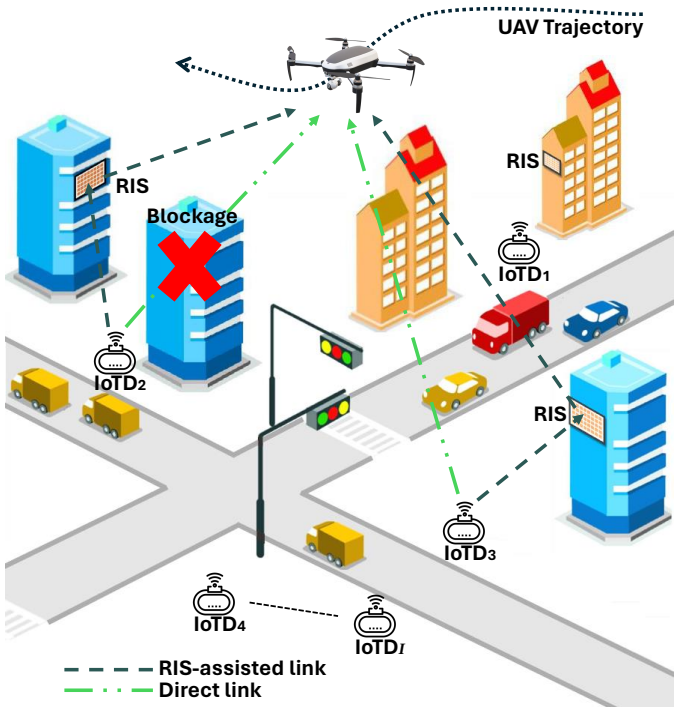

Figure 5.1: RIS-assisted UAV IoT data harvesting system model.

5.3.2 Channel Modelling

The proposed model considers a scenario where IoT devices transmit their data to the UAV using an uplink frequency division multiple access (FDMA) channel, to simplify resource allocation and scheduling, with C radio resources. Moreover, all communications are assumed to be orthogonal, i.e., no interference occurs. The links between the IoT devices and the UAV are categorised into RIS-assisted links and direct links as described in the following

RIS-assisted link

UAVs are known to operate at relatively high distances and RISs are usually deployed on the facade of urban structures [96]. This increases the likelihood of establishing a LoS connection between the RISs and the UAV. Moreover, since RISs are deployed locally, the channels between the IoT devices and the RIS belonging to the same cluster are dominated by a LoS component. Hence, the fading between UAV-RISs and RISs-IoT devices can be represented by a Rician fading with a dominant LoS component. Consequently, the channel gains between the UAV-RISs and designated RIS-i^{th} IoT device can be, respectively, given by [18]

$$h_{R,k\to U}[n] = \sqrt{\rho \left(d_{R,k\to U}[n]\right)^{-\alpha}} \sqrt{\frac{\beta}{1+\beta}} \bar{h}^{\text{LoS}}_{R,k\to U}[n], \tag{5.1}$$

and for the i^{th} IoT device belongs the k^{th}cluster

$$h_{R,k\to i} = \sqrt{\rho\left(d_{R,k\to i}\right)^{-\alpha}}\sqrt{\frac{\beta}{1+\beta}}\bar{h}^{\mathrm{LoS}}_{R,k\to i}, \tag{5.2}$$

respectively, where ρ is the path loss at a reference distance of $1m$, $d_{R,k\to U}$ is the Euclidean distance between the UAV and the k^{th} RIS , α is the path loss exponent, β is the Rice factor, and $d_{R,k\to i}$ is the Euclidean distance between the k^{th} RIS and the i^{th} IoT device. The deterministic LoS components are represented by the RIS array response defined as the steering vector of an incident wave with an elevation departure angle θ and azimuth departure angle ϕ [130]

$$\bar{h}^{\mathrm{LoS}}_{R,k\to U}[n] = a_y(\theta_{R,k\to U}[n], \phi_{R,k\to U}[n]) \otimes a_z(\theta_{R,k\to U}), \tag{5.3}$$

and

$$\bar{h}^{\mathrm{LoS}}_{R,k\to i} = a_y(\theta_{R,k\to i}, \phi_{R,k\to i}) \otimes a_z(\theta_{R,k\to i}), \tag{5.4}$$

where $\otimes$ is the Kronecker product operator. $a_h(\theta,\phi)$ and $a_v(\theta)$ represent the horizontal and vertical array response vectors of a uniform linear array (ULA), respectively

$$\mathbf{a}_h(\theta,\phi) = \left[1, e^{\frac{-j2\pi}{\lambda}d\sin\theta\sin\phi}, \cdots, e^{\frac{-j2\pi}{\lambda}d(M_h-1)\sin\theta\sin\phi}\right]^{\mathrm{T}}, \tag{5.5}$$

and

$$\mathbf{a}_v(\theta) = \left[1, e^{\frac{-j2\pi}{\lambda}d\cdot\cos\theta}, \cdots, e^{\frac{-j2\pi}{\lambda}d\cdot(M_v-1)\cos\theta}\right]^{\mathrm{T}}, \tag{5.6}$$

where d is the separation between the RIS unit cells, and λ is the wavelength.

Direct link

The communication directly established between the UAV and IoT devices is modelled by both LoS and NLoS links. Hence, the channel between the UAV and the i^{th} IoT device is given by [44]

$$h_{U\to i}[n] = P_{\mathrm{LoS}}(\theta_i[n])\left(d_{U\to i}[n]\right)^{-\alpha} + \left(1 - P_{\mathrm{LoS}}(\theta_i[n])\bar{h}_{NLoS}\left(d_{U\to i}[n]\right)^{-\alpha}\right., \tag{5.7}$$

where $P_{\mathrm{LoS}}(\theta_i[n])$ is the probability of establishing a LoS link between UAV and the i^{th} IoT device, $d_{U\to i}[n]$ is the Euclidean distance between the UAV and the i^{th} IoT device, and $\bar{h}_{NLoS}$ is NLoS link attenuation coefficient.

According to [146], the probability of a LoS link is given by

$$P_{\text{LoS}}(\theta_i[n]) = \frac{1}{1 + \xi_1 e^{-\xi_2(\theta_i[n] - \xi_1)}}, \tag{5.8}$$

where $\theta_i[n]$ is the angle between the UAV and the i^{th} ground IoT node, a, and b are environment-dependent variables.

5.4 IoT Devices Clustering

The clustering of IoT devices is crucial for efficient data collection and resource allocation in the wireless network. The proposed approach utilises a novel custom clustering strategy that accounts for the distinct activation patterns of IoT devices. Unlike conventional clustering methods, the proposed strategy incorporates both spatial and temporal considerations, specifically device location and activation period. By integrating these factors, a more refined grouping of devices is achieved, ensuring that neighbouring devices with distinct activation schedules are clustered together. This enables efficient resource allocation and communication scheduling and maximising the overall system performance [37].

IoT devices are systematically assigned to clusters that consider both their geographical locations and active transmission times. This clustering results in the formation of groups consisting of devices that share spatial adjacency and distinct patterns of activation. Once clusters are formed, the RISs are assigned based on the location of the cluster centre, ensuring that the selected RIS is the closest to the devices inside the cluster. Given the distinct activation times of devices within each cluster, the designated RIS passive beamforming will be configured to serve one device within a time slot. Employing a multi-RIS approach within this clustered setup presents a promising solution to address various challenges associated with RIS-based multi-user communication.

At the outset of the clustering process, each IoT device i is characterised by its data transmission period starting time T_i, completion time F_i, and spatial coordinates (x_i, y_i, z_i). To cluster the IoT devices, a customised version of the K-means algorithm is employed, which aligns with the proposed model. In this customised clustering approach, devices with close activation periods are grouped into separate clusters. This can be achieved by defining a threshold value say υ that determines how far apart active periods need to be for devices to be placed in the same cluster. Subsequently, the K-means clustering is applied to the customised clusters. The objective of K-means clustering is to group devices into clusters C_k $(k = 1, 2, \ldots, K)$ by minimising the within-cluster sum of squared distances $W(C_k)$ [147]

$$W(C_k) = \sum_{i \in C_k} \|\nu_i - \mu_k\|^2, \tag{5.9}$$

Algorithm 2 Combined Clustering Algorithm

Custom Clustering by Activation Periods:
Input: K, (x_i, y_i, z_i), T_i, F_i, and δ
Output: K custom clusters based on activation period dissimilarity and spatial proximity
for each IoT device i **do**
    Initialise a new custom cluster
    if no existing custom cluster has activation periods far from i by threshold υ **then**
        Create a new custom cluster with i
    else
        Add i to the existing custom cluster
Return the list of custom clusters
for each custom cluster **do**
    Sort devices within the cluster based on activation periods in descending order
    Select the top device as a representative
Create a list of representatives
Run K-means [147], get C_K
for each K-means cluster of representatives **do**
    Assign the corresponding devices from the original custom clusters to form the final clusters.
Return the list of K clusters

where $\nu_i = (x_i, y_i, z_i)$ is the features vector of the i^{th} IoT device and μ_k represents the centroid of cluster C_k. The centroids are updated iteratively based on the mean of the feature vectors within each cluster. The algorithm proceeds by assigning each IoT device to the cluster with the nearest centroid based on Euclidean distance.

The clustering algorithm follows a two-step approach that combines a customised clustering strategy based on active periods with a spatial-based clustering algorithm. Despite potentially involving multiple iterations, the computational complexity of the proposed clustering algorithm remains manageable for real-world applications.

5.5 Problem Formulation

In this section, an optimisation problem to maximise the number of IoT devices served in an environment covered by UAV and supported by multiple RISs is formulated. This objective is directly aligned with the requirements of smart city applications, where extensive IoT deployment is essential for monitoring various urban infrastructure components such as traffic, waste management, energy usage, and environmental conditions. By maximising the number of served IoT devices, the proposed approach aims to ensure comprehensive coverage and connectivity throughout the city, enabling data collection, analysis, and decision-making in real-time [148].

The SNR for the signal received by the UAV from the i^{th} IoT device belongs to the

k^{th} cluster at the n^{th} time slot can be written as

$$\Gamma_i[n] = \frac{P\left|\boldsymbol{h}_{U\to i}[n] + \boldsymbol{h}^H_{R,k\to U}[n]\boldsymbol{\Theta_k}[n]\boldsymbol{h}_{R,k\to i}\right|^2}{N_0}, \tag{5.10}$$

where $\Theta[n]$ is the RIS phase-shift matrix, P is the IoT device transmit power, and N_0 is the variance of the AWGN.

Hence, the size of data collected at time slot n from each IoT device can then be given by

$$j_i[n] = \eta_i[n]\log_2\left(1+\Gamma_i[n]\right), \tag{5.11}$$

where $\eta_i[n]$ is the scheduling decision for i^{th} IoT device represented as

$$\eta_i[n] = \begin{cases} 1, & \text{if scheduled for service} \\ 0, & \text{otherwise.} \end{cases} \tag{5.12}$$

Each IoT device is allocated a specific number of data packets each comprising Z bits intended for transmission to the UAV. Furthermore, each IoT device is introduced with an associated binary variable, denoting the successful reception of the packets by the UAV. Here, $\Lambda = 1$ signifies successful reception, while $\Lambda = 0$ represents unsuccessful reception. The goal is to maximise the number of IoT devices that can be served by optimising three critical parameters: RISs phase shift matrix $(\Theta_k[n], \forall k \in K)$, the UAV trajectory which is represented by its coordinates in the x and y dimensions $(q[n] = (x_U[n], y_U[n]), \forall n \in N)$, and IoT devices scheduling decision $(\eta_i[n], \forall i \in I)$. To this end, the optimisation problem can be formulated as follows

$$(\text{P1}): \max_{\Theta_k, q, \eta} \quad \sum_{i=1}^{I} \Lambda_i, \tag{5.13}$$

$$\text{s.t.} \quad \theta_{k,m_h,m_v}[n] = \frac{2\pi}{2^B}, \tag{5.14a}$$

$$\|\mathbf{q}[n+1] - \mathbf{q}[n]\|^2 \le V, \tag{5.14b}$$

$$0 \le x_U[n] \le X, \tag{5.14c}$$

$$0 \le y_U[n] \le Y, \tag{5.14d}$$

$$\sum_{i=1}^{I} \eta_i[n] \le L, \tag{5.14e}$$

$$\eta_i[n] \le 1 + \frac{n - T_i - 1}{O}, \tag{5.14f}$$

$$\eta_i[n] \le 1 + \frac{F_i - n}{O}, \tag{5.14g}$$

where (5.13) represents the objective function that quantifies the number of IoT devices that have been effectively flagged as successful in data transmission i.e. fully uploaded their data packets successfully. (5.14a) guarantees that phase shifts are constrained to be chosen from the possible discrete phase shifts for RIS with B control bits. (5.14b) strictly adheres to the UAV's maximum speed V, preventing the UAV from exceeding speed limits. Acting as protective measures, constraints (5.14c) and (5.14d) ensure the UAV remains within a predefined area, where the (x, y) coordinates are bounded by $x \in [0, X]$ and $y \in [0, Y]$. (5.14e) introduces constraints on the number of IoT devices scheduled for transmission during each time slot. (5.14f) and (5.14g) exert precise control over IoT devices, permitting data transmission only within their designated active time windows, and O is a large number [18].

Problem (P1) is nonconvex in nature, primarily due to the presence of the binary variable Λ_i representing successful or unsuccessful reception that introduces non-convexity into the objective function [39]. The discrete nature of the constraint in (5.14a) also contributes to the non-convexity of the optimisation problem. Additionally, the problem is non-convex with respect to the UAV trajectory variable q. Furthermore, The optimisation variable η_i is binary; thus, (5.14e) imposes integer constraints [149] leading to a mixed-integer nonlinear programming (MINLP) problem, which typically increases the computational complexity and difficulty of finding optimal solutions.

The inherent complexity arising from a mixed-integer non-convex problem, compounded by the involvement of variables with anonymous values such as the sleep and active time of IoT devices, makes the problem infeasible to tackle analytically. To address this, ML-empowered algorithms offer a data-driven approach. This will effectively handle the complexity of the problem and find near-optimal solutions.

5.6 Proposed Solution

To make the original optimisation problem tractable, the problem is divided into two distinct sub-problems. Sub-problem-1 addresses the UAV mobility and the scheduling of IoT devices, which are resolved through the application of deep Q-learning. Sub-problem-2 involves optimising the phase shifts of the RISs and is efficiently handled by leveraging a beamforming codebook. In the proposed framework, the joint optimisation of UAV trajectory, radio resource allocation, and RIS phase shifts is facilitated by a centralised optimisation algorithm. This algorithm operates at a distributed network controller responsible for managing IoT devices and data collection activities. Centralising decision-making ensures coordinated optimisation across all components of the system.

Algorithm 3 Deep Q-Learning for sub-problem 1

Input: N, ϵ_{DQL}, Learning Rate, γ_{DQL}
Output: UAV trajectory and scheduling decision
Initialise Q-network weights ξ_{DQL} randomly.
Initialise target network weights $\xi_{\text{target}} = \xi_{DQL}$.
Initialise replay buffer D with maximum capacity κ_{buffer}.
for each episode $e \in \{0, 1, 2, \ldots\}$ **do**
  for time slot n in N **do**
    Select an action a using an exploration strategy

$$\begin{cases} a \text{ is a random action with probability } \epsilon_{DQL} \\ a = \arg\max Q(s, a, \theta_{DQL}) \text{ with probability} \\ (1 - \epsilon_{DQL}) \end{cases}$$

    Execute action a (move the UAV then select devices to be scheduled), observe reward r, and transition to the next state s'.
    Store experience in replay buffer D.
    Sample a mini-batch of experiences from D.
    Calculate target Q-values for the mini-batch using the target network:
      $\text{target} = r + \gamma_{DQL} \cdot \max Q(s', a, \theta_{\text{target}})$
    Update Q-network to minimise the loss:
      $\text{loss} = (Q((s, a, \theta_{DQL}) - \text{target})^2$
      $\theta_{DQL} = \theta_{DQL} - \hat{\alpha} \cdot \nabla(\text{loss})$
    if n is a multiple of κ_{buffer} **then**
      Update target network weights: $\xi_{\text{target}} = \xi_{DQL}$.
    Update the current state s to s'.

5.6.1 Deep Q-Learning

DRL algorithm is used to optimise the UAV trajectory and the scheduling decision. DRL has a set of states **S**, a set of actions **A** and a set of rewards **R**. At each time slot, the agent collects the environment's states $\mathbf{S}[n] \in \mathbf{S}$. Based on the state the agents select an action $\mathbf{A}[n] \in \mathbf{A}$. In the next time step, the environment transitioned to a new state agent to receive a numerical reward. The process of receiving a reward can be considered an arbitrary function that maps state-action pairs to rewards. DRL parameters are defined as follows

- State space:
  - UAV 2D position.
  - IoT devices information, including IoT devices location, active period, amount of uploaded data (in bits), and link condition.
- Action space: The agent controls two aspects:
  - The UAV trajectory, with options such as left, right, forward, backward, and stop.

  - IoT devices wireless scheduling, where the agent selects a subset C from the total IoT devices I.

- Cumulative reward: The cumulative reward is determined by the sum of the number of IoT devices served successfully, given their data is successfully uploaded to the UAV.

The UAV is used as an agent, it uses DRL algorithms to learn optimal flight paths for data collection, considering various factors like the density of IoT devices and signal strength. The UAV adjusts its actions based on feedback from the environment to maximise data throughput and efficiency. The agent's strategy is built on the principles of deep Q-learning as shown in Algorithm 2. Note that two different Q-networks are used, one for each action i.e. UAV trajectory and IoT devices scheduling decision.

5.6.2 Passive Beamforming

After the RL agent has decided on the next UAV state and the scheduled IoT devices set, a codebook is used to optimise the RISs phase shifts. The RIS configuration is changed according to a two-dimensional discrete Fourier transform (2D-DTF) based codebook, and the received signal power is used to find the best configuration from the codebook.

The received signal at the UAV from the i^{th} IoT device belongs to the k^{th} cluster at the n^{th} time slot, can be represented as

$$y_i[n] = ((h_{R,k\to i} \odot h_{R,k\to U}[n])^T w_{\theta,k}[n] + h_{U\to i}[n])x_i[n] + N_0, \tag{5.15}$$

where $x_i[n] \in \mathbb{C}$ is the transmitted signal and $\odot$ is the Hadamard product symbol. The vector $w_{\theta,k} \in \mathbb{C}^{M\times 1}$ represents the k^{th} RIS reflection coefficients that include the phase shifts and amplitude losses.

Hence, the overall power gain can be presented as

$$\begin{aligned}\left|\left(\left(h_{R,k\to i} \odot h_{R,k\to U}[n]\right)^T w_{\theta,k}[n]\right) + h_{U\to i}[n]\right|^2 &= \left|\left(h_{R,k\to i} \odot h_{R,k\to U}[n]\right)^T w_{\theta,k}[n]\right|^2 \\ + 2\,\mathrm{Re}\left\{\left(\left(h_{R,k\to i} \odot h_{R,k\to U}[n]\right)^T w_{\theta,k}[n]\right)^* h_{U\to i}[n]\right\} &+ \left|h_{U\to i}[n]\right|^2,\end{aligned} \tag{5.16}$$

Assuming a weak direct link in the case of RIS-assisted transmission, the power gain can be presented as shown in 5.17 below

$$\left|\left(h_{R,k\to i} \odot h_{R,k\to U}[n]\right)^T w_{\theta,k}[n]\right|^2 = PL_{R,k\to i}PL_{R,k\to U}[n]|\left(\bar{h}_{R,k\to i} \odot \bar{h}_{R,k\to U} w_{\theta,k}\right)|^2, \tag{5.17}$$

where $PL_{R,k\to i}$ and $PL_{R,k\to U}[n]$ are the path losses from the i^{th} IoT device to the RIS and from the RIS to the UAV, respectively.

The best approach is to choose RIS phase shifts such that all reflected signals from the RIS are coherently constructed at the receiver end. Similar to MIMO transmission for a uniform planar array (UPA), optimal RIS phase shifts, for a given transmitted and desired destination angle can defined for RIS-assisted transmission using a two-dimensional discrete Fourier transform (2D-DTF)-based codebook [130]. For large RIS, the optimal phase vector $w_{\theta_o} = \text{argmax}_{|[w_\theta]_i|=1}(((h^n_{R,i} \odot h^n_{R,U})^T w_\theta)^2$ can be approximated by the columns of the DFT matrix denoted by $F(M)$. Therefore, each column of the codebook beamform $F(M_v) \otimes F(M_h) \in \mathbb{C}^{M\times M}$ could potentially serve as a reflection configuration for an incoming signal directed in a specific beam direction. Assuming angular information is unavailable due to the random environment, the codebook can be explored to find the optimal configuration that maximises the received signal power as defined in (5.17).

5.7 Optimising Communication Efficiency in Urban IoT Networks

This section considers the effect of link quality on the performance achieved by the proposed scheme. Introducing link quality, results in a modified objective and additional constraints in the previous optimisation problem (P1). The original objective, which focused on maximising the number of served IoT devices through optimisation of RISs phase shifts, UAV trajectory, and the scheduling decision, can be extended to maximise the average data rate of the served devices.

This extension brings several expected benefits. Firstly, by maximising the average data rate, the enhancement of communication quality is inherently prioritised, which is influenced by link conditions such as multipath fading, LoS probability, and signal attenuation, leading to a better representation of the actual communication environment. Secondly, the extension of the optimisation objective facilitates enhanced system performance by prioritising the maximisation of the cumulative data rate. By optimising resource allocation or scheduling decisions with a focus on data rate, it can be ensured that the system operates at its highest capacity, efficiently utilising available resources to not only serve a greater number of IoT devices but also improve their overall communication quality. Finally, this approach enables the optimised utilisation of resources, ensuring that every component of the system is utilised effectively to achieve the desired communication efficiency. By aligning the objective of maximising the number of served IoT devices with the overarching goal of maximising the average data rate, resources can be allocated in a manner that maximises the number of served devices with minimal resources. This includes efficiently utilising bandwidth and power to ensure optimal network performance.

The average data rate for the i^{th} IoT device over N time slots can be expressed as

$$\bar{R}_i = \frac{1}{N} \sum_{n=1}^{N} j_i[n]. \tag{5.18}$$

The new objective function is modified to prioritise maximising the average data rate of the served devices. It also ensures that the system operates at its highest capacity and efficiently utilising available resources to serve the maximum number of IoT devices. Additionally, to ensure a minimum level of service, an additional constraint is introduced, providing that the system must serve at least a specified minimum number of IoT devices $IoTD_{min}$, as determined by the previous baseline algorithm.

$$(\text{P2}) : \max_{\Theta,q,\eta} \quad \sum_{i=1}^{I} \Lambda_i \times \bar{R}_i, \tag{5.19}$$

$$\text{s.t.} \quad \text{Constraints (11b)-(11i)}, \tag{5.20a}$$

$$\sum_{i=1}^{I} \Lambda_i \geq IoTD_{min}, \tag{5.20b}$$

where the constraint in (5.20b) serves as a safeguard to guarantee a certain level of service delivery, even under varying network conditions and demand fluctuations.

To solve the optimisation problem in (P2), a similar approach as in (P1) is adopted, with adjustments made to accommodate the revised objective function. Specifically, the revised cumulative reward function considers now the average data rate, prioritising the delivery of high-quality services to IoT devices.

5.8 Numerical and Simulation Results

In this section, the simulation results that provide insights into the performance of the proposed solution are presented and analysed. The simulation setup utilises deep-Q learning to construct the agent, and this is implemented using Python and PyTorch. Three linear layers are employed in the DRL component, with the activation function for the middle layers set to be tanh, while softmax is used for the output layer. Each internal layer comprises 128 neurons, and the Adam optimiser is used to minimise the loss function. Notably, the learning rate is configured at 0.003. To ensure robustness and precision, the results are averaged over 500 data tests, i.e. initial state of the environment. The RISs are located within the environment at the following coordinates: $\left(x_{R,1}, y_{R,1}, z_{R,1}\right) = (200, 400, 20)$, $\left(x_{R,2}, y_{R,2}, z_{R,2}\right) = (0, 100, 20)$, and $\left(x_{R,3}, y_{R,3}, z_{R,3}\right) = (400, 100, 20)$. The remaining parameters utilised in the study are detailed in Table 5.1 unless specified otherwise.

Table 5.1: Simulation parameters

Parameter	Value
I	100 devices
T	100 s
K	3
B	2 bits
β	8 dB
α	4
P	20 dBm
C	3
ρ	20 dBm
M	10
Z_i	64 bits
Number of data packets	2
Service Area	400×400 m^2
UAV height	100 m
IoT active period length	10 sec
ξ_1, ξ_2 (for dense urban environment)	11.95, 0.136

The Dragino LHT65 Temperature and Humidity Sensor is an excellent example of a device that aligns well with the parameters discussed. This sensor is specifically designed for environmental monitoring and can measure temperature, humidity, and particulate matter, making it highly suitable for data collection scenarios described in this chapter.

5.8.1 Baseline Data Collection Scheme

This scheme serves as the baseline for the data collection framework introduced in problem (P1), where the goal is to maximise the number of IoT devices served by optimising critical parameters such as RIS phase shift matrix, UAV trajectory, and IoT device scheduling decisions.

First, the performance of the DRL agent is observed. Figure 5.2 shows that the cumulative reward, which reflects the number of IoT devices successfully served, progressively rises as the agent experiences additional episodes. Furthermore, it is noted that the system starts to converge after approximately 400 training episodes.

Figure 5.3 presents data depicting the number of devices successfully served within their specified activation period as the number of the RIS elements is changed, measured in terms of the number of elements. Several key observations can be made from this analysis. First, it is evident that the size of the RIS plays a pivotal role in enhancing system performance. As more RIS elements are introduced, the system can serve a more significant number of devices effectively.

Furthermore, the figure reveals an interesting insight: when the phase shifts of the RIS

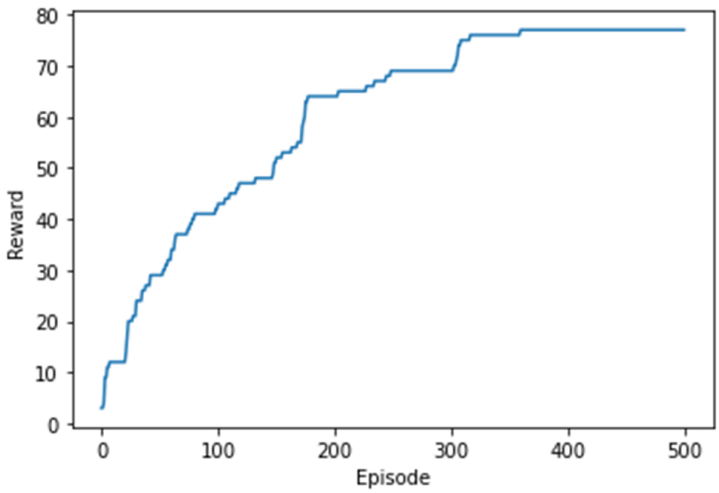

Figure 5.2: DRL reward vs. episodes of training.

elements are randomly selected, the performance improvement is limited. However, when the RIS elements are optimised, significant gains become apparent. This improvement depends on how the UAV trajectory is optimised in conjunction with the RIS elements. Notably, the best performance is achieved when both the UAV trajectory and the RIS phase shifts are jointly optimised.

In Figure 5.4 the simulation varied the number of IoT devices in the network and examined the percentage of devices served. Notably, when the number of devices is relatively small, 20 device, significant performance gains are observed, particularly with the proposed algorithm. The difference in performance between the proposed algorithm and the closest baseline scenario exceeded 50%. However, as the number of IoT devices increases, the rate of successful service delivery decreases. This reduction can be attributed to the constrained availability of the UAV wireless resources. Consequently, when more IoT devices were introduced to the network, the UAV's capacity to meet the network's requirements diminished. Nevertheless, increasing the number of RIS elements can potentially address this challenge.

In Figure 5.5, the influence of different data packet sizes generated by IoT devices on the percentage of served IoT devices is investigated, plotting these percentages against data packet size in bits. In general, it is observed that a smaller data size leads to better service. This is primarily because of the reason that smaller data can be uploaded in shorter time frames, allowing the UAV to allocate more of its resources to serve additional requests. Notably, the DRL+Beamforming codebook method consistently achieved the highest performance compared to the baseline methods across all scenarios.

Similarly, simulation in Figure 5.6 explores the impact of the average activation period of IoT devices on the number of devices successfully served within the stipulated time frame. This investigation reveals noteworthy insights. Firstly, it is clear that the average

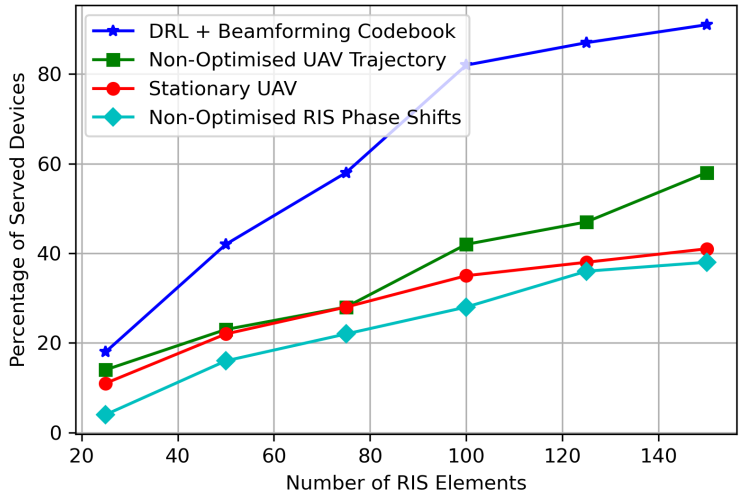

Figure 5.3: Percentage of served devices versus the number of RIS elements.

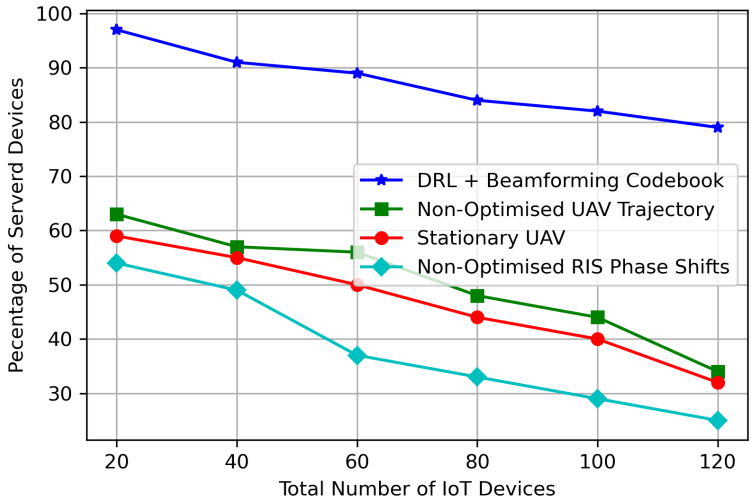

Figure 5.4: Percentage of served devices versus the total number of devices.

activation period has a substantial influence on system performance. When IoT devices have longer activation periods, the system demonstrates a higher capacity to serve a greater number of devices efficiently. This is because longer activation periods create more opportunities for the UAV to fulfil their data collection needs. Moreover, the results indicate that the effectiveness of the system is contingent on how the UAV's trajectory and the operation of the RIS are optimised in response to varying activation periods. When these elements are optimised in a coordinated manner, substantial performance improvements are evident.

5.8.2 Adaptive Link Quality-Based Scheme

This scheme focuses on adapting to link quality variations to improve system performance, particularly by prioritising maximising the average data rate of the served device. The

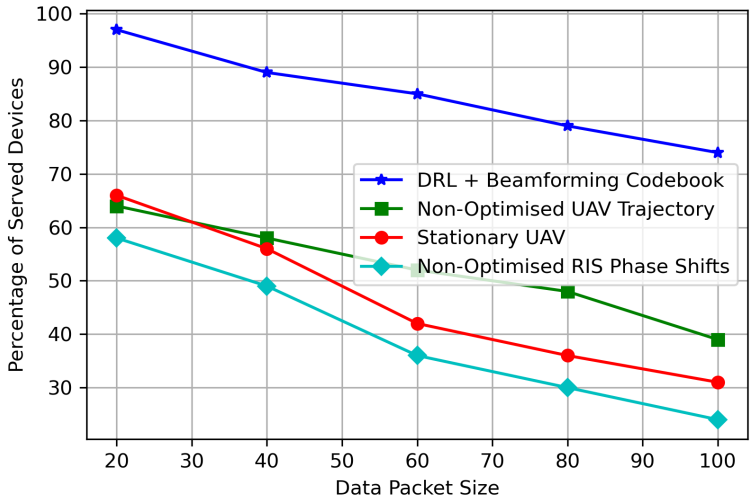

Figure 5.5: Percentage of served devices versus the data packet size.

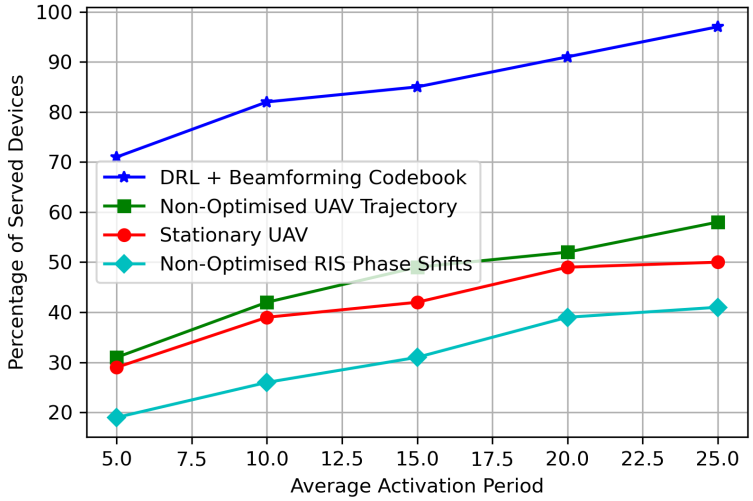

Figure 5.6: Percentage of served devices versus the average active period.

performance of the proposed approach in (P2) to optimise communication efficiency is compared against the baseline method evaluated in the previous simulations, demonstrating significant improvements in communication efficiency and overall system performance. Figure 5.7 and Figure 5.8 highlight the improvements resulting from this adaptive link quality-based scheme.

Figure 5.7 illustrates how the data rate increases with the implementation of the modified optimisation problem. As the optimisation problem now prioritises maximising the data rate of served devices, results show how the system's performance has improved in terms of the data rate compared to the baseline scenario. Additionally, it is evident that the data rate increases with the inclusion of more RIS elements, highlighting the scalability of the proposed approach. Notably, for the baseline scenario without rate optimisation, the data rate remains within a constant range.

Figure 5.8 demonstrates the improvement in the number of devices served by the

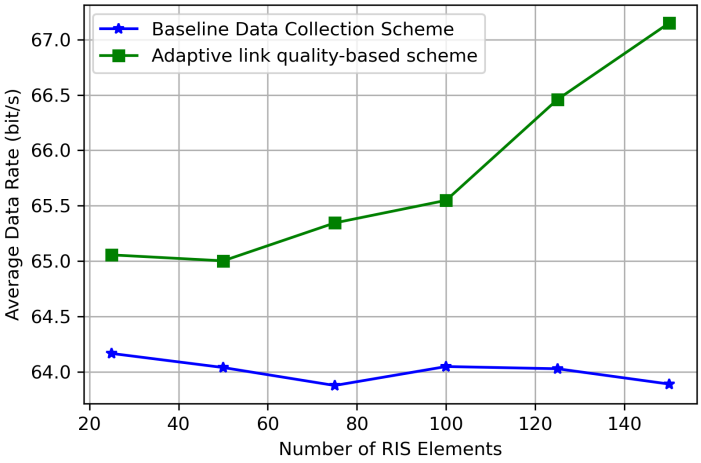

Figure 5.7: Average data rate versus the number of RIS elements.

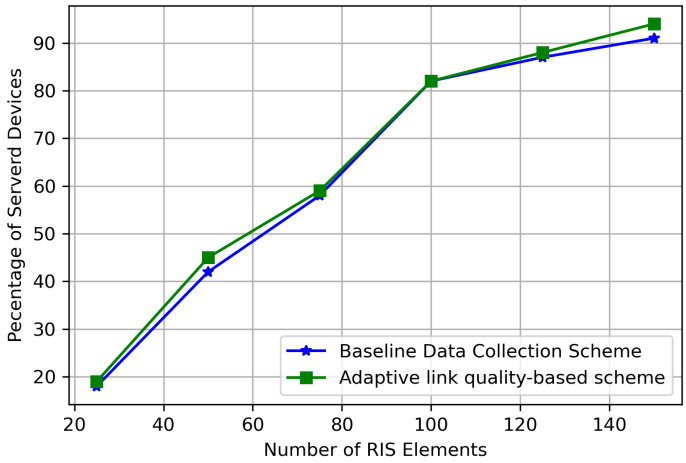

Figure 5.8: Percentage of served devices versus the number of RIS elements.

proposed system as a result of the modifications. It compares the number of devices served before and after the optimisation, highlighting the increase in the number of devices accommodated within the system. This improvement can be attributed to the modified objective function, which now prioritises maximising the cumulative data rate of served devices. By optimising resource allocation and scheduling decisions to maximise data rate, a greater number of devices is effectively served within the system's operational constraints.

Figure 5.8 demonstrates the effectiveness of the adaptive link quality-based scheme in improving the data rate of served devices while maintaining a similar level of service in terms of the number of devices served. A comparison between the number of devices served before and after optimisation reveals a marginal increase, indicating that roughly the same number of devices are accommodated within the system. However, the significant improvement lies in the cumulative data rate of served devices, attributed to the modified objective function prioritising data rate maximisation. By optimising resource allocation and scheduling decisions, the modified scheme enables devices to exploit channel quality

more effectively, resulting in higher data transmission rates without compromising the number of devices served.

These results provide evidence of the effectiveness of the proposed rate maximisation approach. The increase in data rate over time showcases the improved efficiency of the system in transmitting data, while the increase in the number of served devices demonstrates the system's enhanced capacity to accommodate more devices. By prioritising data rate optimisation and introducing additional constraints to ensure a minimum number of served devices, the rate maximisation approach effectively addresses the objectives of improving communication efficiency and system performance.

5.9 Summary

In this study, a RIS-assisted UAV framework for IoT data collection was proposed. DRL algorithm was used to optimise the UAV trajectory and the IoT devices scheduling, and a codebook-based algorithm for RIS beamforming was used to optimise the RIS phase shift matrix to maximise the number of served IoT devices. Findings highlight the potential of combining DRL and RIS to address the challenges of serving IoT devices in wireless networks leading to significant improvements in system performance. Furthermore, the investigation was extended to prioritise data rate maximisation underscoring the importance of addressing link conditions in urban IoT networks. This extension reflects the focus on improving the efficiency of data transmission within the system. By incorporating an adaptive link quality-based scheme, the proposed approach enhanced communication efficiency and overall system performance. Looking forward, findings underscore the potential of this integrated approach and pave the way for future research focusing on RIS-assisted UAV networks' real-world deployment scenarios in similar contexts.

Chapter 6

Conclusions and Future Works

This chapter summarises the conclusions drawn from this thesis and outlines potential directions for future research expansion and exploration.

6.1 Conclusion Remarks

In Chapter 3, a comprehensive performance analysis of RIS-assisted UAV communication systems has been presented, focusing on three distinct scenarios: RIS-assisted UAV-aided communications, RIS-assisted cellular-connected UAV communications, and multi-hop RIS-assisted UAV communications. The proposed theoretical frameworks have enabled a detailed investigation of the coverage and communication reliability of these systems. By deriving accurate closed-form approximations for the statistical distributions of the RIS-assisted channels, analytical expressions for the SNR, outage probability, and BER were obtained. Results highlighted the significant improvements in system performance with the increase in the number of RIS elements, as evidenced by reduced outage probabilities and improved BER under various operational conditions. Furthermore, the validation of analytical expressions through extensive Monte Carlo simulations confirmed the accuracy and practical relevance of the proposed models. The analysis demonstrated that the optimal placement and trajectory of UAVs, in conjunction with the strategic deployment of RIS elements, are crucial for enhancing the reliability and efficiency of wireless communication networks. This research paves the way for future studies to explore more sophisticated optimisation techniques and further integration of RIS-assisted UAV systems, aiming to meet the evolving demands of next-generation communication networks.

In Chapter 4, the impact of RIS technology on enhancing the energy efficiency and sustainability of wireless communication networks has been examined. Within this chapter, a detailed breakdown of RIS-assisted communications power consumption has been introduced, providing a comprehensive breakdown of RIS power dissipation

components. An optimisation problem has been formulated with the objective of minimising the total power consumption of RIS-assisted communication systems while adhering to achievable rate constraints. The problem considered the phase shift configuration and the number of RIS elements as optimisation variables. PSO algorithm has been proposed to solve this non-convex optimisation problem, the algorithm has been shown to effectively handle the complexities of the problem, optimising both the number of RIS elements and their phase shifts to achieve power dissipation reduction. Furthermore, the chapter has undertaken a comparative analysis between RIS and traditional active relaying solutions. Simulation results have demonstrated that RIS-assisted transmission is generally more power-efficient compared to DF and AF relays, especially at higher data rates, highlighting its potential for future high-throughput wireless communication systems. This research has provided a comprehensive study on the optimisation of power efficiency in RIS-assisted communications, laying a solid foundation for future advancements in energy-efficient and sustainable wireless networks.

Chapter 5 has proposed an innovative framework for RIS-assisted UAV communication systems designed to enhance IoT data collection in urban environments. The framework has proposed a novel IoT device clustering algorithm based on their geographical locations and activation periods. Furthermore, to leverage the performance gains of RIS and UAV technologies, the proposed framework optimises UAV trajectory, resource allocation, and RIS phase shifts to maximise the number of served IoT devices and average throughput. DRL algorithm has been proposed to optimise the UAV trajectory and the IoT devices scheduling. Additionally, a codebook-based beamforming algorithm for RIS phase optimisation was introduced to optimise the RIS configuration. The simulation results demonstrated the effectiveness of the proposed framework, highlighting significant improvements in the number of served IoT devices and data rates compared to baseline methods. The analysis of RIS elements' impact revealed that increasing the number of RIS elements significantly enhances system performance, underscoring the importance of RIS configuration in achieving reliable and efficient communication links. This research provides valuable insights into RIS-assisted UAV communication systems applications in IoT data collection, offering a practical solution to address the challenges of dynamic urban environments.

Overall, this thesis has focused on establishing a solid foundation for the deployment of RIS-assisted UAV communication systems. The innovative frameworks, robust mathematical tools, and machine learning-based optimisation strategies, and analyses presented in this thesis, have presented valuable insights to leverage RIS-assisted UAV systems for improved communication efficiency and performance. The work has revealed several key findings that highlight the transformative potential of RIS-assisted UAV systems in modern wireless communication networks. These findings have also presented

a comprehensive understanding of how RIS-assisted UAV communication systems can leverage mathematical tools and optimisation strategies, including machine learning techniques to enhance performance. These findings contribute to the ongoing development of next-generation communication networks, capable of meeting the evolving demands for efficiency, reliability, and sustainability.

6.2 Future Work

The domain of RIS-assisted UAV communications is an extensive and promising research area with numerous potential applications that remain to be thoroughly explored. The contributions presented in this thesis represent the initial steps towards multiple research directions in the study of RIS-assisted UAV communications. In this section, a few interesting research topics are highlighted representing extensions or improvements to the work presented in this thesis.

6.2.1 Optimising Power Efficiency in RIS-Assisted MIMO Communication Systems: Joint Active and Passive Beamforming

The proposed work on examining the impact of RIS technology on enhancing the energy efficiency and sustainability of wireless communication networks was limited by the single antenna assumption at the transmitter. This simplification neglects the potential benefits of MIMO technology, which could provide enhanced spatial diversity and multiplexing gains. Integrating MIMO with RIS would allow for a more comprehensive optimisation, addressing the limitations and unlocking further potential in power-efficient, high-capacity wireless communication systems.

In light of this, adopting MIMO transmission with active beamforming capabilities at the source end can introduce a significant improvement to the framework. The combination of MIMO and RIS will be explored to optimise beamforming strategies, phase shift configurations, and the number of RIS elements to further reduce power consumption while maintaining high data rates and robust communication links. By jointly considering the active beamforming at the source node and the phase shift design at the RIS, the optimisation framework will be adapted to account for the additional degrees of freedom, and advanced algorithms will be developed to jointly optimise the transmitter's beamforming vectors and the RIS phase shifts. These algorithms would need to take into account the complex interactions between the multiple antennas and the RIS elements, and would likely require advanced machine-learning techniques to achieve optimal performance.

6.2.2 Scalable Data Collection in Multi-Region Urban IoT Networks: Federated Learning-Enabled RIS-Assisted UAV Communications

An exciting extension for the IoT data harvesting framework is incorporating Federated Learning (FL) with multiple UAVs serving different regions. The objective is to enhance the scalability and efficiency of the RIS-assisted UAV communication framework for IoT data collection across multiple regions. Each UAV will collect data from IoT devices within its designated region and perform local model training. This ensures data privacy as raw data remains on the UAVs. The locally trained models are sent periodically to a central server for aggregation into a global model, which is then redistributed to the UAVs for further training. Implementing algorithms for coordinating UAV flight paths and resource allocation ensures optimal coverage and data collection efficiency. A hierarchical control system can be used where a central controller coordinates multiple UAVs, each performing FL-based local training. Dynamic clustering algorithms can be employed to assign UAVs to regions based on the geographical distribution and activation patterns of IoT devices. Advanced communication protocols should be utilized to efficiently share model updates between UAVs and the central server, minimising bandwidth usage and latency. The frequency of model updates can be adjusted based on UAV mobility patterns and the dynamics of the IoT environment, balancing training accuracy and communication overhead. The global model is applied to dynamically adjust the phase shifts of RISs in each region. Collaborative management of RIS configurations in overlapping regions by UAVs can help avoid interference and maximise overall system performance.

This extension represents a significant improvement over the existing framework, leveraging advanced machine learning techniques to address the challenges of dynamic urban environments and multi-region IoT data collection, representing an extension or improvement for the work represented in this thesis.

Bibliography

[1] Q. Wu *et al.*, "A Comprehensive Overview on 5G-and-Beyond Networks With UAVs: From Communications to Sensing and Intelligence," *IEEE J. Sel. Areas Commun.*, vol. 39, no. 10, pp. 2912–2945, June 2021.

[2] Y. Zeng, Q. Wu, and R. Zhang, "Accessing From The Sky: A Tutorial on UAV Communications for 5G and Beyond," *Proc. IEEE Proc.*, vol. 107, no. 12, pp. 2327–2375, Dec. 2019.

[3] G. Geraci *et al.*, "What Will the Future of UAV Cellular Communications Be? A Flight From 5G to 6G," *IEEE Commun. Surveys Tuts.*, vol. 24, no. 3, pp. 1304–1335, May 2022.

[4] B. Li, Z. Fei, and Y. Zhang, "UAV Communications for 5G and Beyond: Recent Advances and Future Trends," *IEEE Internet Things J.*, vol. 6, no. 2, pp. 2241–2263, Dec. 2018.

[5] M. Mozaffari *et al.*, "A Tutorial on UAVs for Wireless Networks: Applications, Challenges, and Open Problems," *IEEE Commun. Surveys Tuts.*, vol. 21, no. 3, pp. 2334–2360, Mar. 2019.

[6] Y. Zeng, J. Lyu, and R. Zhang, "Cellular-Connected UAV: Potential, Challenges, and Promising Technologies," *IEEE Wirel. Commun.*, vol. 26, no. 1, pp. 120–127, Sept. 2018.

[7] N.-N. Dao *et al.*, "Survey on Aerial Radio Access Networks: Toward a Comprehensive 6G Access Infrastructure," *IEEE Commun. Surveys Tuts.*, vol. 23, no. 2, pp. 1193–1225, Feb. 2021.

[8] A. Orsino *et al.*, "Effects of Heterogeneous Mobility on D2D-and Drone-Assisted Mission-Critical MTC in 5G," *IEEE Commun. Mag.*, vol. 55, no. 2, pp. 79–87, Feb. 2017.

[9] J. Baek, S. I. Han, and Y. Han, "Energy-Efficient UAV Routing for Wireless Sensor Networks," *IEEE Trans. Veh.*, vol. 69, no. 2, pp. 1741–1750, Dec. 2019.

[10] M. Di Renzo *et al.*, "Smart Radio Environments Empowered by Reconfigurable Intelligent Surfaces: How It Works, State of Research, and The Road Ahead," *IEEE J. Sel. Areas Commun.*, vol. 38, no. 11, pp. 2450–2525, Jul. 2020.

[11] S. Gong *et al.*, "Toward Smart Wireless Communications via Intelligent Reflecting Surfaces: A Contemporary Survey," *IEEE Commun. Surv. Tutor.*, vol. 22, no. 4, pp. 2283–2314, June 2020.

[12] L. Mohjazi *et al.*, "The Journey Toward 6G: A Digital and Societal Revolution in the Making," *IEEE Internet Things Mag.*, vol. 7, no. 2, pp. 119–128, Mar. 2024.

[13] Q. Wu *et al.*, "Intelligent Reflecting Surface-Aided Wireless Communications: A Tutorial," *IEEE Trans. Commun.*, vol. 69, no. 5, pp. 3313–3351, Jan. 2021.

[14] M. Di Renzo *et al.*, "Reconfigurable Intelligent Surfaces vs. Relaying: Differences, Similarities, and Performance Comparison," *IEEE open j. Commun. Soc.*, vol. 1, pp. 798–807, June 2020.

[15] E. Björnson, Ö. Özdogan, and E. G. Larsson, "Reconfigurable Intelligent Surfaces: Three Myths and Two Critical Questions," *IEEE Commun. Mag.*, vol. 58, no. 12, pp. 90–96, Dec. 2020.

[16] L. Yang *et al.*, "On the Performance of RIS-Assisted Dual-Hop UAV Communication Systems," *IEEE Trans. Veh. Technol*, vol. 69, no. 9, pp. 10 385–10 390, June 2020.

[17] L. Ge *et al.*, "Joint Beamforming and Trajectory Optimization for Intelligent Reflecting Surfaces-Assisted UAV Communications," *IEEE Access*, vol. 8, pp. 78 702–78 712, 2020.

[18] A. Al-Hilo *et al.*, "RIS-Assisted UAV for Timely Data Collection in IoT Networks," *IEEE Syst. J.*, vol. 17, no. 1, pp. 431–442, Nov. 2022.

[19] S. Fang, G. Chen, and Y. Li, "Joint Optimization for Secure Intelligent Reflecting Surface Assisted UAV Networks," *IEEE Wirel. Commun. Lett.*, vol. 10, no. 2, pp. 276–280, Sept. 2021.

[20] J. Lyu *et al.*, "Placement Optimization of UAV-Mounted Mobile Base Stations," *IEEE Commun. Lett.*, vol. 21, no. 3, pp. 604–607, Nov. 2016.

[21] M. Alzenad *et al.*, "3-D Placement of an Unmanned Aerial Vehicle Base Station (UAV-BS) for Energy-Efficient Maximal Coverage," *IEEE Wirel. Commun. Lett.*, vol. 6, no. 4, pp. 434–437, MAy 2017.

[22] H. Shakhatreh and A. Khreishah, "Optimal Placement of a UAV to Maximize the Lifetime of Wireless Devices," in *2018 14th International Wireless Communications & Mobile Computing Conference (IWCMC)*, June 2018, pp. 1225–1230.

[23] C.-C. a. Lai, "On-Demand Density-Aware UAV Base Station 3D Placement for Arbitrarily Distributed Users With Guaranteed Data Rates," *IEEE Wirel. Commun. Lett.*, vol. 8, no. 3, pp. 913–916, Feb. 2019.

[24] W. Khawaja *et al.*, "A Survey of Air-to-Ground Propagation Channel Modeling for Unmanned Aerial Vehicles," *IEEE Commun. Surv. Tutor.*, vol. 21, no. 3, pp. 2361–2391, May 2019.

[25] M. A. Jan, S. A. Hassan, and H. Jung, "Chapter Five - UAVs: communication aspects and cellular service provisioning," in *Drones in Smart-Cities*, F. Al-Turjman, Ed. Elsevier, 2020, pp. 79–91. [Online]. Available: https://www.sciencedirect.com/science/article/pii/B9780128199725000057

[26] H. Xiang and L. Tian, "Development of a Low-Cost Agricultural Remote Sensing System Based on an Autonomous Unmanned Aerial Vehicle (UAV)," *Biosystems engineering*, vol. 108, no. 2, pp. 174–190, Feb. 2011.

[27] Q. Feng, J. Liu, and J. Gong, "UAV Remote Sensing for Urban Vegetation Mapping Using Random Forest and Texture Analysis," *Remote sensing*, vol. 7, no. 1, pp. 1074–1094, Jan. 2015.

[28] Y. Li *et al.*, "Geometric Correction Algorithm of UAV Remote Sensing Image for the Emergency Disaster," in *2016 IEEE International Geoscience and Remote Sensing Symposium (IGARSS)*, July 2016, pp. 6691–6694.

[29] H. Chang *et al.*, "Multi-UAV Mobile Edge Computing and Path Planning Platform Based on Reinforcement Learning," *IEEE Trans. Emerg. Top. Comput. Intell.*, vol. 6, no. 3, pp. 1–10, June 2022.

[30] L. Bariah *et al.*, "A Prospective Look: Key Enabling Technologies, Applications and Open Research Topics in 6G Networks," *IEEE Access*, vol. 8, pp. 174 792–174 820, Aug. 2020.

[31] Nokia. (2020) Sendai City Case Study. [Online]. Available: https://www.nokia.com/networks/case-studies/sendai-city/

[32] S. Zhang, Y. Zeng, and R. Zhang, "Cellular-Enabled UAV Communication: A Connectivity-Constrained Trajectory Optimization Perspective," *IEEE Trans. Commun.*, vol. 67, no. 3, pp. 2580–2604, Mar. 2019.

[33] Q. Wu, L. Liu, and R. Zhang, "Fundamental Trade-Offs in Communication and Trajectory Design for UAV-Enabled Wireless Network," *IEEE Wirel. Commun.*, vol. 26, no. 1, pp. 36–44, Feb. 2019.

[34] J. Košmerl and A. Vilhar, "Base stations placement optimization in wireless networks for emergency communications," in *2014 IEEE International Conference on Communications Workshops (ICC)*, Jun. 2014, pp. 200–205.

[35] C. T. Cicek *et al.*, "UAV Base Station Location Optimization for Next Generation Wireless Networks: Overview and Future Research Directions," in *2019 1st International Conference on Unmanned Vehicle Systems-Oman (UVS)*, Feb. 2019, pp. 1–6.

[36] Y. B. Zikria *et al.*, "Next-generation Internet of Things (IoT): Opportunities, Challenges, and Solutions," *Sensors*, vol. 21, no. 4, p. 1174, Feb. 2021.

[37] Z. Wei *et al.*, "UAV-Assisted Data Collection for Internet of Things: A Survey," *IEEE Internet Things J.*, vol. 9, no. 17, pp. 15 460–15 483, May 2022.

[38] P. Tong *et al.*, "UAV-Enabled Age-Optimal Data Collection in Wireless Sensor Networks," in *2019 ICC Workshops*, May 2019, pp. 1–6.

[39] M. Samir *et al.*, "UAV Trajectory Planning for Data Collection From Time-Constrained IoT Devices," *IEEE Trans. Wirel. Commun.*, vol. 19, no. 1, pp. 34–46, Sept. 2019.

[40] D.-H. Tran *et al.*, "UAV Relay-Assisted Emergency Communications in IoT Networks: Resource Allocation and Trajectory Optimization," *IEEE Trans. Wirel. Commun.*, vol. 21, no. 3, pp. 1621–1637, Aug. 2022.

[41] W. Luo *et al.*, "Joint 3-D Trajectory and Resource Optimization in Multi-UAV-Enabled IoT Networks With Wireless Power Transfer," *IEEE Internet Things J.*, vol. 8, no. 10, pp. 7833–7848, Nov. 2020.

[42] A. A. o. Khuwaja, "A Survey of Channel Modeling for UAV Communications," *IEEE Commun. Surv. Tutor.*, vol. 20, no. 4, pp. 2804–2821, July 2018.

[43] X. Li *et al.*, "A Near-Optimal UAV-Aided Radio Coverage Strategy for Dense Urban Areas," *IEEE Trans. Veh. Technol*, vol. 68, no. 9, pp. 9098–9109, Sept. 2019.

[44] A. Al-Hourani, S. Kandeepan, and S. Lardner, "Optimal LAP Altitude for Maximum Coverage," *IEEE Wirel. Commun. Lett.*, vol. 3, no. 6, pp. 569–572, July 2014.

[45] C. She *et al.*, "Ultra-Reliable and Low-Latency Communications in Unmanned Aerial Vehicle Communication Systems," *IEEE Trans. Commun.*, vol. 67, no. 5, pp. 3768–3781, May 2019.

[46] M. M. Azari *et al.*, "Coexistence of Terrestrial and Aerial Users in Cellular Networks," in *2017 IEEE Globecom Workshops (GC Wkshps)*, Dec. 2017, pp. 1–6.

[47] W. Mei, Q. Wu, and R. Zhang, "Cellular-Connected UAV: Uplink Association, Power Control and Interference Coordination," *IEEE Trans. Wirel. Commun.*, vol. 18, no. 11, pp. 5380–5393, Nov. 2019.

[48] M. M. Azari, F. Rosas, and S. Pollin, "Reshaping Cellular Networks for the Sky: Major Factors and Feasibility," in *2018 IEEE International Conference on Communications (ICC)*, May 2018, pp. 1–7.

[49] Z. Zhang *et al.*, "6G Wireless Networks: Vision, Requirements, Architecture, and Key Technologies," *IEEE Veh. Technol. Mag.*, vol. 14, no. 3, pp. 28–41, July 2019.

[50] C. Huang *et al.*, "Reconfigurable Intelligent Surfaces for Energy Efficiency in Wireless Communication," *IEEE Trans. Wirel. Commun.*, vol. 18, no. 8, pp. 4157–4170, June 2019.

[51] E. Basar, "Reconfigurable Intelligent Surface-Based Index Modulation: A New Beyond MIMO Paradigm for 6G," *IEEE Trans. Commun.*, vol. 68, no. 5, pp. 3187–3196, Feb. 2020.

[52] Y. Liu *et al.*, "Reconfigurable Intelligent Surfaces: Principles and Opportunities," *IEEE Commun. Surv. Tutor.*, vol. 23, no. 3, pp. 1546–1577, May 2021.

[53] S. Hassouna *et al.*, "A survey on reconfigurable intelligent surfaces: Wireless communication perspective," *IET Communications*, vol. 17, no. 5, pp. 497–537, Jan. 2023.

[54] E. Basar *et al.*, "Wireless Communications Through Reconfigurable Intelligent Surfaces," *IEEE Access*, vol. 7, pp. 116 753–116 773, Aug. 2019.

[55] H.-T. Chen, A. J. Taylor, and N. Yu, "A review of metasurfaces: physics and applications," *Reports on progress in physics*, vol. 79, no. 7, p. 076401, June 2016.

[56] J. P. Turpin *et al.*, "Reconfigurable and tunable metamaterials: a review of the theory and applications," *International Journal of Antennas and Propagation*, vol. 2014, no. 1, p. 429837, May 2014.

[57] F. Liu *et al.*, "Programmable Metasurfaces: State of the Art and Prospects," in *2018 IEEE International Symposium on Circuits and Systems (ISCAS)*, May 2018, pp. 1–5.

[58] Q. Wu and R. Zhang, "Intelligent Reflecting Surface Enhanced Wireless Network via Joint Active and Passive Beamforming," *IEEE Trans. Wirel. Commun.*, vol. 18, no. 11, pp. 5394–5409, Aug. 2019.

[59] X. Yu, D. Xu, and R. Schober, "MISO Wireless Communication Systems via Intelligent Reflecting Surfaces : (Invited Paper)," in *2019 IEEE/CIC International Conference on Communications in China (ICCC)*, Oct. 2019, pp. 735–740.

[60] Y. Yang *et al.*, "Intelligent Reflecting Surface Meets OFDM: Protocol Design and Rate Maximization," *IEEE Trans. Commun.*, vol. 68, no. 7, pp. 4522–4535, Mar. 2020.

[61] S. Zhang and R. Zhang, "Capacity Characterization for Intelligent Reflecting Surface Aided MIMO Communication," *IEEE J. Sel. Areas Commun.*, vol. 38, no. 8, pp. 1823–1838, Aug. 2020.

[62] Q. Wu and R. Zhang, "Beamforming Optimization for Wireless Network Aided by Intelligent Reflecting Surface With Discrete Phase Shifts," *IEEE Trans. Commun.*, vol. 68, no. 3, pp. 1838–1851, Dec. 2020.

[63] X. Yu, D. Xu, and R. Schober, "Optimal Beamforming for MISO Communications via Intelligent Reflecting Surfaces," in *2020 IEEE 21st International Workshop on Signal Processing Advances in Wireless Communications (SPAWC)*, May 2020, pp. 1–5.

[64] K. Zhi *et al.*, "Power Scaling Law Analysis and Phase Shift Optimization of RIS-Aided Massive MIMO Systems With Statistical CSI," *IEEE Trans. Commun.*, vol. 70, no. 5, pp. 3558–3574, Mar. 2022.

[65] A. Taha *et al.*, "Deep Reinforcement Learning for Intelligent Reflecting Surfaces: Towards Standalone Operation," in *2020 IEEE 21st International Workshop on Signal Processing Advances in Wireless Communications (SPAWC)*, May 2020, pp. 1–5.

[66] E. Björnson, Ö. Özdogan, and E. G. Larsson, "Intelligent Reflecting Surface Versus Decode-and-Forward: How Large Surfaces are Needed to Beat Relaying?" *IEEE Wirel. Commun. Lett.*, vol. 9, no. 2, pp. 244–248, Oct. 2020.

[67] S. Zhou *et al.*, "Spectral and Energy Efficiency of IRS-Assisted MISO Communication With Hardware Impairments," *IEEE Wirel. Commun. Lett.*, vol. 9, no. 9, pp. 1366–1369, Apr. 2020.

[68] C. Liaskos *et al.*, "A new wireless communication paradigm through software-controlled metasurfaces," *IEEE Commun. Mag.*, vol. 56, no. 9, pp. 162–169, Sept. 2018.

[69] J. Zhao, "A Survey of Intelligent Reflecting Surfaces (IRSs): Towards 6G Wireless Communication Networks," *arXiv preprint arXiv:1907.04789*, July 2019.

[70] M. Jung *et al.*, "On the Optimality of Reconfigurable Intelligent Surfaces (RISs): Passive Beamforming, Modulation, and Resource Allocation," *IEEE Trans. Wirel. Commun*, vol. 20, no. 7, pp. 4347–4363, Feb. 2021.

[71] N. S. Perović, M. D. Renzo, and M. F. Flanagan, "Channel Capacity Optimization Using Reconfigurable Intelligent Surfaces in Indoor mmWave Environments," in *ICC 2020 - 2020 IEEE International Conference on Communications (ICC)*, June 2020, pp. 1–7.

[72] L. Yang *et al.*, "Secrecy Performance Analysis of RIS-Aided Wireless Communication Systems," *IEEE Trans. Veh. Technol*, vol. 69, no. 10, pp. 12 296–12 300, July 2020.

[73] J. Qiao and M.-S. Alouini, "Secure Transmission for Intelligent Reflecting Surface-Assisted mmWave and Terahertz Systems," *IEEE Wirel. Commun. Lett.*, vol. 9, no. 10, pp. 1743–1747, June 2020.

[74] X. Yu *et al.*, "Robust and Secure Wireless Communications via Intelligent Reflecting Surfaces," *IEEE J. Sel. Areas Commun.*, vol. 38, no. 11, pp. 2637–2652, July 2020.

[75] H. Yang *et al.*, "Intelligent Reflecting Surface Assisted Anti-Jamming Communications: A Fast Reinforcement Learning Approach," *IEEE Trans. Wirel. Commun.*, vol. 20, no. 3, pp. 1963–1974, Nov. 2021.

[76] A. Damnjanovic *et al.*, "A survey on 3GPP heterogeneous networks," *IEEE Wirel. Commun.*, vol. 18, no. 3, pp. 10–21, June 2011.

[77] A. Asadi, Q. Wang, and V. Mancuso, "A Survey on Device-to-Device Communication in Cellular Networks," *IEEE Communications Surveys Tutorials*, vol. 16, no. 4, pp. 1801–1819, Apr. 2014.

[78] Y. Cao *et al.*, "Sum-Rate Maximization for Multi-Reconfigurable Intelligent Surface-Assisted Device-to-Device Communications," *IEEE Trans. Commun.*, vol. 69, no. 11, pp. 7283–7296, Aug. 2021.

[79] A. U. Makarfi *et al.*, "Reconfigurable Intelligent Surface Enabled IoT Networks in Generalized Fading Channels," in *ICC 2020 - 2020 IEEE International Conference on Communications (ICC)*, June 2020, pp. 1–6.

[80] Y. Zhu *et al.*, "Joint Time Allocation and Beamforming Design for IRS-Aided Coexistent Cellular and Sensor Networks," in *2021 IEEE Global Communications Conference (GLOBECOM)*, Dec. 2021, pp. 1–6.

[81] S. A. Shah and F. Fioranelli, "RF Sensing Technologies for Assisted Daily Living in Healthcare: A Comprehensive Review," *IEEE Aerospace and Electronic Systems Magazine*, vol. 34, no. 11, pp. 26–44, Nov. 2019.

[82] J. u. R. Kazim *et al.*, "Wireless on Walls: Revolutionizing the future of health care," *IEEE Antennas and Propagation Magazine*, vol. 63, no. 6, pp. 87–93, Nov. 2021.

[83] X. Mu *et al.*, "Intelligent Reflecting Surface Enhanced Indoor Robot Path Planning: A Radio Map-Based Approach," *IEEE Trans. Wirel. Commun.*, vol. 20, no. 7, pp. 4732–4747, Mar. 2021.

[84] Y. U. Ozcan, O. Ozdemir, and G. K. Kurt, "Reconfigurable Intelligent Surfaces for the Connectivity of Autonomous Vehicles," *IEEE Trans. Veh. Technol*, vol. 70, no. 3, pp. 2508–2513, Feb. 2021.

[85] Z. Zhang *et al.*, "Wireless Power Transfer—An Overview," *IEEE Trans. Ind. Electron.*, vol. 66, no. 2, pp. 1044–1058, May 2019.

[86] L. Mohjazi *et al.*, "Battery recharging time models for reconfigurable intelligent surfaces-assisted wireless power transfer systems," *IEEE Trans. Green Commun. Netw.*, vol. 6, no. 2, pp. 1173–1185, Oct. 2021.

[87] S. Basharat *et al.*, "Reconfigurable intelligent surfaces: Potentials, applications, and challenges for 6G wireless networks," *IEEE Wirel. Commun.*, vol. 28, no. 6, pp. 184–191, Sept. 2021.

[88] M. Abualhayja'a *et al.*, "Performance of Reconfigurable Intelligent Surfaces vs. Relaying for UAV-Assisted Communications," in *2021 IEEE USNC-URSI Radio Science Meeting (Joint with AP-S Symposium)*, Dec. 2021, pp. 58–59.

[89] F. Rusek *et al.*, "Scaling Up MIMO: Opportunities and Challenges with Very Large Arrays," *IEEE Signal Process. Mag.*, vol. 30, no. 1, pp. 40–60, Dec. 2013.

[90] C. Han *et al.*, "Green radio: radio techniques to enable energy-efficient wireless networks," *IEEE Commun. Mag.*, vol. 49, no. 6, pp. 46–54, June 2011.

[91] O. Osibanjo and I. Nnorom, "The challenge of electronic waste (e-waste) management in developing countries," *Waste management & research*, vol. 25, no. 6, pp. 489–501, Dec. 2007.

[92] E. Yaacoub and M.-S. Alouini, "A Key 6G Challenge and Opportunity—Connecting the Base of the Pyramid: A Survey on Rural Connectivity," *Proceedings of the IEEE*, vol. 108, no. 4, pp. 533–582, Mar. 2020.

[93] M. Abualhayjaa *et al.*, "Intelligent reflective surfaces (IRSs) for green networks," in *The Role of 6G and Beyond on the Road to Net-Zero Carbon*, M. A. Imran *et al.*, Eds. IET, 2023, pp. 193–219.

[94] M. Abualhayja'a *et al.*, "Exploiting Multi-Hop RIS-Assisted UAV Communications: Performance Analysis," *IEEE Wirel. Commun. Lett.*, vol. 28, no. 1, pp. 133–137, Dec. 2023.

[95] ——, "On the Outage Performance of Reconfigurable Intelligent Surface-Assisted UAV Communications," in *2023 IEEE Wireless Communications and Networking Conference (WCNC)*, Mar. 2023, pp. 1–6.

[96] S. Li *et al.*, "Reconfigurable Intelligent Surface Assisted UAV Communication: Joint Trajectory Design and Passive Beamforming," *IEEE Wirel. Commun. Lett.*, vol. 9, no. 5, pp. 716–720, Jan. 2020.

[97] H. Long *et al.*, "Joint Trajectory and Passive Beamforming Design for Secure UAV Networks with RIS," in *2020 IEEE Globecom Workshops (GC Wkshps.* IEEE, Dec. 2020, pp. 1–6.

[98] D. Ma, M. Ding, and M. Hassan, "Enhancing Cellular Communications for UAVs via Intelligent Reflective Surface," in *2020 IEEE Wireless Communications and Networking Conference (WCNC)*, May 2020, pp. 1–6.

[99] A. A. Deshpande *et al.*, "Energy-Efficient Design for RIS-assisted UAV communications in beyond-5G Networks," in *2022 20th Mediterranean Communication and Computer Networking Conference (MedComNet)*, June 2022, pp. 158–165.

[100] K. K. Nguyen *et al.*, "Reconfigurable Intelligent Surface-Assisted Multi-UAV Networks: Efficient Resource Allocation With Deep Reinforcement Learning," *IEEE Signal Process. Mag.*, vol. 16, no. 3, pp. 358–368, Dec. 2022.

[101] X. Liu, Y. Liu, and Y. Chen, "Machine Learning Empowered Trajectory and Passive Beamforming Design in UAV-RIS Wireless Networks," *IEEE J. Sel. Areas Commun.*, vol. 39, no. 7, pp. 2042–2055, Dec. 2021.

[102] X. Mu *et al.*, "Intelligent Reflecting Surface Enhanced Multi-UAV NOMA Networks," *IEEE J. Sel. Areas Commun.*, vol. 39, no. 10, pp. 3051–3066, June 2021.

[103] Z. Mohamed and S. Aïssa, "Leveraging UAVs with Intelligent Reflecting Surfaces for Energy-Efficient Communications with Cell-Edge Users," in *2020 IEEE International Conference on Communications Workshops (ICC Workshops)*, June 2020, pp. 1–6.

[104] X. Fan *et al.*, "RIS-Assisted UAV for Fresh Data Collection in 3D Urban Environments: A Deep Reinforcement Learning Approach," *IEEE Trans. Veh.*, vol. 72, no. 1, pp. 632–647, Aug. 2022.

[105] K. K. Nguyen *et al.*, "RIS-Assisted UAV Communications for IoT With Wireless Power Transfer Using Deep Reinforcement Learning," *IEEE Journal of Selected Topics in Signal Processing*, vol. 16, no. 5, pp. 1086–1096, May 2022.

[106] Z. Zhai *et al.*, "Energy-Efficient UAV-Mounted RIS Assisted Mobile Edge Computing," *IEEE Wirel. Commun. Lett.*, vol. 11, no. 12, pp. 2507–2511, Sept. 2022.

[107] H. Mei *et al.*, "Joint Trajectory-Task-Cache Optimization With Phase-Shift Design of RIS-Assisted UAV for MEC," *IEEE Wirel. Commun. Lett.*, vol. 10, no. 7, pp. 1586–1590, Apr. 2021.

[108] A. V. Savkin, C. Huang, and W. Ni, "Joint Multi-UAV Path Planning and LoS Communication for Mobile-Edge Computing in IoT Networks With RISs," *IEEE Internet Things J.*, vol. 10, no. 3, pp. 2720–2727, Oct. 2023.

[109] L. Yang *et al.*, "Performance Analysis of RIS-Assisted UAV Communication Systems," *IEEE Trans. Veh. Technol.*, vol. 71, no. 8, pp. 9078–9082, May 2022.

[110] A. Mahmoud *et al.*, "Intelligent Reflecting Surfaces Assisted UAV Communications for IoT Networks: Performance Analysis," *IEEE Trans. Green Commun. Netw.*, vol. 5, no. 3, pp. 1029–1040, Mar. 2021.

[111] J. Laneman and G. Wornell, "Distributed Space-Time-Coded Protocols for Exploiting Cooperative Diversity in Wireless Networks," *IEEE Trans. Inf. Theory*, vol. 49, no. 10, pp. 2415–2425, Oct. 2003.

[112] G. K. Karagiannidis, N. C. Sagias, and P. T. Mathiopoulos, "$N*$Nakagami: A Novel Stochastic Model for Cascaded Fading Channels," *IEEE Trans. Commun.*, vol. 55, no. 8, pp. 1453–1458, Aug. 2007.

[113] S. Primak, V. Kontorovich, and V. Lyandres, *Stochastic Methods and Their Applications to Communications: Stochastic Differential Equations Approach.* John Wiley & Sons, 2005.

[114] M. Simon and M.-S. Alouini, *Digital Communication Over Fading Channels*, 2nd ed. Hoboken, NJ, USA: Wiley, 2005.

[115] J. Hu and N. Beaulieu, "Accurate Closed-Form Approximations to Ricean Sum Distributions and Densities," *IEEE Commun. Lett.*, vol. 9, no. 2, pp. 133–135, Jan. 2005.

[116] J. Marcum, "A Statistical Theory of Target Detection by Pulsed Radar," *IRE Transactions on Information Theory*, vol. 6, no. 2, pp. 59–267, Apr. 1960.

[117] N. Temme, "Asymptotic and Numerical Aspects of the Noncentral Chi-Square Distribution," *Computers & Mathematics with Applications*, vol. 25, no. 5, pp. 55–63, Mar. 1993.

[118] A. M. Salhab and M. H. Samuh, "Accurate Performance Analysis of Reconfigurable Intelligent Surfaces Over Rician Fading Channels," *IEEE Wirel. Commun. Lett.*, vol. 10, no. 5, pp. 1051–1055, Feb. 2021.

[119] J. Hu and N. C. Beaulieu, "Performance Analysis of Decode-and-Forward Relaying with Selection Combining," *IEEE Commun. Lett.*, vol. 11, no. 6, pp. 489–491, June 2007.

[120] I. S. Gradshteyn and I. M. Ryzhik, *Tables of Integrals, Series and Products*, 6th ed. San Diego, CA, USA: Academic Press, 2000.

[121] Z. Wang and G. Giannakis, "A Simple and General Parameterization Quantifying Performance in Fading Channels," *IEEE Trans. Commun.*, vol. 51, no. 8, pp. 1389–1398, Aug. 2003.

[122] I. S. Ansari *et al.*, "A New Formula for the BER of Binary Modulations with Dual-Branch Selection over Generalized-K Composite Fading Channels," *IEEE Trans. Commun.*, vol. 59, no. 10, pp. 2654–2658, Jul. 2011.

[123] A. Prudinikov, Y. Brychkov, and O. Marichev, *Integrals and series: special functions.* New York, NY, USA: Gordon and Breach (Publishers, Inc.), 1992, vol. 2.

[124] Iskandar and S. Shimamoto, "The Channel Characterization and Performance Evaluation of Mobile Communication Employing Stratospheric Platform," in *IEEE/ACES International Conference on Wireless Communications and Applied Computational Electromagnetics, 2005.*, Mar. 2005, pp. 828–831.

[125] W. Tang *et al.*, "Wireless Communications With Reconfigurable Intelligent Surface: Path Loss Modeling and Experimental Measurement," *IEEE Trans. Wirel. Commun.*, vol. 20, no. 1, pp. 421–439, Sept. 2021.

[126] X. Pei *et al.*, "RIS-Aided Wireless Communications: Prototyping, Adaptive Beamforming, and Indoor/Outdoor Field Trials," *IEEE Trans. Commun.*, vol. 69, no. 12, pp. 8627–8640, Sept. 2021.

[127] J. Wang *et al.*, "Reconfigurable Intelligent Surface: Power Consumption Modeling and Practical Measurement Validation," *IEEE Trans. Commun.*, pp. 1–1, Mar. 2024.

[128] J. Wang, W. Tang, S. Jin, X. Li, and M. Matthaiou, "Static Power Consumption Modeling and Measurement of Reconfigurable Intelligent Surfaces," in *2023 31st European Signal Processing Conference (EUSIPCO)*, Sept. 2023, pp. 890–894.

[129] T. J. a. Cui, "Coding Metamaterials, Digital Metamaterials and Programmable Metamaterials," *Light: science & applications*, vol. 3, no. 10, pp. e218–e218, Oct. 2014.

[130] X. Pei *et al.*, "RIS-Aided Wireless Communications: Prototyping, Adaptive Beamforming, and Indoor/Outdoor Field Trials," *IEEE Trans. Commun.*, vol. 69, no. 12, pp. 8627–8640, Sept. 2021.

[131] J. Laneman, D. Tse, and G. Wornell, "Cooperative Diversity in Wireless Networks: Efficient Protocols and Outage Behavior," *IEEE Trans. Inf. Theory*, vol. 50, no. 12, pp. 3062–3080, Nov. 2004.

[132] L. Sanguinetti, A. A. D'Amico, and Y. Rong, "A Tutorial on the Optimization of Amplify-and-Forward MIMO Relay Systems," *IEEE J. Sel. Areas Commun.*, vol. 30, no. 8, pp. 1331–1346, Aug. 2012.

[133] R. Nabar, H. Bolcskei, and F. Kneubuhler, "Fading Relay Channels: Performance Limits and Space-Time Signal Design," *IEEE J. Sel. Areas Commun.*, vol. 22, no. 6, pp. 1099–1109, Aug. 2004.

[134] A. Pandey *et al.*, "Secrecy Performance of Cooperative Cognitive AF Relaying Networks With Direct Links Over Mixed Rayleigh and Double-Rayleigh Fading Channels," *IEEE Trans. Veh. Technol*, vol. 69, no. 12, pp. 15 095–15 112, Oct. 2020.

[135] L. Sboui *et al.*, "A New Relation Between Energy Efficiency and Spectral Efficiency in Wireless Communications Systems," *IEEE Wirel. Commun.*, vol. 26, no. 3, pp. 168–174, Apr. 2019.

[136] X. Qi *et al.*, "Energy Efficient Resource Allocation for 5G Heterogeneous Networks Using Genetic Algorithm," *IEEE Access*, vol. 9, pp. 160 510–160 520, Nov. 2021.

[137] X. Ma *et al.*, "Energy Consumption Optimization of 5G Base Stations Considering Variable Threshold Sleep Mechanism," *Energy Reports*, vol. 9, pp. 34–42, Aug. 2023.

[138] B. Bossy, P. Kryszkiewicz, and H. Bogucka, "Energy-Efficient OFDM Radio Resource Allocation Optimization With Computational Awareness: A Survey," *IEEE Access*, vol. 10, pp. 94 100–94 132, Sept. 2022.

[139] Q. Wu and R. Zhang, "Intelligent Reflecting Surface Enhanced Wireless Network: Joint Active and Passive Beamforming Design," in *2018 IEEE Global Communications Conference (GLOBECOM)*, Dec. 2018, pp. 1–6.

[140] J. D. Griffin and G. D. Durgin, "Complete Link Budgets for Backscatter-Radio and RFID Systems," *IEEE Antennas Propag. Mag.*, vol. 51, no. 2, pp. 11–25, Apr. 2009.

[141] B. Bossy, P. Kryszkiewicz, and H. Bogucka, "Energy Efficient Wireless Relay Networks With Computational Awareness," *IEEE Trans. Commun.*, vol. 68, no. 2, pp. 825–840, Nov. 2020.

[142] H. o. Bayerlein, "Multi-UAV Path Planning for Wireless Data Harvesting With Deep Reinforcement Learning," *IEEE Open J. Commun. Soc.*, vol. 2, pp. 1171–1187, May 2021.

[143] D. Ebrahimi *et al.*, "Data Collection in Wireless Sensor Networks Using UAV and Compressive Data Gathering," in *2018 IEEE Global Communications Conference (GLOBECOM)*, Dec. 2018, pp. 1–7.

[144] S. Alfattani *et al.*, "Multi-UAV Data Collection Framework for Wireless Sensor Networks," in *2019 IEEE Global Communications Conference (GLOBECOM)*, Dec. 2019, pp. 1–6.

[145] T. A. Al-Janabi and H. S. Al-Raweshidy, "An Energy Efficient Hybrid MAC Protocol With Dynamic Sleep-Based Scheduling for High Density IoT Networks," *IEEE Internet Things J.*, vol. 6, no. 2, pp. 2273–2287, Mar. 2019.

[146] M. Mozaffari *et al.*, "Unmanned Aerial Vehicle With Underlaid Device-to-Device Communications: Performance and Tradeoffs," *IEEE Trans. Wirel. Commun.*, vol. 15, no. 6, pp. 3949–3963, Feb. 2016.

[147] T. Kanungo *et al.*, "An Efficient K-Means Clustering Algorithm: Analysis and Implementation," *IEEE Trans. Pattern Anal. Mach. Intell.*, vol. 24, no. 7, pp. 881–892, July 2002.

[148] Y. Mehmood *et al.*, "Internet-of-Things-Based Smart Cities: Recent Advances and Challenges," *IEEE Commun. Mag.*, vol. 55, no. 9, pp. 16–24, Sept. 2017.

[149] Q. Wu, Y. Zeng, and R. Zhang, "Joint Trajectory and Communication Design for Multi-UAV Enabled Wireless Networks," *IEEE Trans. Wirel. Commun.*, vol. 17, no. 3, pp. 2109–2121, Jan. 2018.